AN EMPIRICAL MODEL FOR VORTEX-INDUCED VIBRATIONS

Thesis by

Dirceu Luiz Rodrigues Botelho

In Partial Fulfillment of the Requirements

for the Degree of

Doctor of Philosophy

California Institute of Technology

Pasadena, California

1983

(Submitted July 26, 1982)

ACKNOWLEDGMENTS

I wish to express my appreciation to my advisor Dr. W.D. Iwan, for his guidance and suggestions during the course of this investigation. I also wish to thank Dr. A. Roshko with whom I have had valuable discussions.

The financial support received through the CNPq-Conselho Nacional de Desenvolvimento Científico e Tecnólogico (Brazilian Council for Scientific and Technological Development) and the California Institute of Technology is gratefully acknowledged.

To the members of the Civil Engineering Department with whom I have had the opportunity of working, I want to extend my appreciation. Thanks is also extended to Ms. Anne Swatfigure for her patience in typing this manuscript and to Ms. Cecilia Lin for her assistance in finalizing the figures in this manuscript.

Lastly, and most importantly, I thank my wife Anne, for her support and encouragement through the difficult moments we shared in the course of my graduate work. To her, with love, this thesis is dedicated.

ABSTRACT

Through an analytical-empirical approach, the vortex-excited transverse oscillations of flexibly-mounted circular cylinders in a uniform flow is studied.

A new model is derived, assuming spanwise constant flow velocity within the sub-critical range of Reynolds numbers and using only experimental data obtained from forced cylinders in water.

The steady-state response of flexibly-mounted cylinders is obtained as a function of the structural system and flow parameters and its stability is analyzed. Several characteristics observed experimentally and also present in the model response are discussed.

The resultant model's capability for predicting structural response for a wide range of fluid mediums is illustrated through comparisons between model predictions and results obtained experimentally from flexibly-mounted cylinders in air and in water.

This model developed is expected to yield better results for structures in water, by virtue of being based only on experimental results obtained in water.

TABLE OF CONTENTS

NOTATION

a	Parameter appearing in the analytical interpolation expression for C_{dl}
a_i	Wake Oscillator Model constants, i=0,1,2,....,6
a_{ij}	Parameters appearing in the stability matrix, i,j=1,2
A	Cylinder amplitude (=1/2 peak-to-peak displacement)
b	Parameter appearing in the analytical interpolation expression for C_{dl}
B	Normalized cylinder amplitude (=A/D)
B_{max}	Maximum value of the normalized amplitude B
B_{ss}	Steady-state normalized cylinder amplitude-response
c	Parameter appearing in the analytical interpolation expression for C_{dl}
$\bar{c}$	Structural damping per unit length for the flexibly mounted cylinder
C_{dh}	Drag coefficient, component of F out-of-phase with cylinder displacement, normalized by $(1/2\rho DV^2)$
C_{dl}	Drag coefficient, component of F out-of-phase with cylinder displacement, normalized by $(1/2\rho DA^2\omega^2)$
C_{mh}	Inertia coefficient, component of F in-phase with cylinder displacement, normalized by $(1/2\rho DV^2)$
C_{ml}	Inertia coefficient, component of F in-phase with cylinder displacement, normalized by $(1/2\rho DA^2\omega^2)$
d	Parameter appearing in the analytical interpolation expression for C_{dl}
D	Cylinder diameter
e	Parameter appearing in the analytical interpolation expression for C_{ml}
e_1	$a_0 + a_3 + a_5$
f	Parameter appearing in the analytical interpolation expression for C_{ml}

F	Experimentally measured force acting on a cylinder being forced to vibrate transversally to a uniform flow
F_{int}	Wake Oscillator Model prediction of the force acting on a cylinder being forced to vibrate transversally to a uniform flow
k	Structural stiffness per unit length for the flexibly mounted cylinder
m	Structural mass per unit length for the flexibly mounted cylinder
R	Real part of a complex number
Re	Reynolds number
S	Strouhal number
V	Uniform free stream flow velocity
V_n	Normalized flow velocity ($= \omega_s/\omega_n = 2\pi SV/\omega_n D$)
V_r	Reduced flow velocity ($= \omega_s/S\omega$)
V_{ro}	Parameter appearing in the analytical interpolation expression for C_{ml}
y	Normalized cylinder displacement ($=Y/D$)
Y	Cylinder displacement
z	Normalized fluid oscillator variable in the Wake Oscillator Model ($=Z/D$)
Z	Fluid oscillator variable in the Wake Oscillator Model
α	Perturbation of Ω about Ω_{ss}
α_o	Amplitude of the perturbation α
$\Delta\omega_1$	1/2 power method bandwidth
$\Delta\omega_2$	Frequency entrainment bandwidth
ζ	Structural damping ratio (fraction of critical damping)
$\hat{\zeta}$	Reduced damping ($= 2(2\pi S)^2\ \zeta/\eta$)
η	Mass ratio ($= \rho D^2/m$)

λ	Eigenvalue in the stability analysis
ν	Kinematic viscosity of a fluid
ξ	Perturbation of B about B_{ss}
ξ_o	Amplitude of the perturbation ξ
ρ	Fluid density
τ	Normalized time (= $\omega_s t$)
ϕ	Phase angle in the assumed form of the Non-Lock-in Model response
ϕ_{ss}	Phase angle of the steady-state Non-Lock-in Model response
ψ	Perturbation of ϕ about ϕ_{ss}
ψ_o	Amplitude of the perturbation ψ
ω	Angular cylinder frequency, either in the induced or in the forced oscillations case
ω_n	Angular natural frequency of the flexibly mounted cylinder
ω_s	Angular Strouhal frequency
ω_v	Angular vortex-shedding frequency
Ω	Normalized cylinder frequency (= ω/ω_s)
Ω_{ss}	Normalized steady-state cylinder frequency response

CHAPTER I

INTRODUCTION

A bluff structure exposed to a flowing fluid, may be subjected to vortex induced vibrations. In structural engineering applications, these strumming oscillations are of great interest not only because of their potentially large amplitudes which can overstress a structural member but also because of their equally destructive long term effects, which may cause failure by fatigue.

The most common examples of structures subjected to this kind of excitation are structures composed by cables and beams such as power transmission lines, mooring cables, towers and risers. More complex structures like bridges may also be subjected to vortex excited oscillations, however the phenomenon may be even further complicated by reattachment of the vortices.

1.1 BASIC PHENOMENA

The oscillating forces induced by vortex shedding, are brought about by the fluid pressure on the structure's surface which fluctuates as vortices are shed alternately from each side of the structure. A sequence of this oscillating pressure field on a cylinder is pictured in Fig. 1.1.1.

The major regimes of flow behavior, in which vortex-shedding from a stationary cylinder may occur are presented in Fig. 1.1.2. For low flow velocities (i.e., $Re = \frac{VD}{\nu} < 5$) the flow is able to negotiate its way around the cylinder and thus, no vortices are shed. As the flow velocity is increased a pair of Föppl vortices is formed in the wake and when

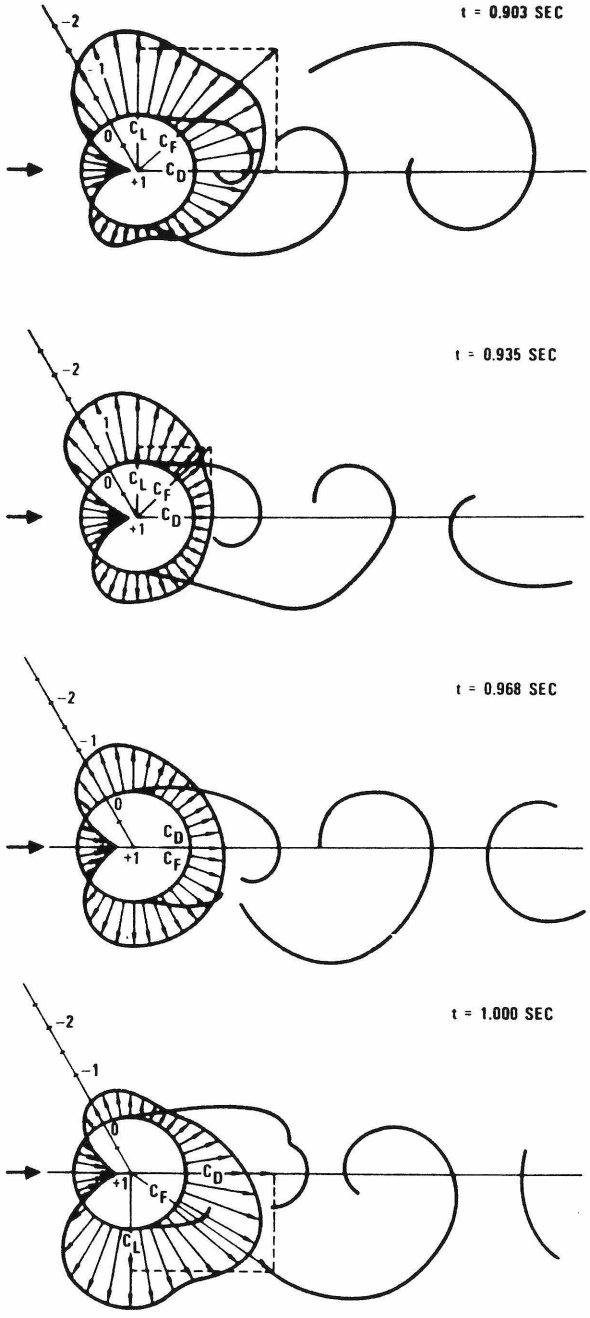

Fig. 1.1.1

A Sequence of Surface Pressure Fields Around a Circular Cylinder [5]

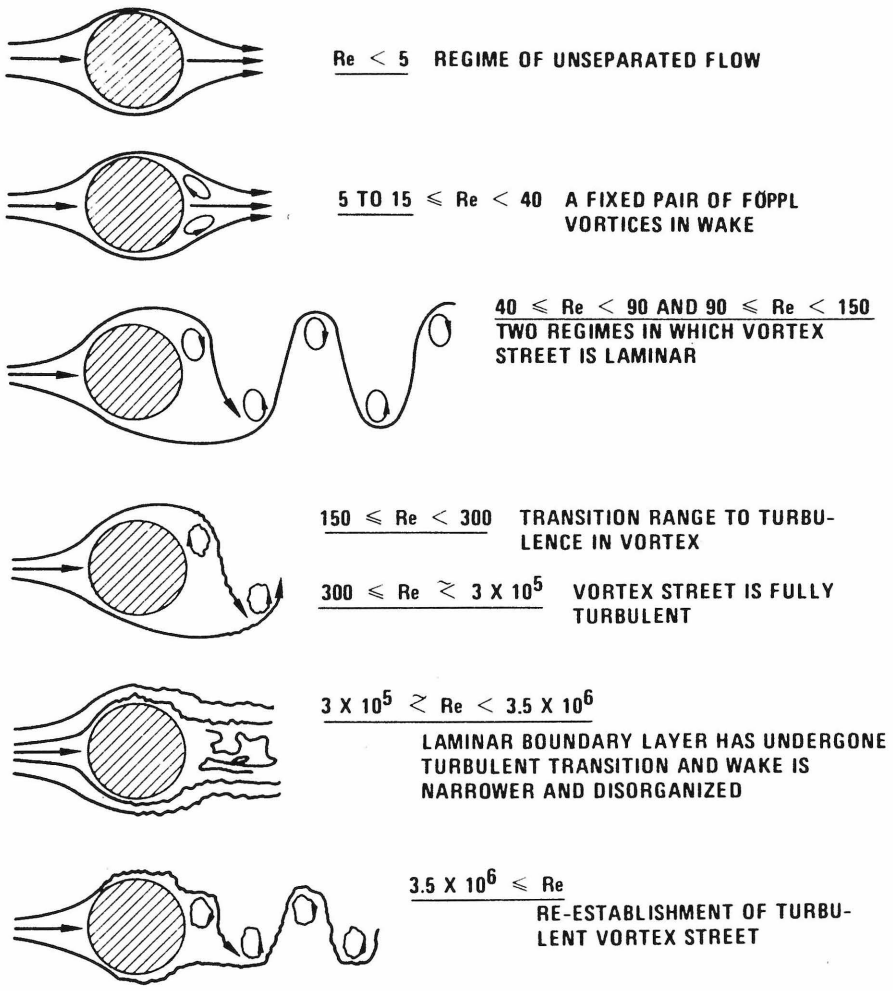

Fig. 1.1.2

Vortex Shedding Regimes from a Fixed Circular Cylinder [5]

$Re \geqslant 40$, there is periodic shedding of vortices. Vortex-shedding persists within the entire subcritical range of the Reynolds number. In the transcritical range, $3 \times 10^5 \lesssim Re \lesssim 3.5 \times 10^6$, periodic shedding ceases to exist. It appears again in the supercritical range of the Reynolds number, [5].

In the absence of structural oscillations, the vortex-shedding frequency ω_v, satisfies [29]

$$\omega_v \equiv \omega_s \tag{1.1.1}$$

where the Strouhal frequency (ω_s) is given by an experimentally determined relationship [73] as

$$\omega_s = 2\pi S \frac{V}{D} \tag{1.1.2}$$

V is the free stream flow velocity, D is the diameter of the cylinder, and S is the Strouhal number. The experimental constant S is a function of the structure's geometry and of the Reynolds number, as shown in Fig. 1.1.3. Within the subcritical range of Reynolds number, the Strouhal number and, consequently, the Strouhal frequency are quite well defined. But this is not true within the transcritical range, where the Strouhal number can take on any value between the dashed lines, resulting in a wide band of shedding frequencies. Finally, in the supercritical range, the Strouhal number is again quite well defined.

Induced oscillations will occur at some frequency ω, when a structural system with natural frequency ω_n is exposed to the oscillating forces due to vortex shedding. For sufficiently small amplitudes of oscillation, the vortex shedding process is undisturbed. In this case, the vortex shedding frequency is equal to the Strouhal frequency and the system also responds at the Strouhal frequency

$$\omega = \omega_v = \omega_s \tag{1.1.3}$$

However, in the range of flow velocities V for which the Strouhal frequency is in the neighborhood of the structural system's natural frequency, the induced amplitudes of oscillation may be large enough to establish the lock-in condition. Under the lock-in condition, Eq. (1.1.1) ceases to hold and the actual vortex shedding frequency is very close to the natural frequency of the system [29]

$$\omega \cong \omega_n \cong \omega_v \tag{1.1.4}$$

On the other hand, when the structural system exposed to vortex shedding is forced to oscillate at a frequency ω, lock-in occurs whenever the flow velocity is such that $\omega_s \cong \omega$ and then the actual vortex shedding frequency is very close to the forcing frequency, i.e.,

$$\omega_v \cong \omega \tag{1.1.5}$$

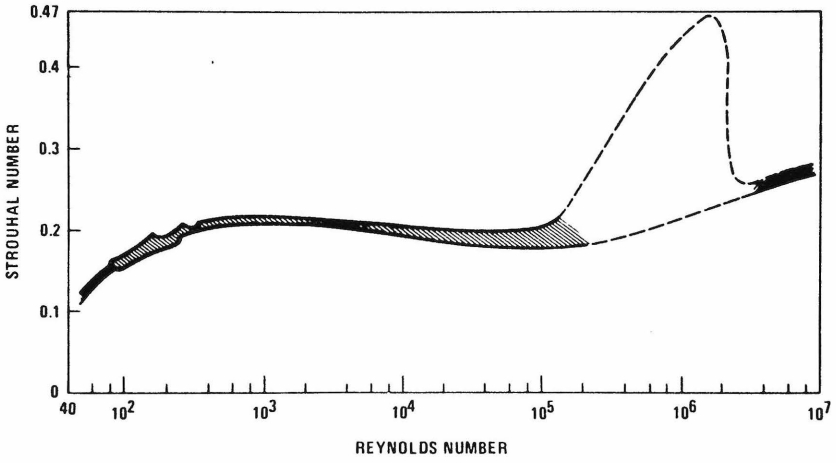

Fig. 1.1.3
Strouhal Number versus Reynolds Number [5]

1.2. SCOPE OF THIS INVESTIGATION

Reported herein is research done to develop an analytical-empirical model for the response of elastically mounted cylinders subjected to vortex shedding. Assuming spanwise constant flow velocity, in the sub-critical range of Reynolds number (i.e., S = 0.20) and using only experimental data obtained from experiments with forced cylinders in water, a new approach in the development of the model is followed. The resultant model's capability for predicting structural response for a wide range of fluid mediums is illustrated through comparison between model predictions and experimental results from flexibly mounted cylinders in air and water. Although comparison between experimental results obtained in air with those obtained in water has been current practice for many years, doubts concerning the appropriateness of such practice are raised. The model developed is expected to yield better results for structures in water, by virtue of being based only on experimental results obtained in water.

CHAPTER II

DISCUSSION OF PREVIOUS WORK

2.1 A BRIEF HISTORICAL REVIEW

Even though Aeolian tones emitted by taut wires in the wind were known in ancient time, it was only in 1878 that the first systematic study on vortex-shedding [73] was published. Experimenting with a variety of pipes and rods, Strouhal [73] derived the expression (Eq. (1.1.2)) for the vortex-shedding frequency and determined constant S was equal to 0.185. Further experimenting with wires, Strouhal came across more complex problems, such as frequency entrainment[1] and modal interaction. But it was Lord Rayleigh [57] in 1879, who discovered that vortex shedding oscillations occur primarily in a plane perpendicular to the flow velocity. von Kármán, in 1912 published his theoretical work [77] on vortex-street stability which motivated many subsequent works. Until the early 1940's, however, most of the experimental and theoretical studies were confined to wakes of fixed cylinders and development of curves such as drag coefficient versus Reynolds number and Strouhal number versus Reynolds number. Then, the first observations on wakes of vibrating cylinders [41] were published and subsequent experimental [2, 8, 9, 11, 12, 14, 15, 33, 36, 39, 40, 47, 49-51, 53, 55, 56, 60-62, 74-76], theoretical [1, 3, 4, 17-20, 22, 23,

---

[1] It is clear that Strouhal [73] did not understand the frequency entrainment phenomenon as it is understood today. However, he noted that when the "friction sound" frequency (i.e., Strouhal frequency) was equal to the natural frequency of one of the wires, the sound produced was greatly increased.

28-32, 34, 42, 45, 59, 62, 65-67, 69] and theoretical-experimental [16, 37, 54, 58, 70] studies became broader in scope. They ranged from studies with fixed cylinders in uniform and sheared flow to studies with prototype-size cables in almost uniform flow. The extreme complexity of the problem not only precludes solutions based on first principles but has also restricted the range of application of approximate theories and models.

This subject still generates very much interest not only academically but also in practice where engineers are faced with problems caused by vortex induced vibrations [13].

2.2 EXPERIMENTAL INVESTIGATIONS

By virtue of being relatively more complete, particular interest is given, herein, to the experimental observations obtained by Sarpkaya [61, 62] and by Feng [9]. The former, on the forces acting on harmonically forced cylinders in uniform aqueous flow, will serve as the basis for development of the present model. The latter, on the response of flexibly mounted cylinders in a uniform flow of air, will be used to gauge the predictions produced by the model.

2.2.1 Forced Cylinders

Sarpkaya [61, 62] measured the forces acting on a rigid cylinder forced to vibrate transverse to a uniform flow, as pictured in Fig. 2.2.1. The cylinder was forced to displace harmonically with a displacement given by

$$Y = A \sin \omega t \qquad (2.2.1)$$

with prescribed amplitude A and frequency ω. The component of the force in the frequency of excitation acting on the cylinder was measured as a function of time. Since this force closely resembles a sinusoidal wave, Sarpkaya chose to decompose it into two orthogonal Fourier components defined by

$$F(t) \equiv \frac{1}{2} \rho D V^2 [C_{mh} \sin \omega t - C_{dh} \cos \omega t] \qquad (2.2.2)$$

or alternatively

$$F(t) \equiv \frac{1}{2} \rho D V^2 \left[C_{ml} \frac{2\pi^3 A}{V_r^2 D} \sin \omega t - C_{dl} \frac{32\pi A^2}{3V_r^2 D^2} \cos \omega t\right] \qquad (2.2.3)$$

where the reduced velocity V_r is defined as

$$V_r \equiv \frac{1}{S \frac{\omega}{\omega_s}} \qquad (2.2.4)$$

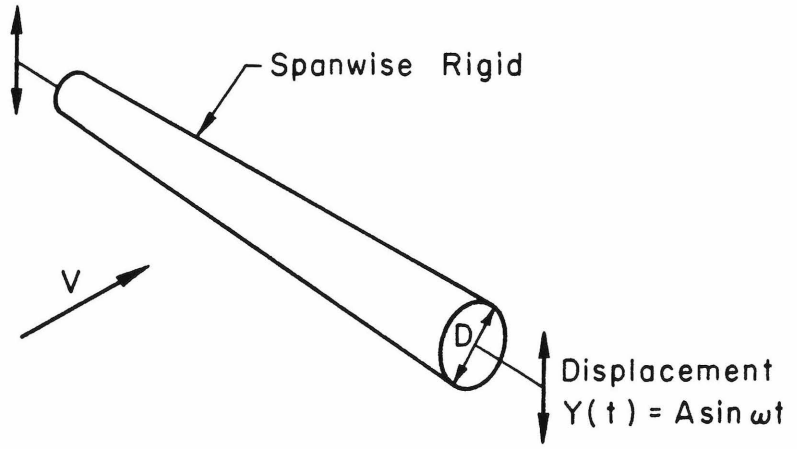

Fig. 2.2.1
Forced Cylinder

The inertia coefficients C_{mh} and C_{ml} and drag coefficients C_{dh} and C_{dl} as presented in [62] are herein reproduced as Figs. 2.2.2 and 2.2.3.

Also reproduced in Fig. 2.2.4 is a comparison between the time trace of F(t) given by Eq. (2.2.2) and its experimentally measured counterpart. It is noted that this relatively good agreement was attained only when the cylinder was vibrating under lock-in conditions, i.e., when the vortex shedding frequency ω_v is very close to the frequency ω at which the cylinder is forced to vibrate (i.e., $\omega_v \cong \omega$). However outside the lock-in range, vortices are shed at the Strouhal frequency ω_s while the cylinder is forced at a frequency ω, (i.e., $\omega_v = \omega_s \neq \omega$). Thus a frequency-content analysis of the measured F(t) will show energy concentration around the forcing frequency ω and around the Strouhal frequency ω_s [33, 70, 71]. This implies that the actual experimental time trace of F(t), outside the lock-in range would show a beating-like characteristic, [61, 70, 71] which cannot be accounted for by Eq. (2.2.2). It is important that this limitation be recognized and if possible taken into account in any formulation that uses Eq. (2.2.2) to model the force acting on a cylinder vibrating in a cross flow.

2.2.2 Flexibly Mounted Cylinders

Placing a flexibly mounted cylinder, as shown in Fig. 2.2.5, in a wind tunnel, Feng [9] measured the cylinder amplitude and frequency response as a function of the flow velocity. Sample experimental results for two different values of structural damping are reproduced in Figs. 2.2.6 and 2.2.7, where the natural frequency of the cylinder is defined as

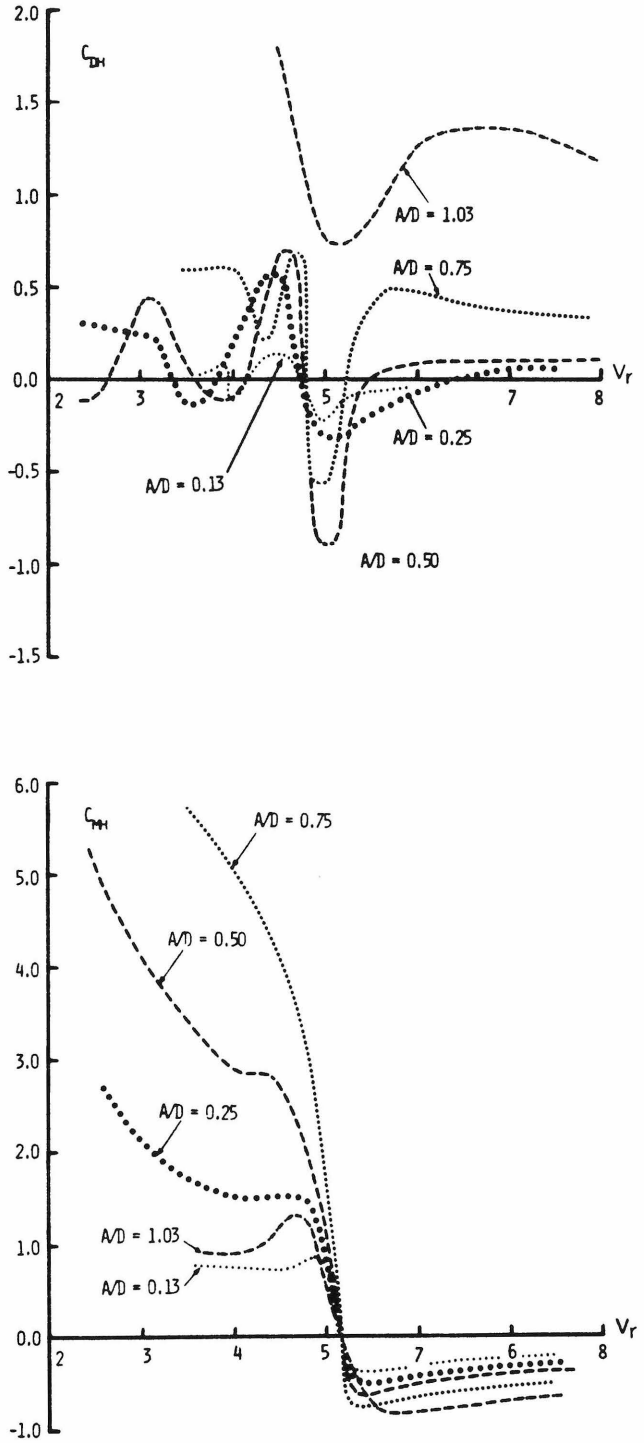

Fig. 2.2.2

Inertia Coefficients C_{mh} and Drag Coefficients C_{dh} versus Reduced Velocity for Various Values of Normalized Amplitude [62]

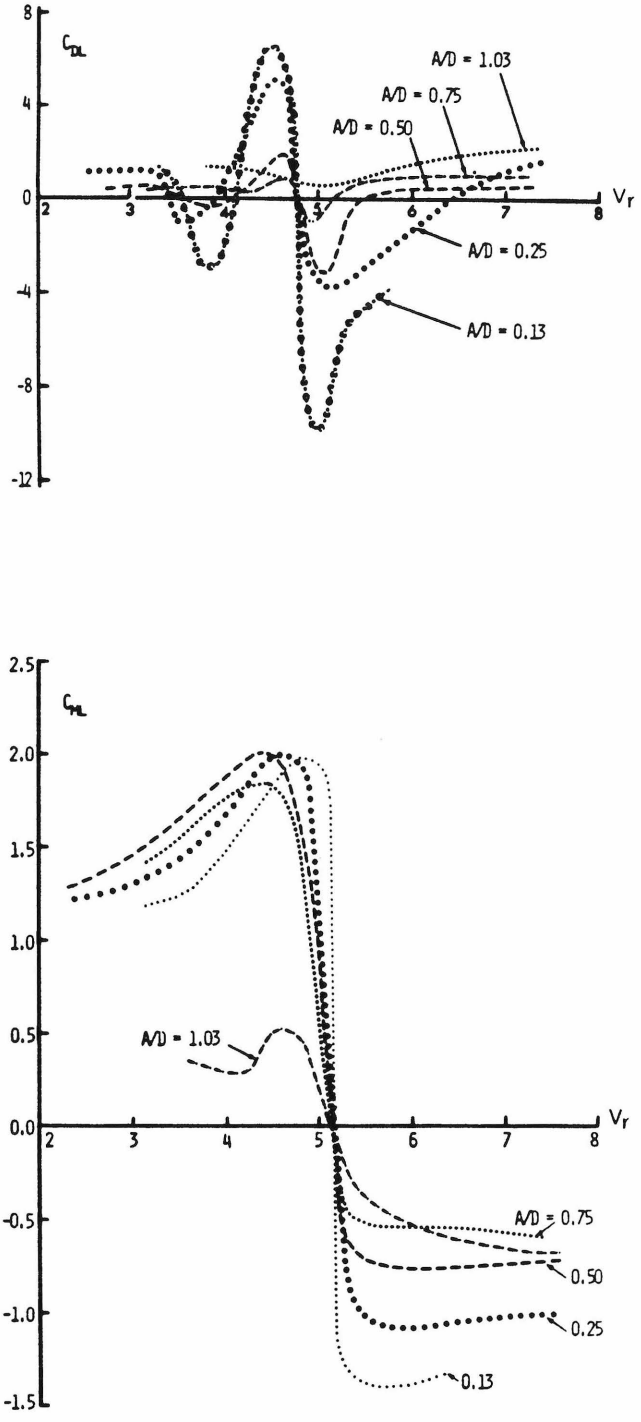

Fig. 2.2.3

Inertia Coefficients C_{ml} and Drag Coefficients C_{dl} versus Reduced Velocity for Various Values of Normalized Amplitude [62]

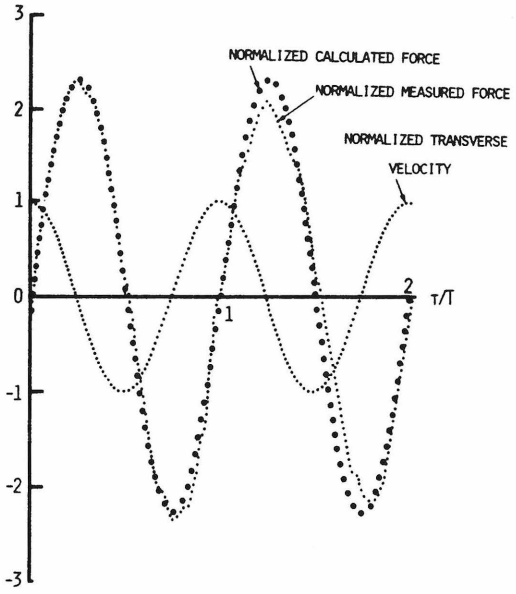

Fig. 2.2.4
Comparison of Measured and Calculated Transverse Force, F(t) [62]

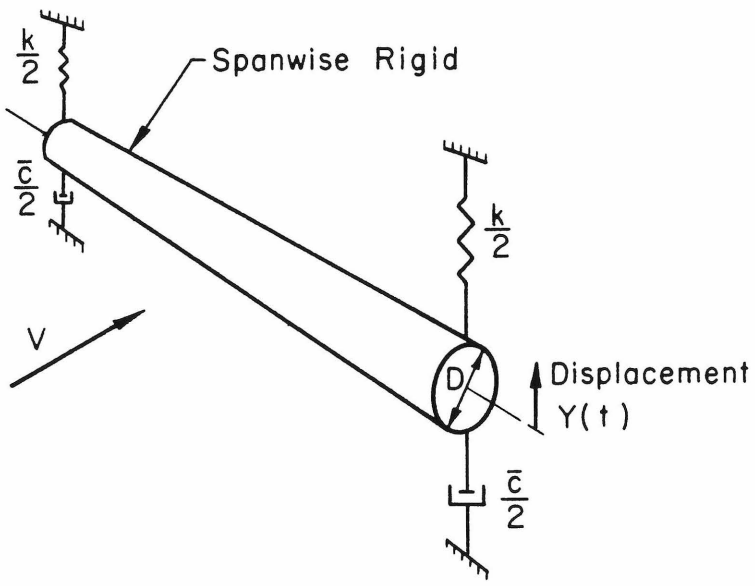

Fig. 2.2.5
Flexibly Mounted Cylinder

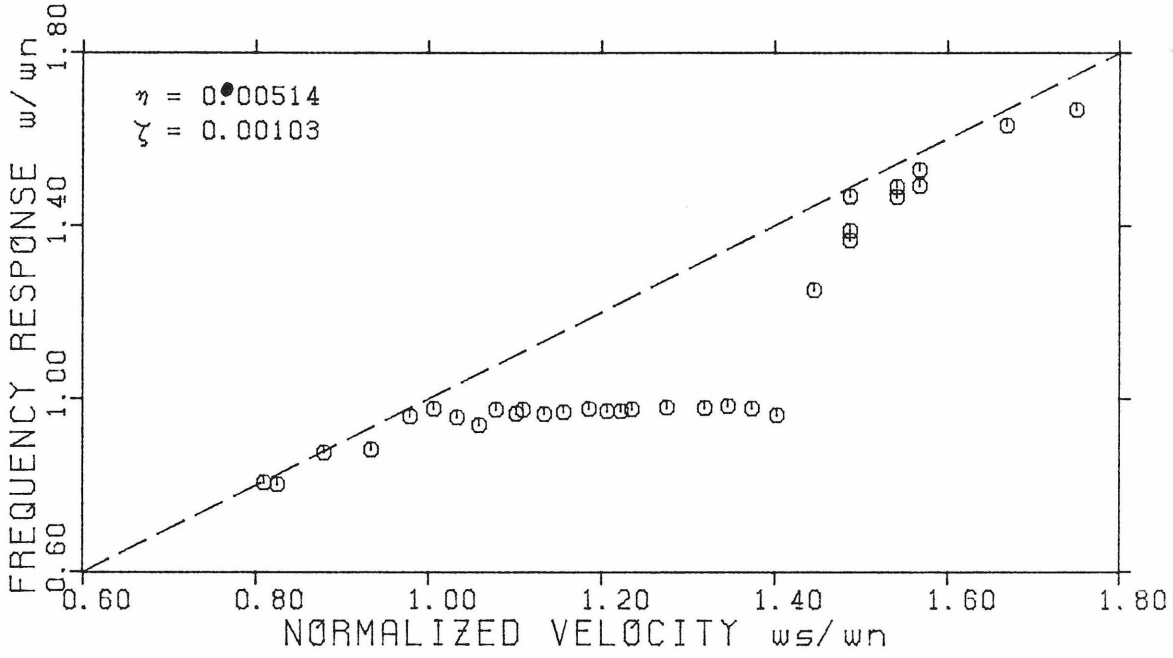

Fig. 2.2.6a

Experimental Frequency Response [9]

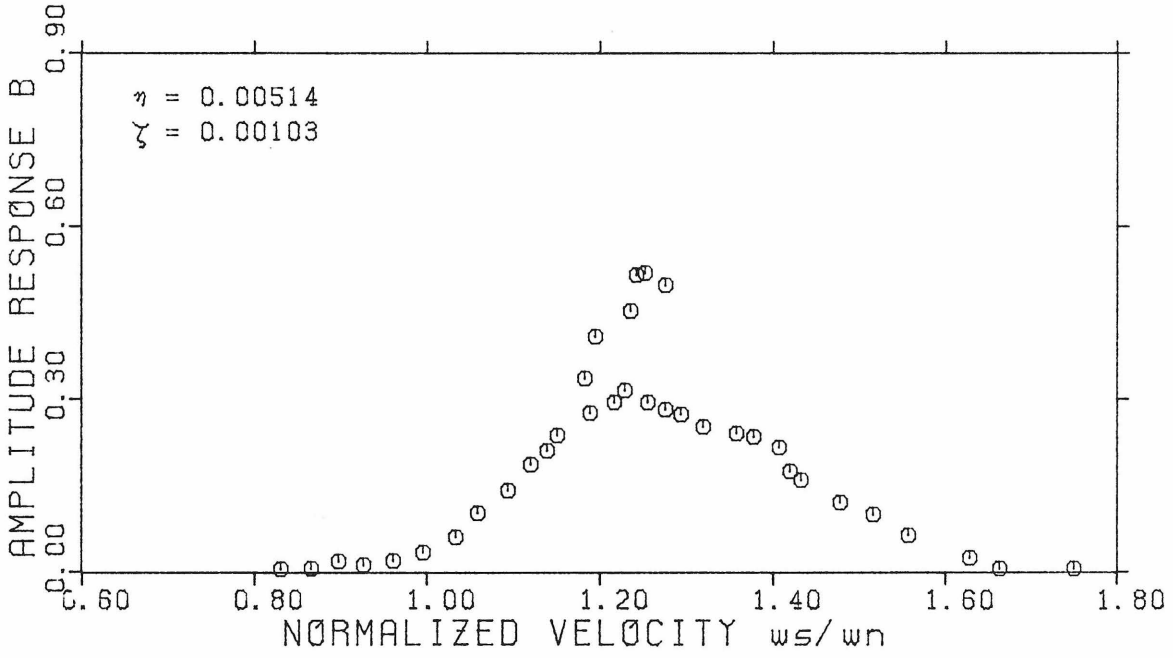

Fig. 2.2.6b

Experimental Amplitude Response [9]

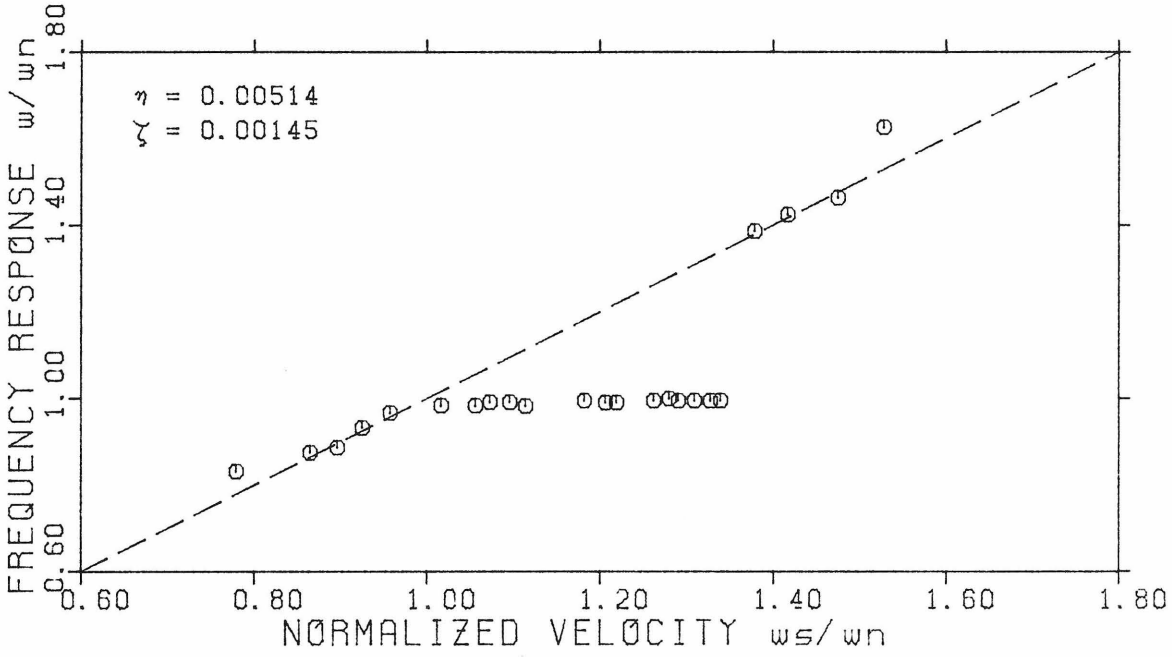

Fig. 2.2.7a

Experimental Frequency Response [9]

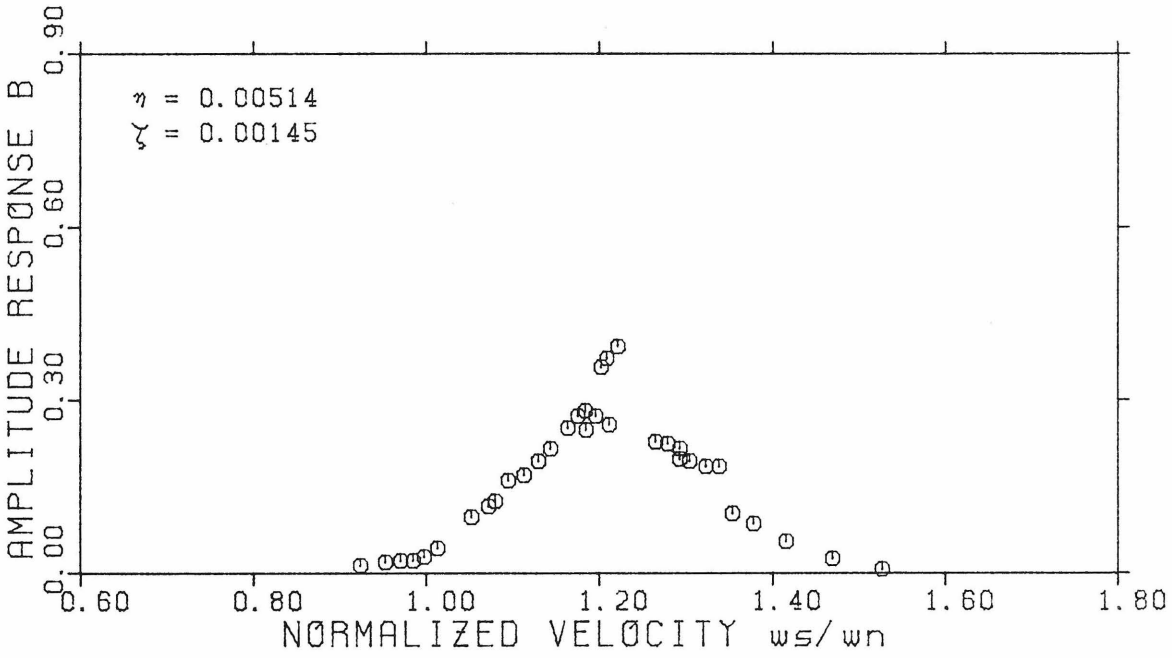

Fig. 2.2.7b

Experimental Amplitude Response [9]

$$\omega_n \equiv \sqrt{\frac{k}{m}} \tag{2.2.5}$$

and the fraction of critical damping is given by

$$\zeta \equiv \frac{\bar{c}}{2\sqrt{km}} \tag{2.2.6}$$

where m, $\bar{c}$, and k are the structural mass, damping and stiffness, per unit length, respectively. The mass ratio is defined as

$$\eta \equiv \frac{\rho D^2}{m} \tag{2.2.7}$$

where ρ is the fluid density. Thus, the mass ratio is proportional to the ratio of the fluid mass dislocated by the cylinder and the mass of the cylinder.

In Figs. 2.2.6 and 2.2.7, the response is plotted as a function of the normalized velocity V_n defined as

$$V_n \equiv \frac{\omega_s}{\omega_n} \equiv \frac{2\pi S \frac{V}{D}}{\omega_n} \tag{2.2.8}$$

where S = 0.20 has been assumed. The normalized amplitude B is given by

$$B \equiv \frac{1/2 \text{ (peak to peak displacement)}}{D} \tag{2.2.9}$$

The frequency of response ω is normalized by ω_n. Also plotted, is a reference dashed line $\omega/\omega_n \equiv \omega_s/\omega_n$ on which will lie all points corresponding to a non-locked-in response. On the other hand, points corresponding to a locked-in response will lie on the horizontal line $\omega/\omega_n = 1$ within a region where $\omega \cong \omega_n$ defined as the lock-in bandwidth.

2.3 ANALYTICAL MODELING

2.3.1 Introduction

Theoretical studies have, in general, lagged behind their more numerous experimental counterparts by several years. Theoretical modeling of wakes behind fixed cylinders began in 1912 [77]. It was only in 1964, however, that Bishop and Hassan [2] suggested, based on experimental observations, that the wake behind a vibrating cylinder behaved very much like a nonlinear self excited oscillator. Many analytical models stemmed from this suggestion. Hartlen and Currie [28] proposed a Lift-Oscillator Model using a Van der Pol equation to model the fluid behavior. Iwan and Blevins [30] proposed a similar model, the Wake Oscillator Model, in which the Van der Pol equation is tentatively derived from the gross fluid behavior. Both formulations have been further pursued [29, 31, 65, 66, 67][1] with results that can, in general, be considered good.

In the remainder of this section, the Wake Oscillator Model is used to predict the forces acting on forced cylinders. These forces are herein, presented in terms of the inertia coefficient C_{mh} and the drag coefficient C_{dh}, and will be used in later sections as an aid, not only to understand the experimental data, but also to interpret some of the results obtained by the present model.

---

[1] For other analytical formulations, see papers [48] and [64] where several formulations are reviewed.

2.3.2 The Wake Oscillator Model

Based on other assumptions besides the fluid momentum equation, Hall [29] arrived at the following Van der Pol type equation for the fluid oscillator

$$a_0\rho D^2 \frac{d^2Z}{dt^2} - a_1\rho DV\frac{dZ}{dt} + a_2\rho\frac{D}{V}\left(\frac{dZ}{dt}\right)^3 + a_6\rho V^2 Z = -F_{int}(t) \qquad (2.3.1)$$

$$F_{int}(t) = a_3\rho D^2\left(\frac{d^2Z}{dt^2} - \frac{d^2Y}{dt^2}\right) + a_4\rho DV\left(\frac{dZ}{dt} - \frac{dY}{dt}\right) + a_5\rho D^2\frac{d^2Z}{dt^2} \qquad (2.3.2)$$

It is noted that by setting $a_5 = 0$, Eqs. (2.3.1) and (2.3.2) reduce to the expressions derived by Blevins [3]. The constants a_0 to a_6 are model constants, determined by the fitting of experimental data. Y is the cylinder displacement and Z is a fluid oscillator variable defined such that its first derivative with respect to time is "the average vertical fluid velocity in a unit depth of a control volume surrounding the cylinder", [29].

The cylinder displacement, the fluid oscillator variable and time are normalized as follows

$$y \equiv \frac{Y}{D} \quad ; \quad z \equiv \frac{Z}{D} \qquad (2.3.3)$$

$$\tau = \omega_s t \qquad (2.3.4)$$

$$\frac{d}{dt} \equiv \omega_s \frac{d}{d\tau} \equiv \omega_s (\quad)' \qquad (2.3.5)$$

then, substituting into Eqs. (2.3.1) and (2.3.2), yields

$$a_0 \rho D^3 \omega_s^2 \, z'' - a_1 \rho D^2 V \omega_s \, z' + a_2 \frac{\rho D^4 \omega_s^3}{V} (z')^3 + a_6 \rho D V^2 \, z = F_{int}(\tau) \tag{2.3.6}$$

and

$$F_{int}(\tau) = a_3 \rho D^3 \omega_s^2 \, (z'' - y'') + a_4 \rho D^2 \rho V \omega_s \, (z' - y') + a_5 \rho D^3 \omega_s^2 \, z'' \tag{2.3.7}$$

Dividing by $\frac{1}{2} \rho D V^2$, the above expression can be written as

$$a_0 (2\pi S)^2 \, z'' - a_1 2(2\pi S) \, z' + a_2 2(2\pi S)^3 \, (z')^3 + a_6 2z = \frac{F_{int}(\tau)}{1/2 \rho D V^2} \tag{2.3.8}$$

and

$$\frac{F_{int}(\tau)}{1/2 \rho D V^2} = a_3 2(2\pi S)^2 \, (z'' - y'') + a_4 2(2\pi S)(z' - y') + a_5 2(2\pi S)^2 \, z'' \tag{2.3.9}$$

Substituting Eq. (2.3.9) into Eq. (2.3.8) and rearranging, yields

$$z'' - \frac{1}{(2\pi S)} \frac{a_1 - a_4}{e_1} z' + 2\pi S \frac{a_2}{e_1} (z')^3 + \frac{a_6}{e_1} \frac{1}{(2\pi S)^2} z = \frac{1}{(2\pi S)} \frac{a_4}{e_1} y' + \frac{a_3}{e_1} y'' \tag{2.3.10}$$

where

$$e_1 = a_0 + a_3 + a_5 \tag{2.3.11}$$

To reproduce conditions similar to those in Sarpkaya's experiment, a cylinder is assumed to be harmonically driven with a motion

$$y = B \sin \frac{\omega}{\omega_s} \tau \tag{2.3.12}$$

Eq. (2.3.10) can then be solved for z and the normalized interaction force determined through Eq. (2.3.9)

Based upon several different data sets obtained from experiments performed in air and in water, Blevins [3] arrived at the following values for the model constants

$$a_0 = 0.48 \qquad a_2 = 0.20 \qquad a_4 = 0.38 \qquad a_6 = e_1(2\pi S)^2$$
$$a_1 = 0.44 \qquad a_3 = 0 \qquad a_5 = 0^{1} \qquad (2.3.13)$$

The resultant predicted inertia coefficient C_{mh} and drag coefficient C_{dh} are presented in Fig. 2.3.1, for $4.0 < V_r < 7.0$. The amplitude and frequency responses of a rigid flexibly mounted cylinder obtained using model constants (2.3.13) are shown in Fig. 2.3.2, so to enable future comparisons.

Whereas Hall [29] used several different data sets obtained from experiments performed only in air to determine model constants with the following values

$$a_0 = 0.4611 \qquad a_2 = 0.0558 \qquad a_4 = 0.2413 \qquad a_6 = e_1 (2\pi S)^2$$
$$a_1 = 0.2824 \qquad a_3 = -0.3000 \qquad a_5 = 0.0985 \qquad (2.3.14)$$

and again, the predicted inertia coefficient C_{mh} and drag coefficient C_{dh} are plotted in Fig. 2.3.3, for $4.8 < V_r < 7.8$. Plotted in Fig. 2.3.4 are the amplitude and frequency response of the same rigid flexibly mounted cylinder using model constants given in (2.3.14).

---

[1] As previously explained, setting $a_5 = 0$, reduces Eq. (2.3.9) and (2.3.10) to those originally derived by Blevins [3].

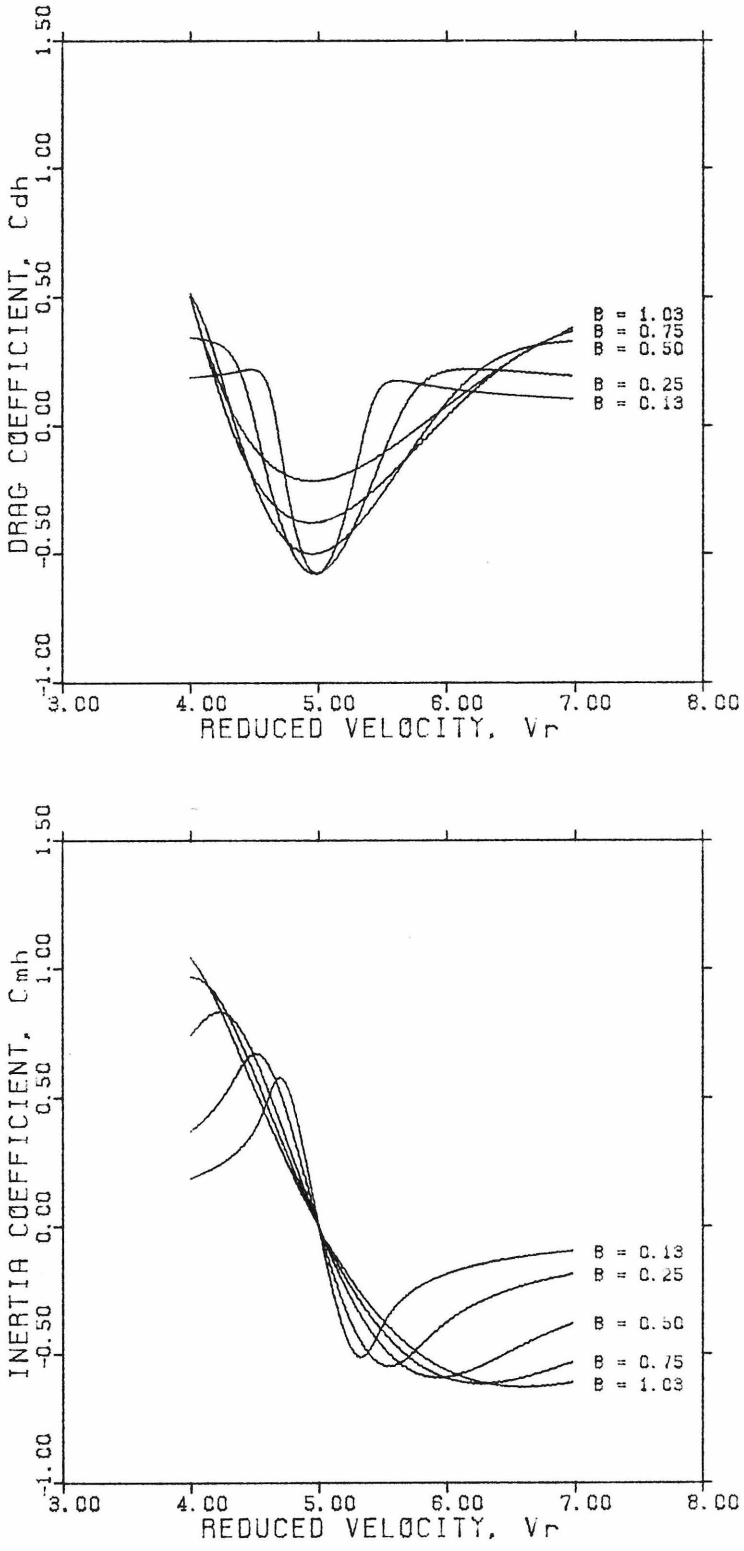

Fig. 2.3.1

Inertia Coefficient C_{mh} and Drag Coefficient C_{dh} Versus Reduced Velocity Obtained through the Wake Oscillator Model using set of Constants (2.3.13)

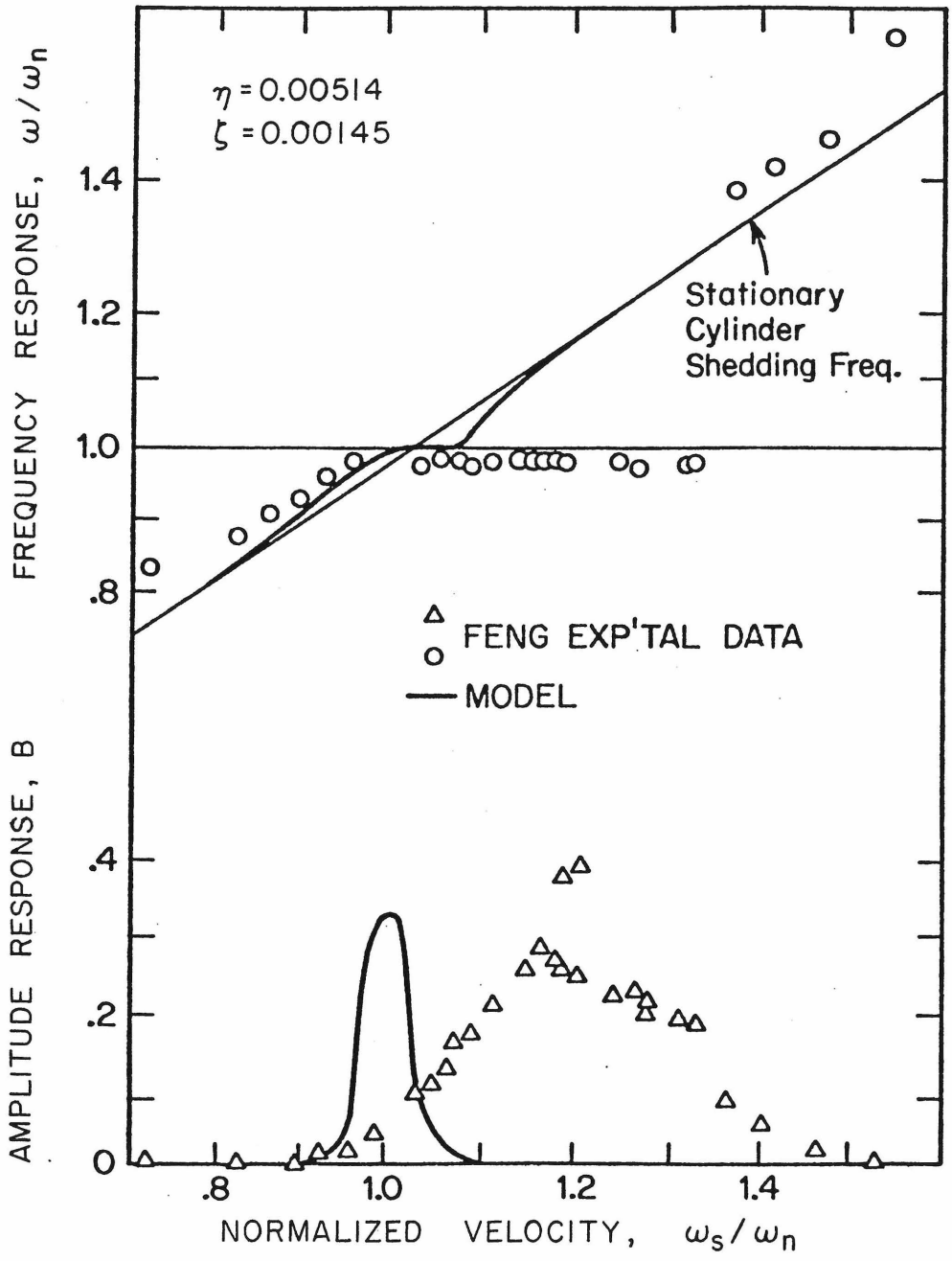

Fig. 2.3.2

Wake Oscillator Model Response using

Set of Constants (2.3.13), [3]

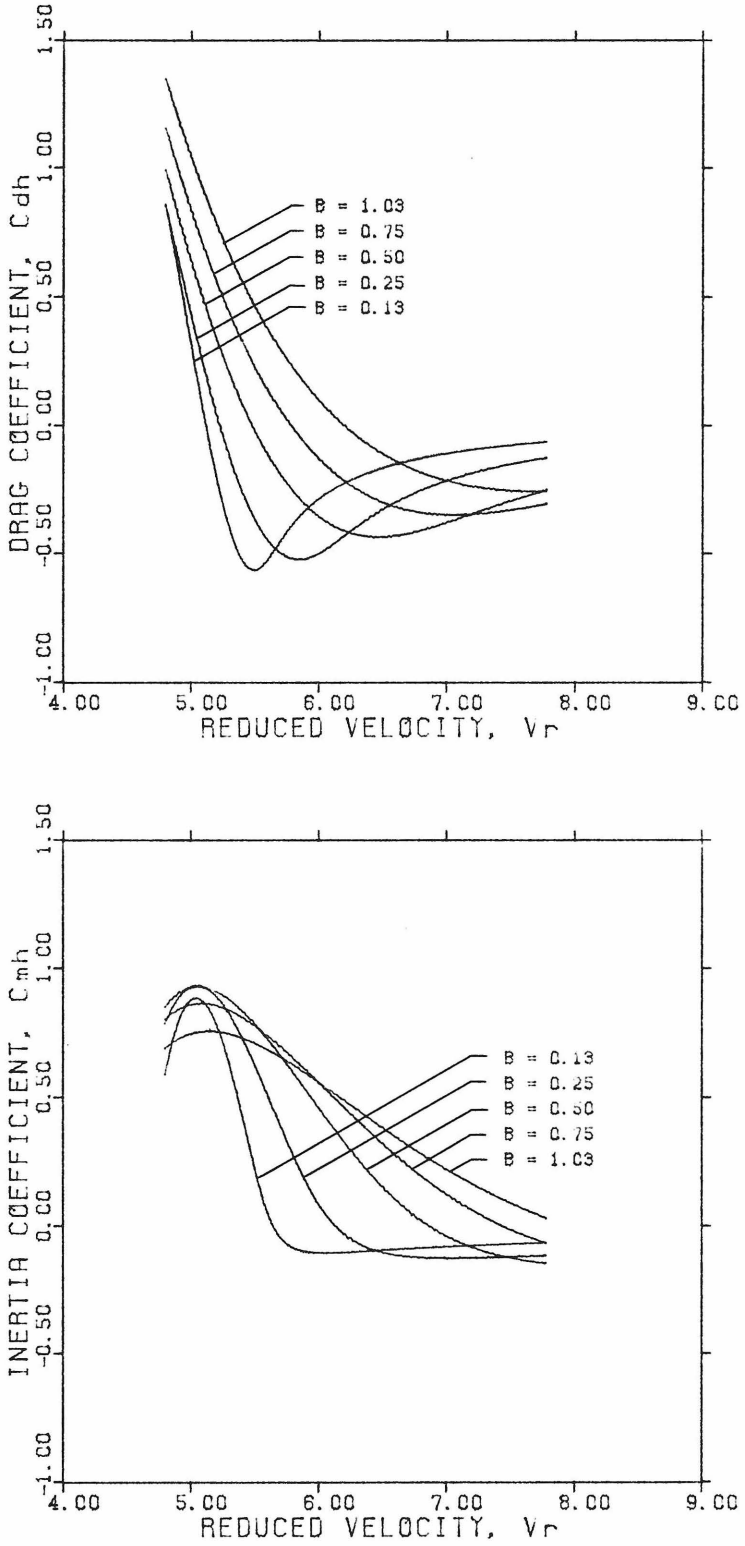

Fig. 2.3.3

Inertia Coefficient C_{mh} and Drag Coefficient C_{dh} Versus Reduced Velocity Obtained Through the Wake Oscillator Model using set of Constants (2.3.15)

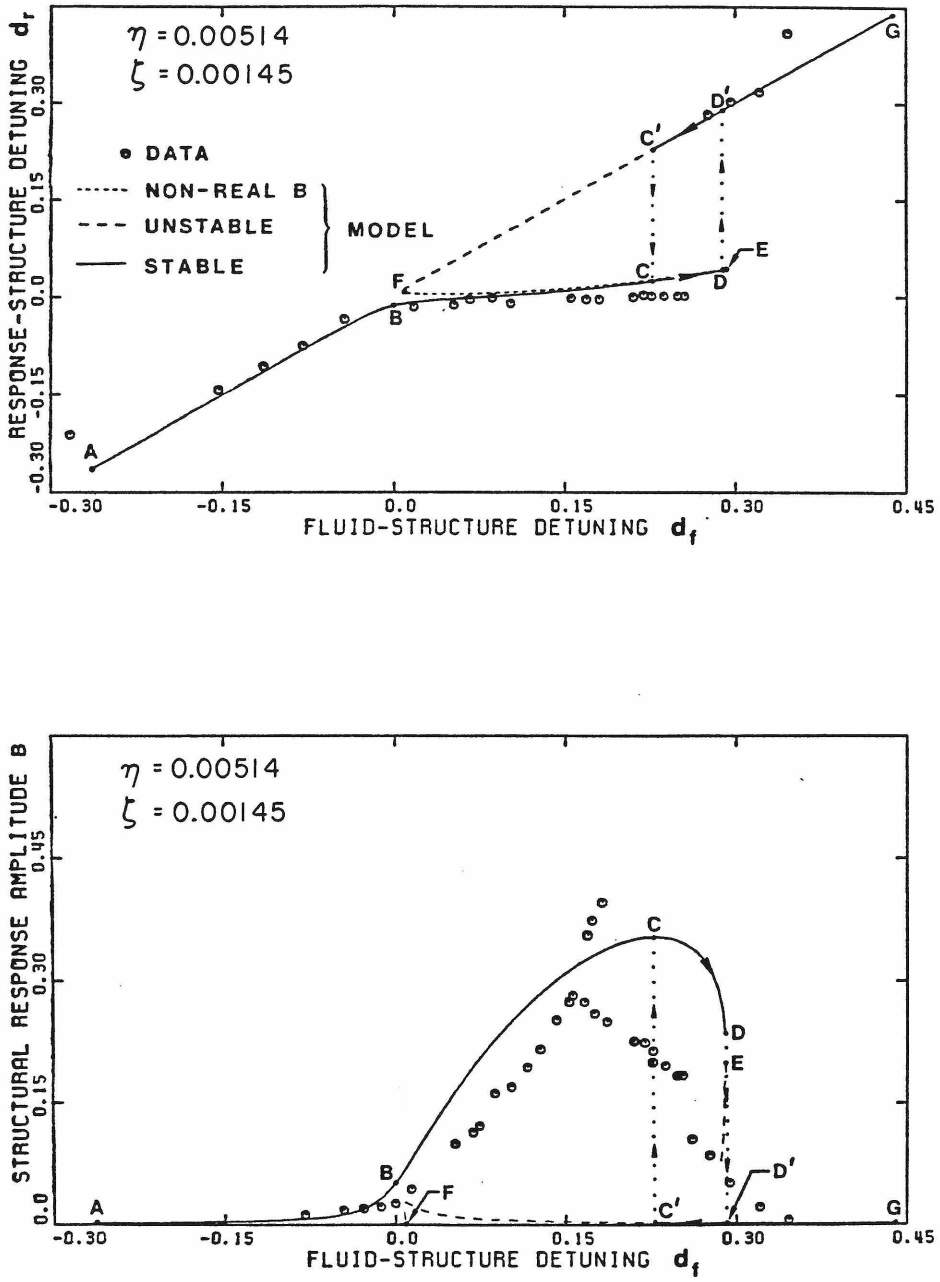

Fig. 2.3.4

Wake Oscillator Response Using set of Constants (2.3.14) [29]

CHAPTER III

AN ANALYTICAL-EMPIRICAL MODEL

3.1 INTRODUCTION

The merit of any approximate model resides basically in its ability to predict structural response, amplitude and frequency, as a function of the structural system and flow parameters. As a by product of the modeling process it is hoped that one may be able to better understand some aspects of the intricate phenomenon of fluid-structure interaction. However, a total understanding of this phenomenon will only be possible through a formulation based on first principles. Given the present knowledge, this still appears to be far away.

In view of this situation, approximate models, for either the structural response or the fluid response, and ideally involving both responses, are and will be of interest and value for some time to come. Models based on the Van der Pol equation for the modeling of the fluid behavior [3, 28, 29, 66], have been and still are useful, but like any other approximate model have their drawbacks and shortcomings. Some of the most important shortcomings are:

1) the model constants are not directly measurable quantities. Rather, other parameters, functions of these constants, are evaluated through the solution of a system of differential equations;
2) the data used to calibrate the models are generally taken from several different experiments which may not be directly comparable;

3) the models rely heavily for calibration on experiments performed in air but are applied without adjustment to water. Since the model constants, by virtue of approximations involved in the solution of the system of differential equations, make use of the nature of the fluid considered, strictly speaking there should be a reassessment of the model whenever a new fluid is introduced;

4) the extension of Van der Pol oscillator type models to other situations of interest, such as spanwise variable flow and infinite cables has proven extremely difficult, if not impossible.

Motivated by these drawbacks, an alternate approach to the modeling of vortex-induced oscillation of structures has been developed, based on measurements of forced cylinders in uniform flow. As in previous formulations [3, 28, 29, 66], it is not intended to solve the fluid-structure interaction problem precisely, but rather to give another tool for dealing with this class of problem. The proposed empirical model makes use only of "forced cylinder" data to predict behavior of flexibly mounted structures. This approach was suggested quite a few years ago [15], but never fully exploited.

It is hoped that the proposed model will provide another step towards the understanding of an important physical phenomenon.

3.2 STEADY-STATE RESPONSE FORMULATION

Based upon experimental results, as the ones discussed in Chapter II, one may conclude that the phenomenon of flow-induced vibrations of cylinders can be separated into two distinct categories:

1) A locked-in oscillation with the following characteristics:
   a) there is vortex shedding frequency entrainment. The vortex shedding frequency is captured by the frequency of oscillation of the mechanical system;
   b) the amplitude of vibration of the mechanical system is large;
   c) the frequency of vibration of the mechanical system is close to its own natural frequency though unknown "a priori".
2) A non-locked-in oscillation with the following characteristics:
   a) there is no vortex shedding frequency entrainment and vortices are shed at the Strouhal frequency;
   b) the amplitude of vibration of the mechanical system is small;
   c) the frequency of vibration of the mechanical system is essentially the Strouhal frequency, i.e., the system responds at the frequency of excitation.

The present model is formulated separately for each of the above categories of response and is based upon experimental data for a forced cylinder in uniform flow, as reported by Sarpkaya [61].

In these particular experiments, a rigid cylinder, placed transverse to the flow, was harmonically driven with a motion

$$Y = A \sin \omega t \tag{3.2.1}$$

The force acting on the cylinder, recorded as a function of time, was decomposed into two orthogonal Fourier components at the frequency of oscillation and is expressed as

$$F(t) = \frac{1}{2} \rho LDV^2 [C_{mh} \sin \omega t - C_{dh} \cos \omega t] \tag{3.2.2}$$

The coefficients C_{mh} and C_{dh} are presented as functions of a normalized amplitude (A/D) and reduced velocity (V_r), where

$$V_r = \frac{1}{S \frac{\omega}{\omega_s}} \tag{3.2.3}$$

3.2.1 The Lock-in Model

Consider the rigid flexibly mounted cylinder of Fig. 2.2.4. It is important to note, if experimental results (such as those of Sarpkaya) are used, that built into those results, there is a definite phase between the displacement and the measured force, for each prescribed amplitude and frequency of vibration. Thus, in solving the induced vibration case, this should be and is accounted for by assuming the force as given in Eq. (3.2.2)[1] and the response as in Eq. (3.2.1).

The problem of induced vibrations is hereby formulated in terms of structural parameters per unit length as

---

[1] Refer to discussion on Sarpkaya's experimental results presented in Chapter II

$$m\frac{d^2Y}{dt^2} + \bar{c}\frac{dY}{dt} + kY = \frac{1}{2}\rho DV^2[C_{mh}\sin\omega t - C_{dh}\cos\omega t] \qquad (3.2.4)$$

with

$$Y = A\sin\omega t \qquad (3.2.5)$$

where the amplitude and frequency of vibration are unknowns.

The time, displacement, amplitude and frequency are normalized as follows

$$y \equiv \frac{Y}{D} \quad ; \quad B \equiv \frac{A}{D} \qquad (3.2.6)$$

$$\Omega \equiv \frac{\omega}{\omega_s} \quad ; \quad \Omega_n \equiv \frac{\omega_n}{\omega_s} \qquad (3.2.7)$$

$$\tau \equiv \omega_s t \qquad (3.2.8)$$

$$\frac{d}{dt} \equiv \omega_s \frac{d}{d\tau} \equiv \omega_s (\quad)' \qquad (3.2.9)$$

then, substituting into Eq. (3.2.4) and (3.2.5) yields

$$y'' + 2\zeta\Omega_n y' + \Omega_n^2 y = \frac{\eta}{2(2\pi S)^2}[C_{mh}\sin\Omega\tau - C_{dh}\cos\Omega\tau] \qquad (3.2.10)$$

where

$$y = B\sin\Omega\tau \qquad (3.2.11)$$

$$C_{mh} = C_{mh}(\Omega, B) \qquad (3.2.12)$$

$$C_{dh} = C_{dh}(\Omega, B) \qquad (3.2.13)$$

ζ is the fraction of critical damping defined in the usual way; Ω_n is

the natural frequency of the system, normalized by the Strouhal frequency

$$\Omega_n = \frac{\omega_n}{\omega_s} = \frac{1}{\omega_s}\sqrt{\frac{k}{m}} \tag{3.2.14}$$

η is a dimensionless fluid-structure mass ratio parameter defined [29] as

$$\eta = \frac{\rho D^2}{m} \tag{3.2.15}$$

and ω_s is the Strouhal frequency as defined by Eq. (1.1.2).

Substituting Eq. (3.2.11) and its derivatives into Eq. (3.2.10) and collecting the $\sin\Omega\tau$ and the $\cos\Omega\tau$ terms, yields

$$(\Omega_n^2 - \Omega^2)B = \frac{\eta}{2(2\pi S)^2} C_{mh}(\Omega,B) \tag{3.2.16}$$

$$2\zeta\Omega_n\Omega B = -\frac{\eta}{2(2\pi S)^2} C_{dh}(\Omega,B) \tag{3.2.17}$$

With respect to the system of Eqs. (3.2.16) and 3.2.17), it is noted that:

1) the equations form a coupled set of nonlinear algebraic equations as opposed to a coupled system of nonlinear differential equations as obtained in the Van der Pol Oscillator formulations [3, 28, 29, 66];
2) a very small ratio η, as well as other approximations are generally required to solve the system of equations in the Van der Pol Oscillator formulations. In the present

formulation, however, no approximations are necessary to implement the solution scheme. Also, for the first time it is possible to vary the mass ratio within a range covering both structures in water and in air, without reassessment of the model;

3) analysis of Eq. (3.2.17) indicates that induced oscillations are restricted to regions where

$$C_{dh}(\Omega,B) \leqslant 0 \qquad (3.2.18)$$

Should the present approach prove worth pursuing hereupon more experimental data will be needed and Eq. (3.2.18) will provide a criterion as to where experimental efforts should be concentrated. In Fig. 2.2.2 the two regions where Eq. (3.2.18) is satisfied are given by $3.3 \lesssim V_r \lesssim 4.3$ and by $V_r \gtrsim 4.8$. This thesis will be concerned with the second region, $V_r \gtrsim 4.8$, where the forces are relatively larger thus yielding greater amplitudes and where almost perfect "synchronization", i.e., $\Omega \cong 1.0$ occurs ;

4) to implement the solution of the system of Eqs. (3.2.16) and (3.2.17), $C_{mh}(\Omega,B)$ and $C_{dh}(\Omega,B)$ must be defined for all points where Eq. (3.2.18) is satisfied. But at this stage, available experimental data are far from sufficient to allow the interpolation of these points by a numerical procedure. Instead, one has to resort to what is done in Section 3.3, i.e., interpolation of these points through an analytical surface.

3.2.2 The Non-Lock-in Model

Assuming the hypotheses presented at the beginning of section 3.2 and by reasoning similar to those for the Lock-in Model, the problem can again be formulated in terms of structural parameters per unit length, as follows

$$m \frac{d^2Y}{dt^2} + \bar{c} \frac{dY}{dt} + kY = \frac{1}{2} \rho D V^2 [C_{mh} \sin \omega_s t - C_{dh} \cos \omega_s t] \qquad (3.2.19)$$

with

$$Y = A \sin (\omega_s t - \emptyset) \qquad (3.2.20)$$

where amplitude and phase of vibration are unknowns. Using Eq. (3.2.6) to Eq. (3.2.9) gives

$$y'' + 2\zeta \Omega_n y' + \Omega_n^2 y = \frac{\eta}{2(2\pi S)^2} [C_{mh} \sin\tau - C_{dh} \cos\tau) \qquad (3.2.21)$$

$$y = B \sin (\tau - \emptyset) \qquad (3.2.22)$$

$$C_{mh} = C_{mh}(\Omega=1, B) \qquad (3.2.23)$$

$$C_{dh} = C_{dh}(\Omega=1, B) \qquad (3.2.24)$$

It is important to note, that although assuming that the oscillator will respond at the Strouhal frequency ω_s, the problem is still non-linear because of the nonlinearity of the forcing function.

The non-lock-in problem is substantially simpler than the lock-in problem. One is required to solve only one nonlinear algebraic equation under non-locked-in conditions, as opposed to a coupled system of

nonlinear algebraic equations under the locked-in condition.

Substituting Eq. (3.2.22) and its derivatives into Eq. (3.2.21) a solving for B and $\emptyset$ yields

$$B = \frac{\eta}{2(2\pi S)^2} \frac{(C_{mh}^2 + C_{dh}^2)^{1/2}}{[(\Omega_n^2 - 1)^2 + (2\zeta\Omega_n)^2]^{1/2}} \tag{3.2.25}$$

$$\sin\emptyset = \frac{(\Omega_n^2 - 1)\, C_{dh} + (2\zeta\Omega_n)C_{mh}}{(C_{mh}^2 + C_{dh}^2)^{1/2}\, [(\Omega_n^2 - 1)^2 + (2\zeta\Omega_n)^2]^{1/2}} \tag{3.2.26}$$

$$\cos\emptyset = \frac{(\Omega_n^2 - 1)\, C_{mh} - (2\zeta\Omega_n)C_{dh}}{(C_{mh}^2 + C_{dh}^2)^{1/2}\, [(\Omega_n^2 - 1)^2 + (2\zeta\Omega_n)^2]^{1/2}} \tag{3.2.27}$$

Solution is implemented by first solving Eq. (3.2.25) for B, and then solving Eq. (3.2.26) and (3.2.27) for $\emptyset$.

3.3. STABILITY ANALYSIS OF STEADY-STATE RESPONSE

Multiple solutions are anticipated due to the nonlinear nature of the present problem [9], so the determination of stability of each solution becomes essential.

Application of asymptotic methods are rigorously justified for certain nonlinear systems which, however, do not include the proposed system. Still, the Method of Slowly Varying Parameters[1], developed by Krylov and Bogoliubov [38], and by Bogoliubov and Mitropolsky [7], does

---

[1] Also known as Method of Averaging or Krylov-Bogoluibov-Mitropolsky (KBM) Method.

lend itself to the perturbation approach used in carrying out the aforementioned analyses. The Method of Slowly Varying Parameters, when applied to the equation of motion of a single degree of freedom oscillator yields a pair of first order ordinary differential equations given in terms of precisely the same variables used in section 3.2, that is, the amplitude and frequency of the system. This analogy primarily motivates the perturbation analysis done herein.

3.3.1 The Lock-in Model

From Eq. (3.2.10), the equation governing the locked-in response is

$$y'' + 2\zeta\Omega_n y' + \Omega_n^2 y = \frac{\eta}{2(2\pi S)^2}[C_{mh}(\Omega,B)\ \sin\Omega\tau - C_{dh}(\Omega,B)\ \cos\Omega\tau]$$

Assume

$$y = B(\tau)\ \sin\Omega(\tau)\tau \tag{3.3.2}$$

where the amplitude B and frequency Ω are slowly varying functions of the normalized time. Differentiating Eq. (3.3.2) once, with respect to the time τ yields

$$y' = B\Omega\ \cos\Omega\tau + B'\ \sin\Omega\tau + B\Omega'\tau\ \cos\Omega\tau \tag{3.3.3}$$

By analogy to the Method of Slowly Varying Parameters, let it be further assumed that

$$y' = B\Omega\ \cos\Omega\tau \tag{3.3.4}$$

then from Eq. (3.3.3) it is clear that

$$B'\ \sin\Omega\tau + B\Omega'\tau\ \cos\Omega\tau = 0 \tag{3.3.5}$$

Differentiating Eq. (3.3.4), with respect to the normalized time gives

$$y'' = -B\Omega^2 \sin\Omega\tau - B\Omega\Omega'\tau \sin\Omega\tau + B'\Omega \cos\Omega\tau + B\Omega' \cos\Omega\tau \quad (3.3.6)$$

Substituting Eqs. (3.3.2), (3.3.4) and (3.3.6) into Eq. (3.3.1) then yields

$$(\Omega_n^2 - \Omega^2)B \sin\Omega\tau - B\Omega\Omega'\tau \sin\Omega\tau + B'\Omega \cos\Omega\tau + B\Omega' \cos\Omega\tau +$$

$$+ 2\zeta\Omega_n\Omega B \cos\Omega\tau = \frac{\eta}{2(2\pi S)^2} (C_{mh} \sin\Omega\tau - C_{dh} \cos\Omega\tau) \quad (3.3.7)$$

Equation (3.3.5) together with Eq. (3.3.7) form a coupled system of first order ordinary differential equations that replaces Eq. (3.3.1), a single second order ordinary differential equation. By first, multiplying Eq. (3.3.5) by $\cos\Omega\tau$, Eq. (3.3.7) by $\sin\Omega\tau$ and subtracting term by term; and then multiplying Eq. (3.3.7) by $\cos\Omega\tau$, Eq. (3.3.5) by $\sin\Omega\tau$ and adding term by term, the following set of equations results

$$(\Omega_n^2 - \Omega^2)B \sin^2\Omega\tau - B\Omega\Omega'\tau + (\Omega' + 2\zeta\Omega_n\Omega)B \sin\Omega\tau \cos\Omega\tau =$$

$$= \frac{\eta}{2(2\pi S)^2} (C_{mh} \sin^2\Omega\tau - C_{dh} \sin\Omega\tau \cos\Omega\tau) \quad (3.3.8)$$

and

$$(\Omega_n^2 - \Omega^2)B \sin\Omega\tau \cos\Omega\tau + B'\Omega + (\Omega' + 2\zeta\Omega_n\Omega)B \cos^2\Omega\tau =$$

$$= \frac{\eta}{2(2\pi S)^2} (C_{mh} \sin\Omega\tau \cos\Omega\tau - C_{dh} \cos^2\Omega\tau) \quad (3.3.9)$$

Averaging Eq. (3.3.8) and (3.3.9) over one cycle of oscillation yields

$$\int_0^{2\pi} (\Omega_n^2 - \Omega^2)B \sin^2\Theta \, d\Theta - \int_0^{2\pi} B\Omega'\Theta \, d\Theta + \int_0^{2\pi} (\Omega' + 2\zeta\Omega_n\Omega)B \sin\Theta \cos\Theta \, d\Theta$$

$$= \frac{\eta}{2(2\pi S)^2} \left(\int_0^{2\pi} C_{mh} \sin^2\Theta \, d\Theta - \int_0^{2\pi} C_{dh} \sin\Theta \cos\Theta \, d\Theta \right) \tag{3.3.10}$$

and

$$\int_0^{2\pi} (\Omega_n^2 - \Omega^2)B \sin\Theta \cos\Theta \, d\Theta + \int_0^{2\pi} B'\Omega \, d\Theta + \int_0^{2\pi} (\Omega' + 2\zeta\Omega_n\Omega)B \cos^2\Theta \, d\Theta$$

$$= \frac{\eta}{2(2\pi S)^2} \left(\int_0^{2\pi} C_{mh} \sin\Theta \cos\Theta \, d\Theta - \int_0^{2\pi} C_{dh} \cos^2\Theta \, d\Theta \right) \tag{3.3.11}$$

where

$$\Theta = \Omega\tau \tag{3.3.12}$$

Assuming that B and Ω remain essentially constant over one cycle of oscillation, they can be replaced by their average values over that cycle, which will be approximately B and Ω. Then Eqs. (3.3.10) and (3.3.11) yield

$$(\Omega_n^2 - \Omega^2)B - 2\pi B\Omega' = \frac{\eta}{2(2\pi S)^2} C_{mh}(\Omega, B) \tag{3.3.13}$$

$$2\zeta\Omega_n\Omega B + 2B'\Omega + B\Omega' = -\frac{\eta}{2(2\pi S)^2} C_{dh}(\Omega, B) \tag{3.3.14}$$

Note that under steady-state conditions, that is, $\Omega' = B' = 0$, the system of Eqs. (3.3.13) and (3.3.14) reduces to

$$(\Omega_n^2 - \Omega^2)B = \frac{\eta}{2(2\pi S)^2} C_{mh}(\Omega, B) \tag{3.3.15}$$

$$2\zeta\Omega_n\Omega B = -\frac{\eta}{2(2\pi S)^2}\, C_{dh}(\Omega,B) \tag{3.3.16}$$

which is, as expected, identical to the system of Eqs. (3.2.16) and (3.2.17) derived directly for the steady state response in section 3.2. The system of Eqs. (3.2.13) and (3.2.14), by virtue of being more complete allows for the analysis of stability of these solutions, which is undertaken as follows.

Let the steady state solution be denoted by

$$y_{ss} = B_{ss}\, \sin\Omega_{ss}\tau \tag{3.3.17}$$

Then, consider a perturbation to this solution of the following form

$$B(\tau) = B_{ss} + \xi(\tau) \tag{3.3.18}$$

$$\Omega(\tau) = \Omega_{ss} + \alpha(\tau) \tag{3.3.19}$$

where $\xi(\tau)$ and $\alpha(\tau)$ are small perturbations about B_{ss} and Ω_{ss}, respectively. Furthermore, expand the forcing terms $C_{mh}(\Omega,B)$ and $C_{dh}(\Omega,B)$ about B_{ss} and Ω_{ss}, as a function of ξ and α as

$$C_{mh}(\Omega,B) = C_{mh}(\Omega_{ss},B_{ss}) + \left.\frac{\partial C_{mh}}{\partial B}\right|_{\substack{\Omega=\Omega_{ss}\\B=B_{ss}}} \cdot\, \xi + \left.\frac{\partial C_{mh}}{\partial \Omega}\right|_{\substack{\Omega=\Omega_{ss}\\B=B_{ss}}} \cdot\, \alpha + \ldots \tag{3.3.20}$$

$$C_{dh}(\Omega,B) = C_{dh}(\Omega_{ss},\, B_{ss}) + \left.\frac{\partial C_{dh}}{\partial B}\right|_{\substack{\Omega=\Omega_{ss}\\B=B_{ss}}} \cdot\, \xi + \left.\frac{\partial C_{dh}}{\partial \Omega}\right|_{\substack{\Omega=\Omega_{ss}\\B=B_{ss}}} \cdot\, \alpha + \ldots \tag{3.3.21}$$

where only the first order terms in the expansion are shown.

Substituting Eqs. (3.3.20) and (3.3.21) into Eqs. (3.3.13) and (3.3.14), retaining only terms of first order in ξ and α, and making use of Eqs. (3.3.15) and (3.3.16) one obtains

$$(\Omega_n^2 - \Omega_{ss}^2)\xi - 2\Omega_{ss}B_{ss}\,\alpha - 2\pi B_{ss}\alpha' = \frac{\eta}{2(2\pi S)^2}\left(\frac{\partial C_{mh}}{\partial B}\bigg|_{\substack{\Omega=\Omega_{ss}\\B=B_{ss}}} \cdot \xi + \frac{\partial C_{dh}}{\partial \Omega}\bigg|_{\substack{\Omega=\Omega_{ss}\\B=B_{ss}}} \cdot \alpha\right) \tag{3.3.22}$$

$$2\zeta\Omega_n\Omega_{ss}\xi + 2\zeta\Omega_n B_{ss}\alpha + 2\Omega_{ss}\xi' + B_{ss}\alpha' = \frac{\eta}{2(2\pi S)^2}\left(\frac{\partial C_{mh}}{\partial B}\bigg|_{\substack{\Omega=\Omega_{ss}\\B=B_{ss}}} \cdot \xi + \frac{\partial C_{dh}}{\partial \Omega}\bigg|_{\substack{\Omega=\Omega_{ss}\\B=B_{ss}}} \cdot \alpha\right) \tag{3.3.23}$$

Eqs. (3.3.22) and (3.3.23) form a coupled system of first order differential equations in the perturbed variables ξ and α, and will be referred to as the perturbed system of equations.

Assume solution of the form

$$\xi = \xi_o\, e^{\lambda t} \tag{3.3.24}$$

$$\alpha = \alpha_o e^{\lambda t} \tag{3.3.25}$$

where ξ_o, α_o and λ are constants. The steady state solution will then be stable if and only if λ has negative real parts, i.e., $R(\lambda) < 0$, so that the perturbations ξ and α decrease in time. Otherwise, the solution will be unstable. Substitute Eqs. (3.3.24) and (3.3.25) into Eqs. (3.3.22) and (3.3.23) to obtain

$$\begin{bmatrix} a_{11} & a_{12} - 2\pi B_{ss}\lambda \\ a_{21} + 2\Omega_{ss}\lambda & a_{22} + B_{ss}\lambda \end{bmatrix} \begin{pmatrix} \xi_o \\ \alpha_o \end{pmatrix} = \underset{\sim}{0} \qquad (3.3.26)$$

where

$$a_{11} = (\Omega_n^2 - \Omega_{ss}^2) - \frac{\eta}{2(2\pi S)^2} \left.\frac{\partial C_{mh}}{\partial B}\right|_{\substack{\Omega=\Omega_{ss} \\ B=B_{ss}}} \qquad (3.3.27a)$$

$$a_{12} = -2\Omega_{ss}B_{ss} - \frac{\eta}{2(2\pi S)^2} \left.\frac{\partial C_{dh}}{\partial \Omega}\right|_{\substack{\Omega=\Omega_{ss} \\ B=B_{ss}}} \qquad (3.3.27b)$$

$$a_{21} = 2\zeta\Omega_n\Omega_{ss} + \frac{\eta}{2(2\pi S)^2} \left.\frac{\partial C_{dh}}{\partial B}\right|_{\substack{\Omega=\Omega_{ss} \\ B=B_{ss}}} \qquad (3.3.27c)$$

$$a_{22} = 2\zeta\Omega_n B_{ss} + \frac{\eta}{2(2\pi S)^2} \left.\frac{\partial C_{dh}}{\partial \Omega}\right|_{\substack{\Omega=\Omega_{ss} \\ B=B_{ss}}} \qquad (3.3.27d)$$

The system of Eqs. (3.3.26) will have a nontrivial solution only if the determinant of the coefficient matrix is zero. This leads to the characteristic equation for λ

$$4\pi\Omega_{ss}B_{ss}\lambda^2 + (B_{ss}a_{11} - 2\Omega_{ss}a_{12} + 2\pi B_{ss}a_{21})\lambda + (a_{11}a_{22} - a_{12}a_{21}) = 0 \qquad (3.3.28)$$

3.3.1.1 Stability Boundaries

Analysis of Eq. (3.3.28) leads to the conclusion that a necessary and sufficient condition for instability is

$$a_{11}\, a_{22} - a_{12}\, a_{21} < 0 \qquad (3.3.29)$$

since under this condition, at least one of the roots of Eq. (3.3.28) will contain a positive real part, $R(\lambda) > 0$. However, because of the complexity of each a_{ij} $(i,j = 1,2)$ term, no sufficient condition for instability can be derived in terms of the basic variables involved in Eq. (3.3.28).

A parametric study has shown that for most of the range of parameters considered herein[1], the real part of at least one of the roots is postive, whenever $a_{21} < 0$. Therefore, as an approximation, the stability boundaries may be given by

$$a_{21} \equiv 2\zeta\Omega_n\Omega_{ss} + \frac{\eta}{2(2\pi S)^2} \left.\frac{\partial C_{dh}}{\partial B}\right|_{\substack{\Omega=\Omega_{ss} \\ B=B_{ss}}} = 0 \qquad (3.3.30)$$

Thus, a steady state solution lying on a stability boundary not only has to satisfy Eqs. (3.3.15) and (3.3.16) but also Eq. (3.3.30). That is, the stability boundary is the solution for the following set of equations:

$$(\Omega_n^2 - \Omega_{ss}^2)B_{ss} = \frac{\eta}{2(2\pi S)^2} C_{mh}(\Omega_{ss}, B_{ss}) \qquad (3.3.31)$$

---

[1] See section 3.4.

$$2\zeta\Omega_n\Omega_{ss}B_{ss} = -\frac{\eta}{2(2\pi S)^2}\, C_{dh}(\Omega_{ss},B_{ss}) \qquad (3.3.32)$$

$$2\zeta\Omega_n\Omega_{ss} + \frac{\eta}{2(2\pi S)^2}\left.\frac{\partial C_{dh}}{\partial B}\right|_{\substack{\Omega=\Omega_{ss}\\ B=B_{ss}}} = 0 \qquad (3.3.33)$$

Substituting Eq. (3.3.32) into Eq. (3.3.33), the stability boundary will be given by

$$(\Omega_n^2 - \Omega_{ss}^2)B_{ss} = \frac{\eta}{2(2\pi S)^2}\, C_{mh}(\Omega_{ss},B_{ss}) \qquad (3.3.31)$$

$$\left.\frac{\partial C_{dh}}{\partial B}\right|_{\substack{\Omega=\Omega_{ss}\\ B=B_{ss}}} - \frac{C_{dh}(\Omega_{ss},B_{ss})}{B_{ss}} = 0 \qquad (3.3.34)$$

An examination of Eqs. (3.3.31) and (3.3.34) leads to two main conclusions, valid within a certain range of the parameters η and ζ:

1) The stability of the steady-state response depends only on C_{dh} (Ω,B) coefficients, as evidenced by Eq. (3.3.34). According to the present approximation, stability is independent of the C_{mh} (Ω,B) coefficient.
2) Stability boundaries depend only on the mass ratio parameter η. According to the present approximation the stability boundaries are independent of the structural damping ratio ζ.

3.3.2 The Non Lock-in Model

Consider the non-lock-in formulation given by Eqs. (3.3.21) and (3.2.22). Bearing in mind the differences between the Lock-in and the Non-Lock-in models with respect to the assumed form of response and of force coefficients, the perturbation analysis framework laid down in subsection 3.3.1 yields

$$y'' + 2\zeta\Omega_n y' + \Omega_n^2 y = \frac{\eta}{2(2\pi S)^2}\,(C_{mh}\,\sin\tau - C_{dh}\,\cos\tau) \tag{3.3.35}$$

where

$$C_{mh} = C_{mh}(\Omega=1,B) \tag{3.3.36}$$

$$C_{dh} = C_{dh}(\Omega=1,B) \tag{3.3.37}$$

In applying the perturbation approach, the response of the oscillator is assumed to be of the form

$$y = B(\tau)\,\sin[\tau - \emptyset(\tau)] \tag{3.3.38}$$

with amplitude B and phase $\emptyset$ assumed to be slowly varying functions of the normalized time. Assuming that

$$y' = B\,\cos(\tau - \emptyset) \tag{3.3.39}$$

yields

$$B'\sin(\tau - \emptyset) - B\emptyset'\,\cos(\tau - \emptyset) = 0 \tag{3.3.40}$$

Differentiating Eq. (3.3.39) once with respect to τ and substituting it along with Eq. (3.3.38) and (3.3.39) into Eq. (3.3.25) yields

$$(\Omega_n^2 - 1)B \sin(\tau - \phi) + 2\zeta\Omega_n B \cos(\tau - \phi) + B' \cos(\tau - \phi) +$$

$$+ B\phi' \sin(\tau - \phi) = \frac{\eta}{2(2\pi S)^2} (C_{mh} \sin\tau - C_{dh} \cos\tau) \qquad (3.3.41)$$

The system of Eq. (3.3.40) and (3.3.41) must be solved for $B(\tau)$ and $\phi(\tau)$. This is done by first multiplying Eq. (3.3.40) by $\sin(\tau - \phi)$, Eq. (3.3.41) by $\cos(\tau - \phi)$ and adding term by term; and then multiplying Eq. (3.3.40) by $\cos(\tau - \phi)$, Eq. (3.3.41) by $\sin(\tau - \phi)$ and subtracting term by term. The resulting set of equations is as follows

$$(\Omega_n^2 - 1)B \sin(\tau - \phi) \cos(\tau - \phi) + 2\zeta\Omega_n B \cos^2(\tau - \phi) + B' =$$

$$= \frac{\eta}{2(2\pi S)^2} [C_{mh} \sin\tau \cos(\tau - \phi) - C_{dh} \cos\tau \cos(\tau - \phi)] \qquad (3.3.42)$$

and

$$(\Omega_n^2 - 1)B \sin^2(\tau - \phi) + 2\zeta\Omega_n B \sin(\tau - \phi) \cos(\tau - \phi) + B\phi' =$$

$$= \frac{\eta}{2(2\pi S)^2} [C_{mh} \sin\tau \sin(\tau - \phi) - C_{dh} \cos\tau \sin(\tau - \phi)] \qquad (3.3.43)$$

Averaging Eqs. (3.3.42) and (3.3.43) over one cycle of oscillation and assuming that B and ϕ remain essentially constant over this cycle of oscillation, then Eqs. (3.3.42) and (3.3.43) can be rewritten as

$$(\Omega_n^2 - 1)B + 2B\phi' = \frac{\eta}{2(2\pi S)^2} (C_{mh} \cos\phi + C_{dh} \sin\phi) \qquad (3.3.44)$$

$$2\zeta\Omega_n B + 2B' = \frac{\eta}{2(2\pi S)^2} (C_{mh} \sin\phi - C_{dh} \cos\phi) \qquad (3.3.45)$$

Under steady-state conditions $B' = \emptyset' = 0$, Eqs. (3.3.44) and (3.3.45) become

$$(\Omega_n^2 - 1)B = \frac{\eta}{2(2\pi S)^2}(C_{mh}\cos\emptyset + C_{dh}\sin\emptyset) \tag{3.3.46}$$

$$2\zeta\Omega_n B = \frac{\eta}{2(2\pi S)^2}(C_{mh}\sin\emptyset - C_{dh}\cos\emptyset) \tag{3.3.47}$$

If solved for B and $\emptyset$, these equations yield Eqs. (3.2.25), (3.2.26) and (3.2.27) as expected.

Let the steady state solution be

$$y_{ss} = B_{ss}\sin(\tau - \emptyset_{ss}) \tag{3.3.48}$$

Consider small perturbation $\xi(\tau)$ and $\psi(\tau)$, such that

$$B(\tau) = B_{ss} + \xi(\tau) \tag{3.3.49}$$

$$\emptyset(\tau) = \emptyset_{ss} + \psi(\tau) \tag{3.3.50}$$

Expand the forcing terms C_{mh} (Ω=1,B) and C_{dh} (Ω=1,B) about B_{ss} as a function of ξ only and make use of small angle assumption. Then the resulting perturbed system of first order differential equations is obtained as

$$(\Omega_n^2 - 1)\xi + 2B_{ss}\psi' = \frac{\eta}{2(2\pi S)^2}\left(-C_{mh}\sin\emptyset_{ss}\,\psi + \left.\frac{\partial C_{mh}}{\partial B}\right|_{\substack{\Omega=1\\B=B_{ss}}}\cos\emptyset_{ss}\,\xi + \right.$$

$$\left. + C_{dh}\cos\emptyset_{ss}\,\psi + \left.\frac{\partial C_{dh}}{\partial B}\right|_{\substack{\Omega=1\\B=B_{ss}}}\sin\emptyset_{ss}\,\xi\right) \tag{3.3.51}$$

$$2\zeta\Omega_n\xi + 2\xi' = \frac{\eta}{2(2\pi S)^2}\left(C_{mh}\cos\phi_{ss}\,\psi \quad \left.\frac{\partial C_{mh}}{\partial B}\right|_{\substack{\Omega=1\\B=B_{ss}}} \sin\phi_{ss}\,\xi + \right.$$

$$\left. + C_{dh}\sin\phi_{ss}\,\psi - \left.\frac{\partial C_{dh}}{\partial B}\right|_{\substack{\Omega=1\\B=B_{ss}}} \cos\phi_{ss}\,\xi\right) \qquad (3.3.52)$$

Assume a solution of the form

$$\xi = \xi_o\, e^{\lambda t} \qquad (3.3.53)$$

$$\psi = \psi_o\, e^{\lambda t} \qquad (3.3.54)$$

where ξ_o, ψ_o and λ are constants.

As in the lock-in formulation, the same criteria for stability apply . Thus the steady state solution is stable if and only if λ has negative real parts, $R(\lambda)<0$, so that perturbations die out in time. Otherwise the solution is said to be unstable.

Substituting Eqs. (3.3.53) and (3.3.54) into Eqs. (3.3.51) and (3.3.52) yields

$$\begin{bmatrix} (2B_{ss}\lambda + a_{11}) & a_{12} \\ a_{21} & (2\lambda + a_{22}) \end{bmatrix} \begin{pmatrix} \psi_o \\ \xi_o \end{pmatrix} = \underset{\sim}{0} \qquad (3.3.55)$$

with

$$a_{11} = -\frac{\eta}{2(2\pi S)^2}(-C_{mh}\sin\phi_{ss} + C_{dh}\cos\phi_{ss}) \qquad (3.3.56a)$$

$$a_{12} = (\Omega_n^2 - 1) - \frac{\eta}{2(2\pi S)^2}\left(\left.\frac{\partial C_{mh}}{\partial B}\right|_{\substack{\Omega=1\\B=B_{ss}}} \cos\phi_{ss} + \left.\frac{\partial C_{dh}}{\partial B}\right|_{\substack{\Omega=1\\B=B_{ss}}} \sin\phi_{ss}\right) \tag{3.3.56b}$$

$$a_{21} = \frac{\eta}{2(2\pi S)^2}\left(C_{mh}\cos\phi_{ss} + C_{dh}\sin\phi_{ss}\right) \tag{3.3.56c}$$

$$a_{22} = 2\zeta\Omega_n - \frac{\eta}{2(2\pi S)^2}\left(\left.\frac{\partial C_{mh}}{\partial B}\right|_{\substack{\Omega=1\\B=B_{ss}}} \sin\phi_{ss} - \left.\frac{\partial C_{dh}}{\partial B}\right|_{\substack{\Omega=1\\B=B_{ss}}} \cos\phi_{ss}\right) \tag{3.3.56d}$$

Note that by using Eqs. (3.3.46) and (3.3.47), Eqs. (3.3.56a) and (3.3.56c) can be further simplified to give

$$a_{11} = 2\zeta\Omega_n B_{ss} \tag{3.3.57a}$$

$$a_{21} = -(\Omega_n^2 - 1)B_{ss} \tag{3.3.57b}$$

The system of equations Eq. (3.3.55) will have a nontrivial solution, only if the determinant of the coefficient matrix is zero. This yields the characteristic equation for λ

$$4B_{ss}\lambda^2 + 2(a_{11} + B_{ss}\, a_{22})\lambda + (a_{11}a_{22} - a_{12}a_{21}) = 0 \tag{3.3.58}$$

3.3.2.1 Stability Boundaries

Analysis of Eq. (3.3.58), again leads to the conclusion that a necessary and sufficient condition for instability is

$$a_{11}a_{22} - a_{12}a_{21} < 0$$

Once more, due to the complexity of the quantities involved, the above condition cannot be translated in terms of the basic variables present in Eq. (3.3.58). However, a parametric study has shown that no instability occurs within the range of parameters considered herein.

Ideally, the regions of stability of each model would be mutually exclusive allowing the stable solution in each region to be considered the only solution in that particular region, i.e., the criteria for transition between the responses of the Lock-in and the Non-Lock-in models would be based upon the stability character of each response. But due to the lack of instability in the Non-Lock-In model response, the aforementioned criteria will apply only when transitioning from the Lock-in model to the Non-Lock-in model. Nevertheless, this is understood not to be a severe shortcoming, since from the practical point of view, interest lies primarily in the larger amplitude response that may be induced under lock-in conditions. Therefore, at this time no alternate criterion has been developed.

CHAPTER IV

ANALYSIS OF THE MODEL

4.1 INTRODUCTION

It has been suggested [15], that results from the forced cylinder experiments could be used in understanding the case of induced oscillations. Sarpkaya [61], besides obtaining experimental data, also attempted to use these data to predict the induced response of cylinders, but restricted himself to predictions of the maximum amplitude of vibration. Rather recent research [29], however, casts some doubts on the analogy between the forced cylinder and the spring mounted cylinder, and the experimental use of one situation to understand the other. Despite these doubts, the present approach is directly applied to forced cylinder experimental data in order to illustrate its potential and to uncover possible inconsistencies in the data. To further emphasize the potential of this formulation, suitably interpolated experimental data are used to produce continuous model response curves.

4.2 A PURELY EMPIRICAL APPROACH

The actual experimental data points for coefficients C_{mh} and C_{dh}, as published in [61], have been digitized and reproduced in Figs. 4.2.1a and 4.2.1b. They are shown as functions of reduced velocity V_r, but could just as well have been plotted as functions of the frequency of vibration Ω. Note that in each of these figures, only the region of interest, i.e., where Eq. (3.2.18) is satisfied, has been reproduced.

To apply the Lock-in Model, Eqs. (3.2.16) and (3.2.17) must be

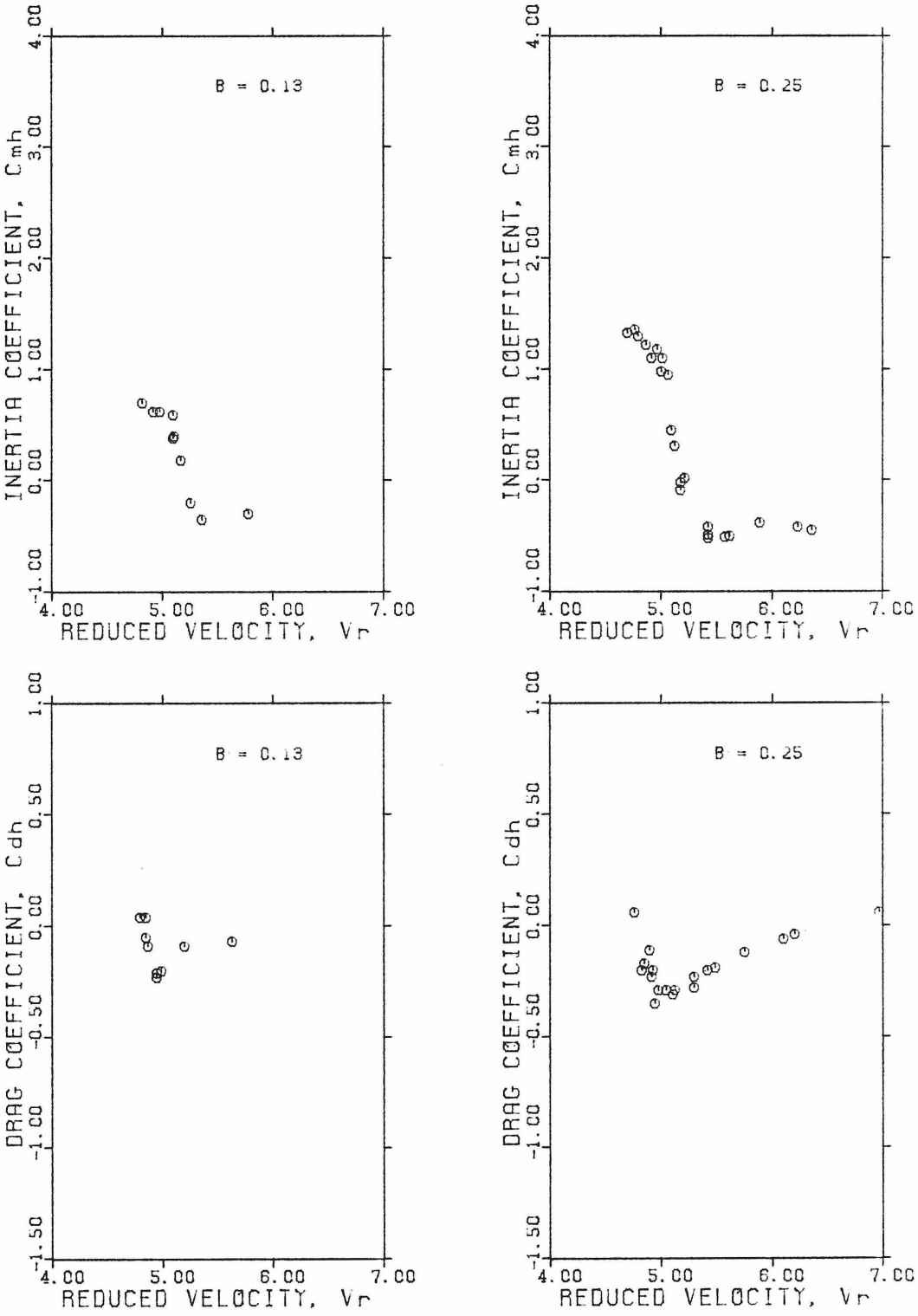

Fig. 4.2.1a

Actual Experimental Data Points of C_{mh} and C_{dh} Coefficients [61]

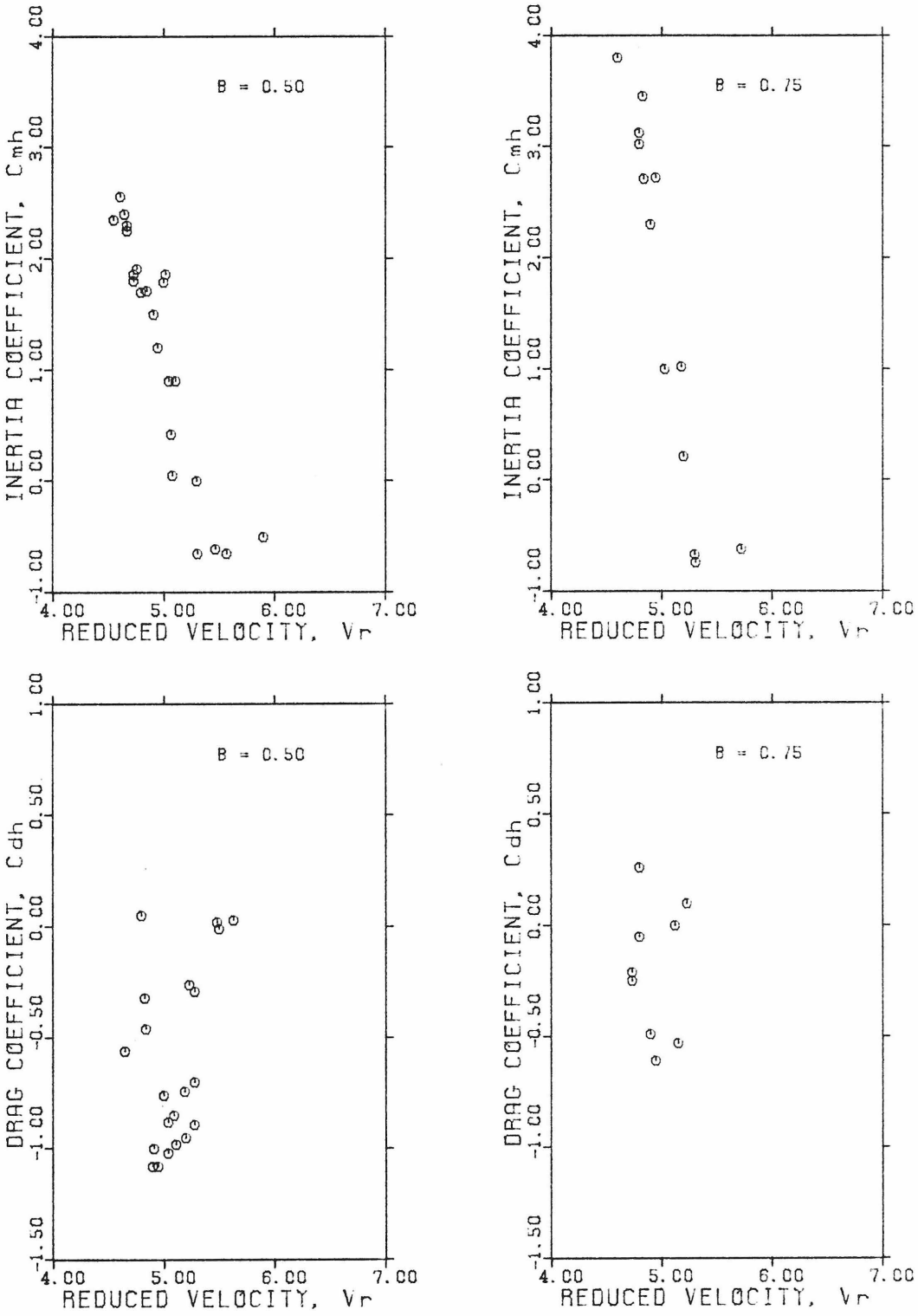

Fig. 4.2.1b

Actual Experimental Data Points of C_{mh} and C_{dh} Coefficients [61]

solved simultaneously for B and Ω, given the other parameters Ω_n, η, ζ, and S. However, since B is known only at four discrete points, those equations are solved instead for Ω_n and Ω, given B, η, ζ, and S. From Eqs. (3.2.16) and (3.2.17), one obtains two different expressions for Ω_n,

$$\Omega_n = \frac{\eta}{2(2\pi S)^2}\left[\frac{C_{mh}(\Omega,B)}{B} + \Omega^2\right]^{1/2} \tag{4.2.1}$$

which does not contain the coefficient C_{dh}, and

$$\Omega_n = -\frac{\eta}{2(2\pi S)^2}\,\frac{C_{dh}(\Omega,B)}{2\zeta\Omega B} \tag{4.2.2}$$

which does not contain the coefficient C_{mh}. Through Eqs. (4.2.1) and (4.2.2), Ω_n is evaluated as a function of Ω for each of the four values of B and at each experimental data point for C_{mh} and C_{dh} given in Figs. 4.2.1a and 4.2.1b. Ω_n is plotted as a function of Ω in Figs. 4.2.2a to 4.2.2g, for values of parameters S, η, and ζ chosen as follows:

Table 4.2.1

Values of Parameters for Purely Empirical Approach

Case	Figure	S	η	ζ
1	4.2.2a	0.20	.00514	.00103
2	4.2.2b	0.20	.00514	.00145
3	4.2.2c	0.20	.00514	.00181
4	4.2.2d	0.20	.05	.01
5	4.2.2e	0.20	.50	.10
6	4.2.2f	0.20	.20	.05
7	4.2.2g	0.20	.20	.005

In cases 1 to 3, the parameters were chosen so to enable direct comparison with Feng's experiments [9]. By maintaining the ratio η/ζ

constant in cases 4 and 5, the effect of η on the solutions could be verified. Finally, the manner in which ζ affects the solution is shown in cases 6 and 7.

For each of the four B values, Eq. (4.2.1) and (4.2.2) may at most intersect at two points. Just to aid visual interpretations of those intersections, interpolation curves (dashed lines) were also drawn in Fig. 4.2.2g. The intersection points obtained in the case considered in Fig. 4.2.2g form the amplitude and frequency response curves plotted in Fig. 4.2.3. These curves, though rather sketchy, show the same qualitative behavior encountered experimentally [9, 27, 46] and are the first indications that indeed forced vibration data can be used to generate the response of the induced vibration case.

4.2.1 Observations on the Available Data

Based on the results of Fig. 4.2.2 it is observed that:

1) What appeared to be an extensive set of $C_{mh}(\Omega,B)$ and $C_{dh}(\Omega,B)$ coefficient data for the purpose of response prediction is, in fact, not so. As indicated by Figs. 4.2.1, there are only four values for the variable B that yielded meaningful results. Even so, the considerable scatter of data points makes defining a smooth interpolation curve difficult.

2) In past experiments, the total force acting on the cylinder was measured and then decomposed into its orthogonal components, as given by Eq. (3.2.2). In this manner, each experiment, for a certain amplitude B and reduced velocity V_r, yielded only one value for each forcing coefficient C_{mh}

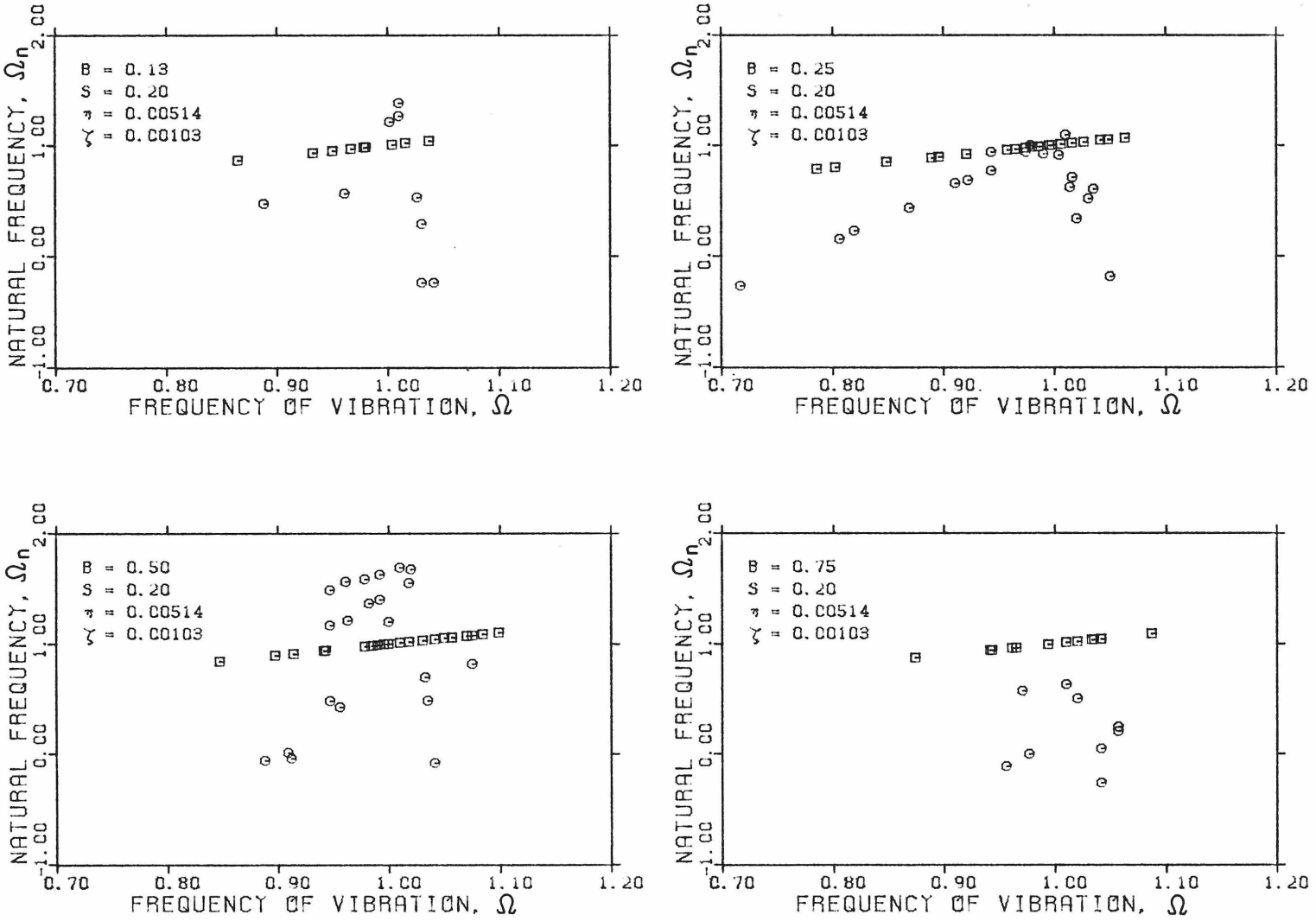

Fig. 4.2.2a

Solution of Eq. (4.2.1) ⊡, and Eq. (4.2.2) ⊙

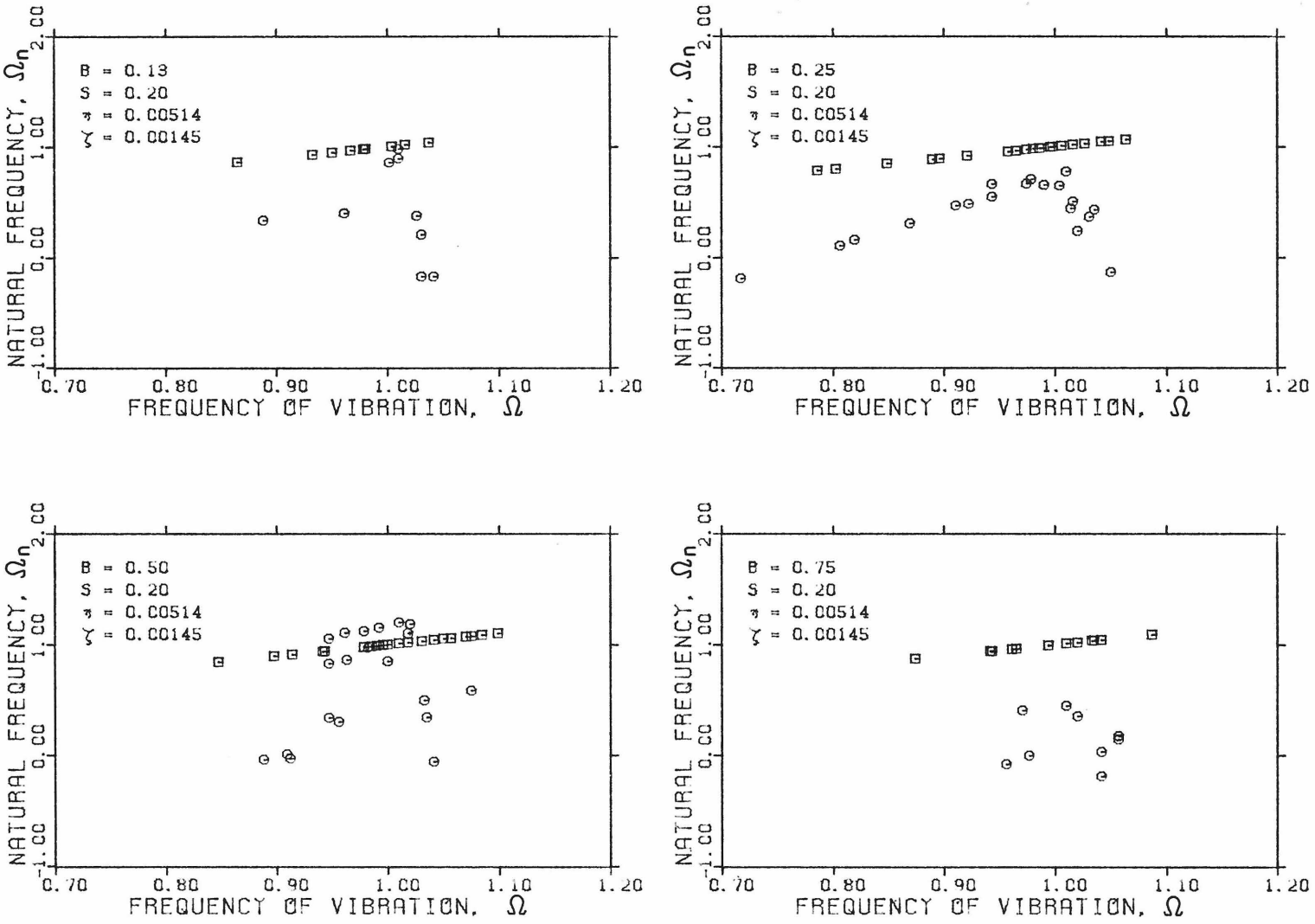

Fig. 4.2.2b

Solution of Eq. (4.2.1) ⊡, and Eq. (4.2.2) ⊙

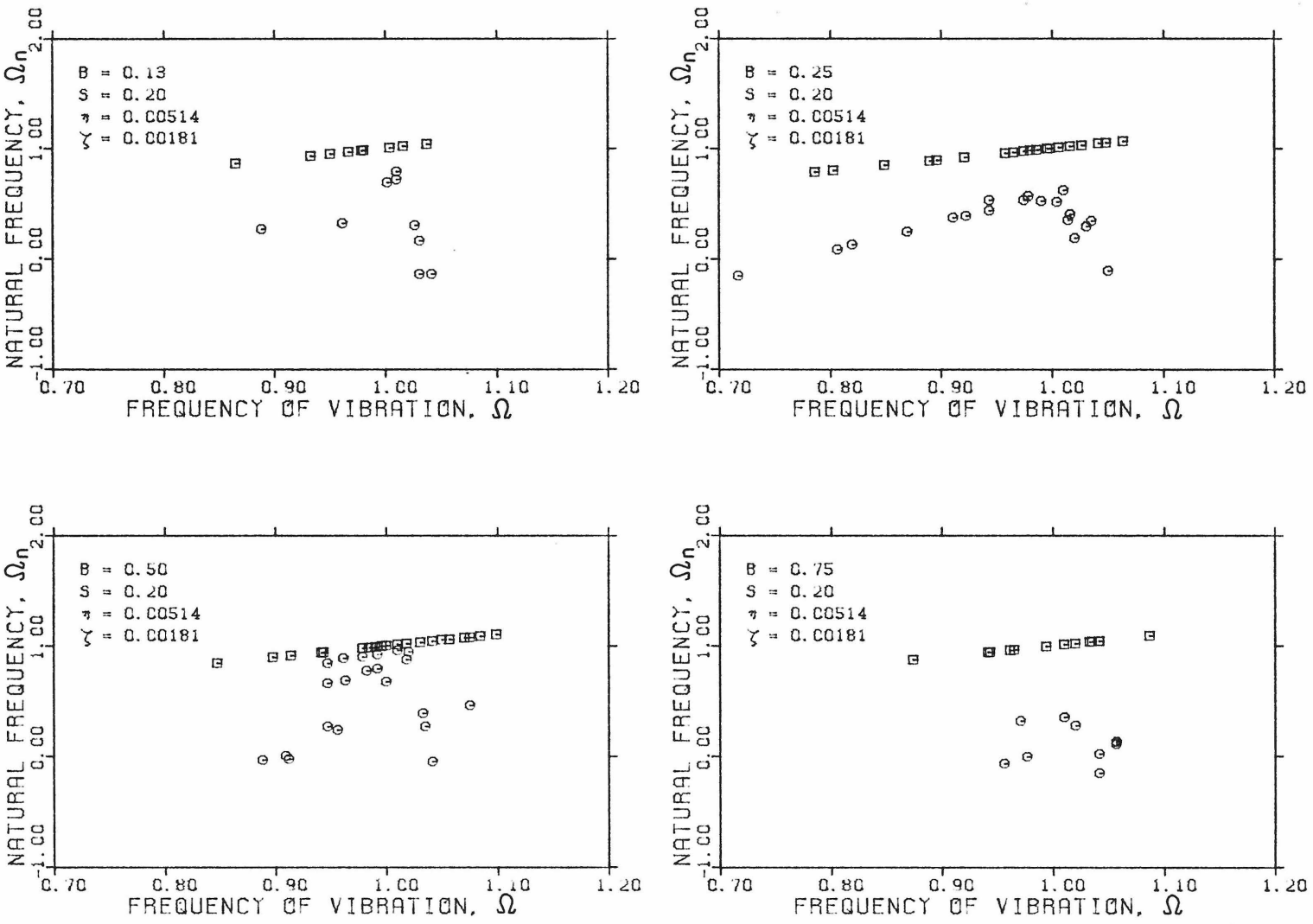

Fig. 4.2.2c

Solution of Eq. (4.2.1) ⊡, and Eq. (4.2.2) ⊙

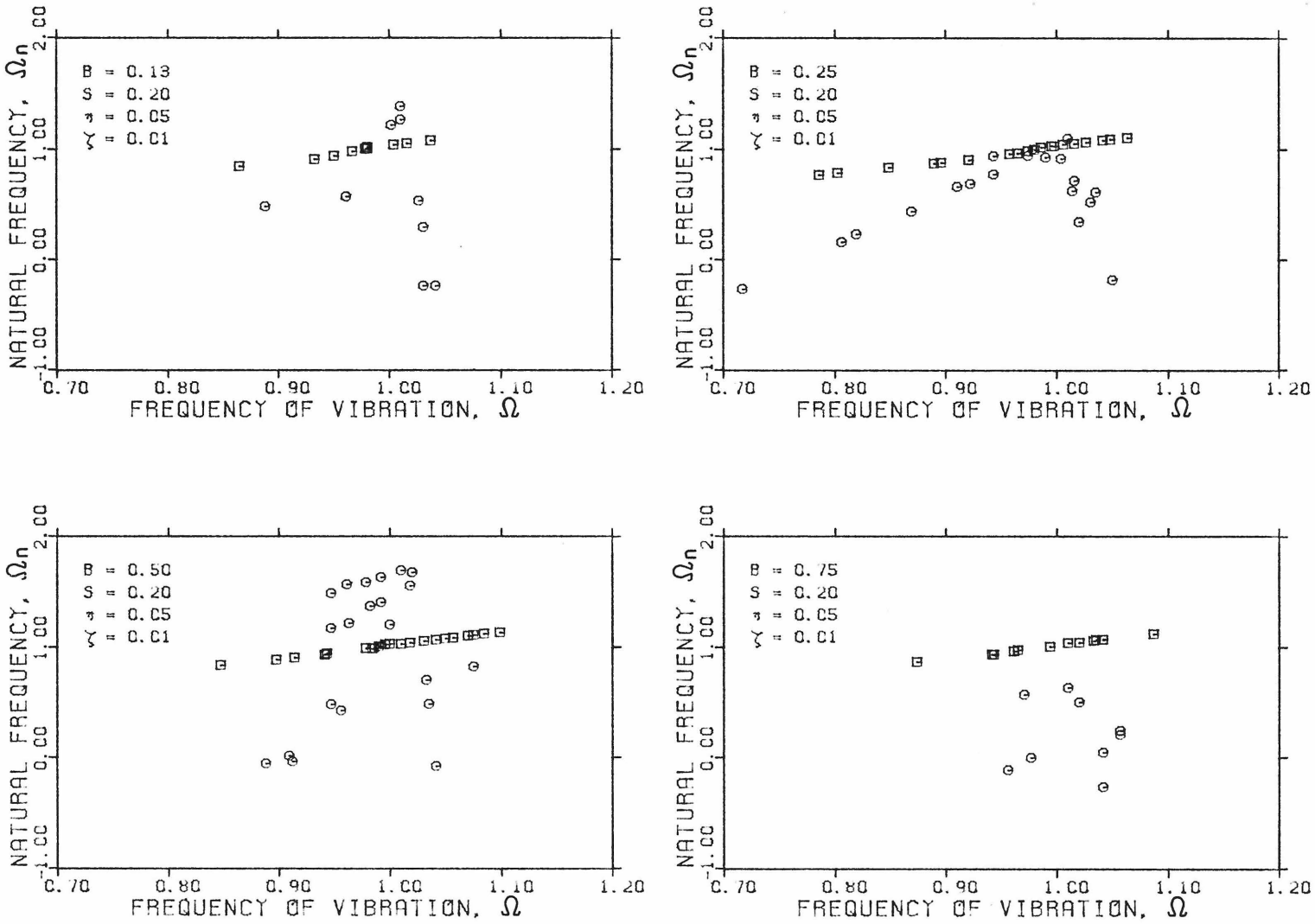

Fig. 4.2.2d

Solution of Eq. (4.2.1) ⊡, and Eq. (4.2.2) ⊙

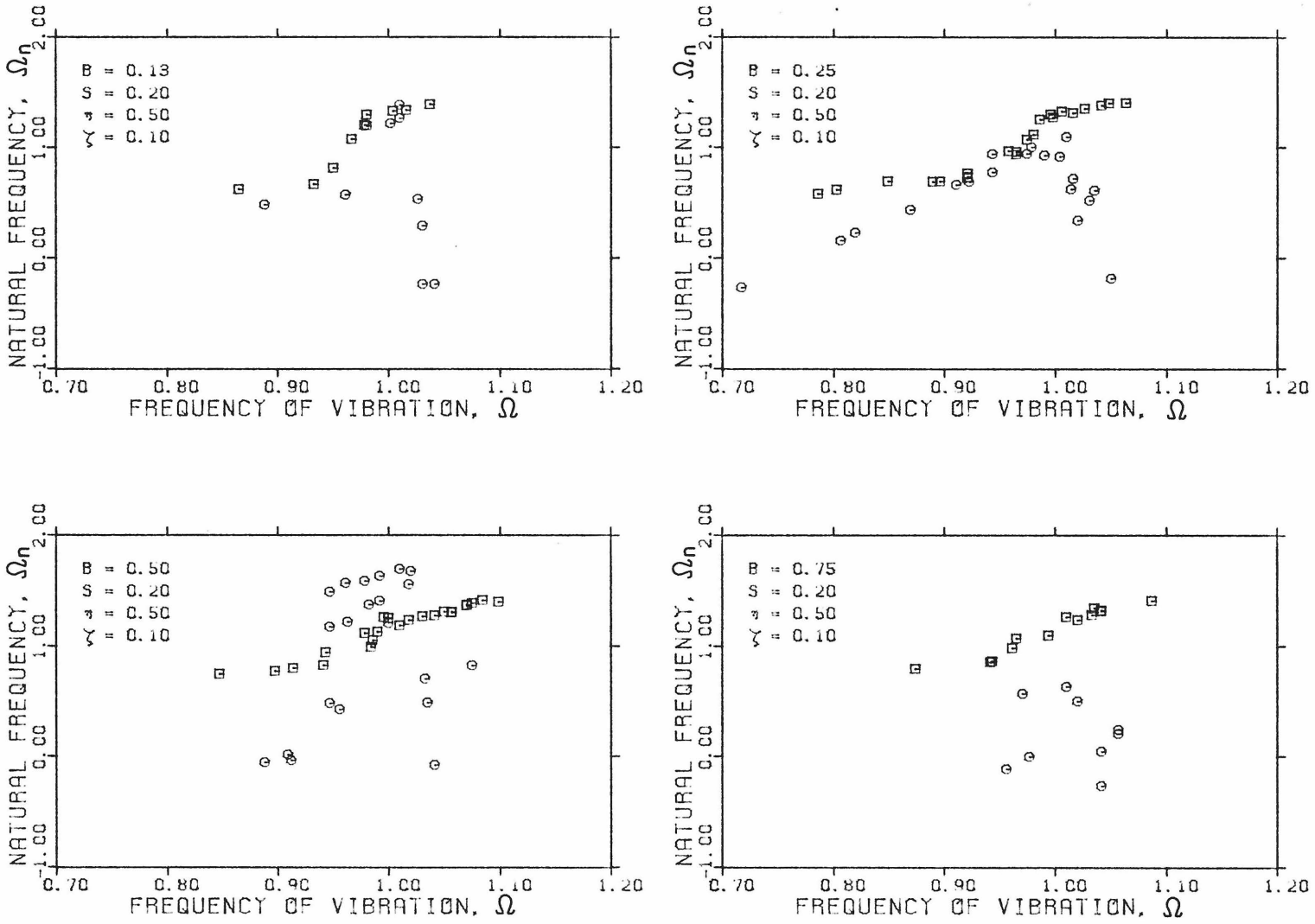

Fig. 4.2.2e

Solution of Eq. (4.2.1) ⊡, and Eq. (4.2.2) ⊙

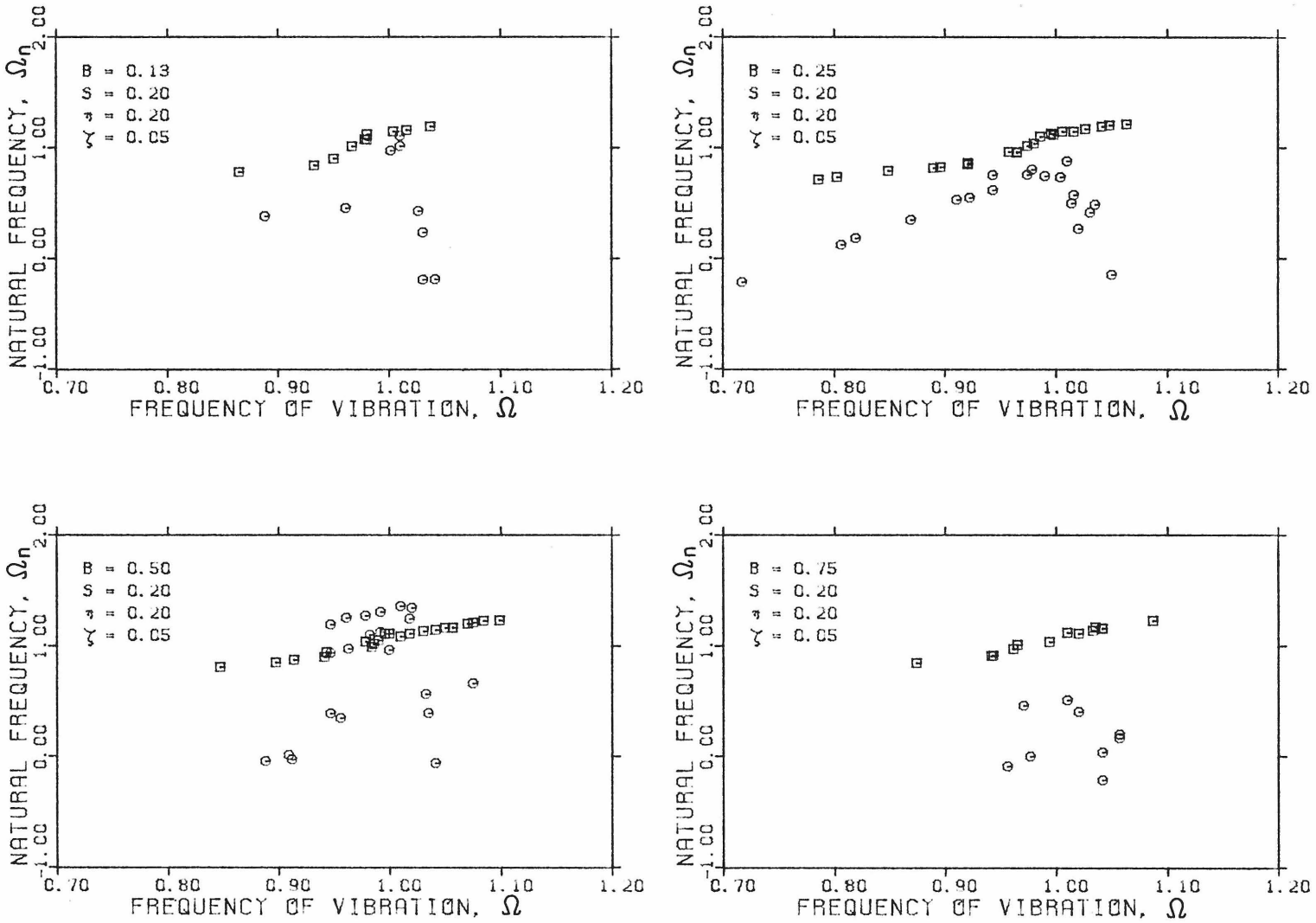

Fig. 4.2.2f

Solution of Eq. (4.2.1) ⊡, and Eq. (4.2.2) ⊙

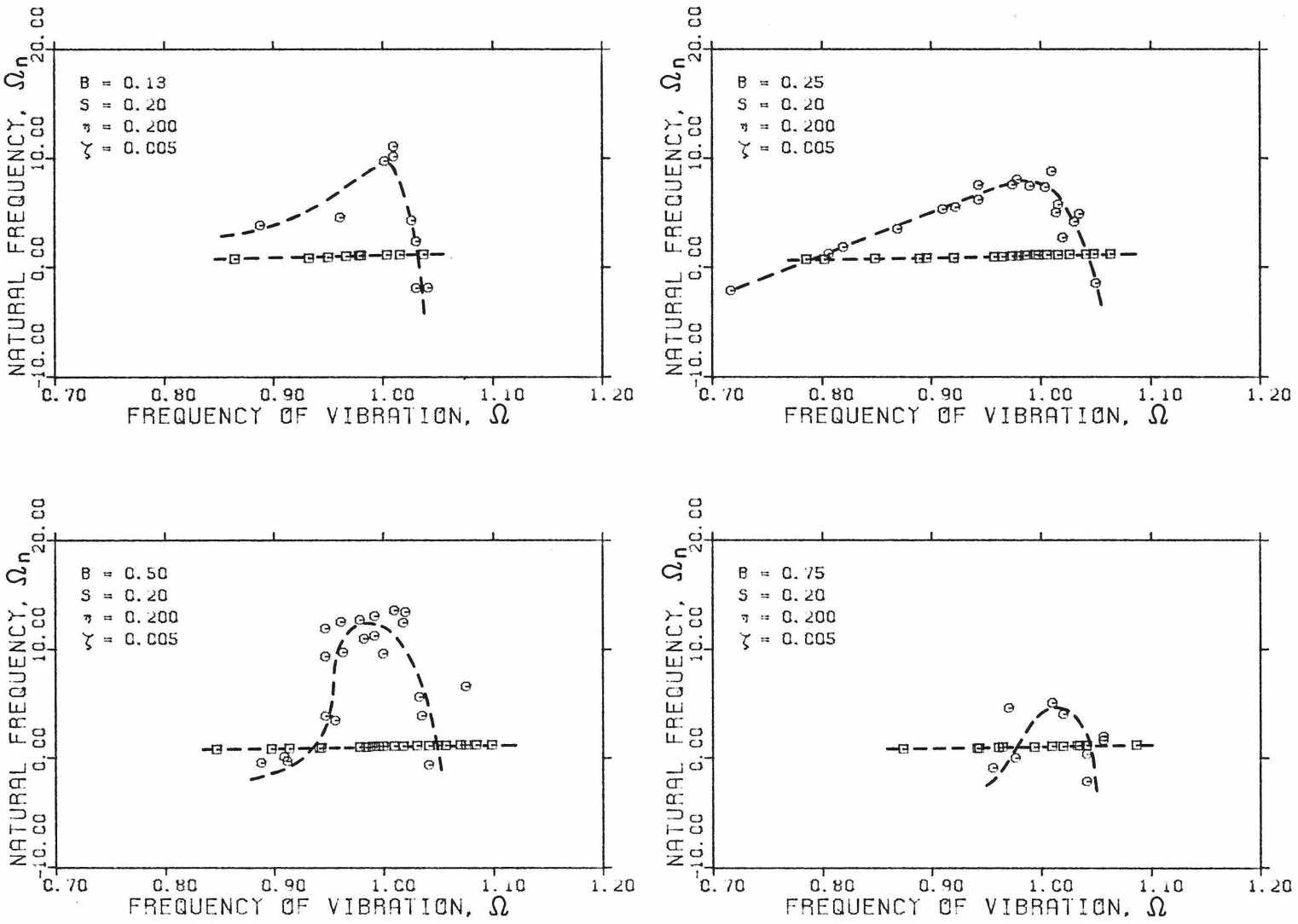

Fig. 4.2.2g

Solution of Eq. (4.2.1) ⊡, and Eq. (4.2.2) ⊙

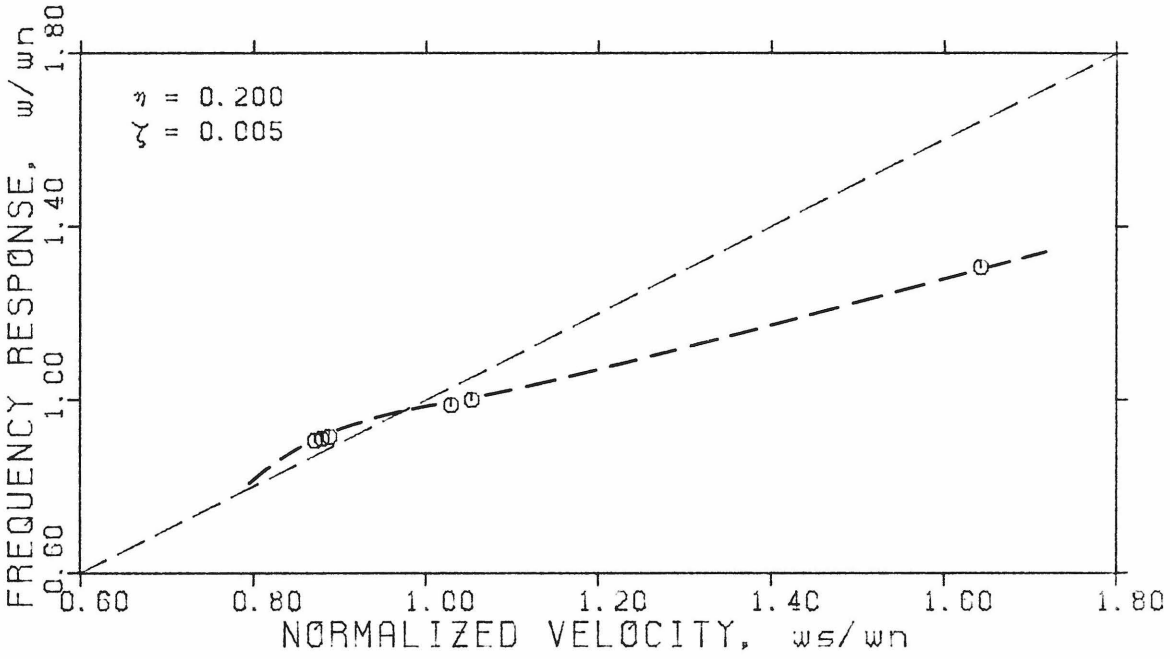

Fig. 4.2.3a

Frequency Response for Case 7

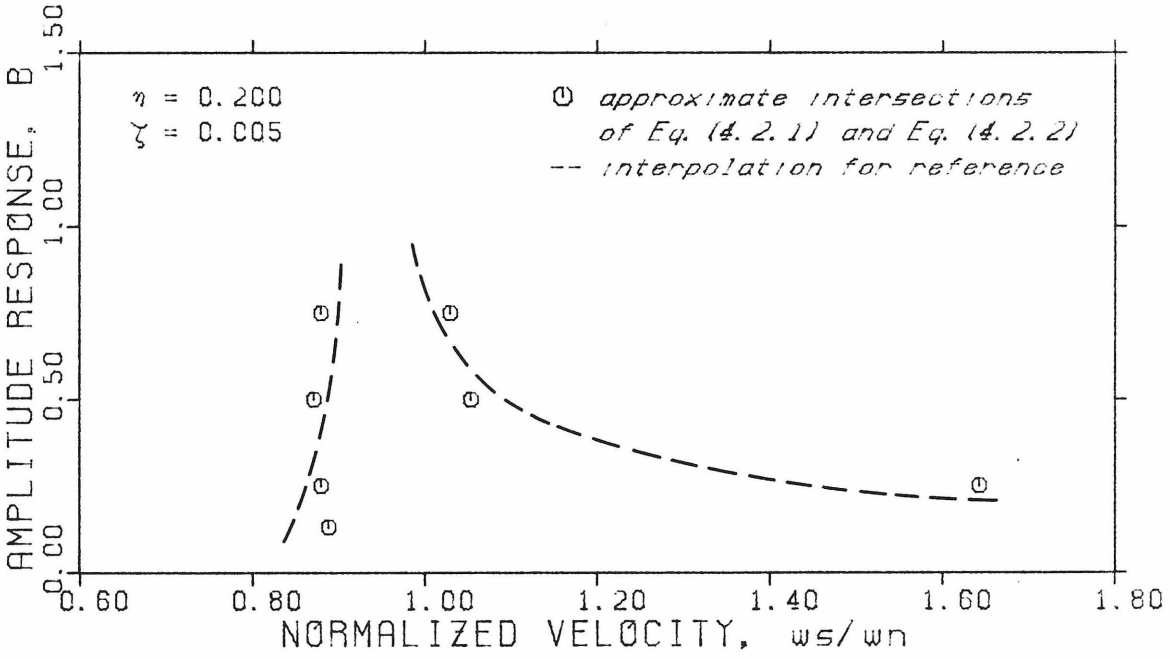

Fig. 4.2.3b

Amplitude Response for Case 7

and C_{dh}. Thus, the resulting C_{mh} and C_{dh} values when plotted should align under their corresponding V_r value. But close examination of the actual experimental data points [61] shows that there appears to be a shift between the C_{mh} and C_{dh} coefficients obtained within each experimental run.

3) From Figs. 4.2.2, it is noted that if the experimental points C_{mh} and C_{dh} were aligned under the same V_r value, then instead of plotting the results from Eq. (4.2.1) and (4.2.2) separately, one could have plotted the difference between these two equations. After all, the sole purpose of the procedure is to determine the simultaneous solution of Eqs. (3.2.16) and (3.2.17) in terms of Ω and Ω_n.

4) Upon examining Figs. 4.2.2b and 4.2.2c, it appears that either there is something wrong with the data, or else, there is a new characteristic of the vortex induced vibration phenomenon never before encountered or reported experimentally. Fig. 4.2.2b shows that Eqs. (3.2.16) and (3.2.17) barely have a solution for B = 0.13, have no solution for B = 0.25 and B = 0.75 and have some sort of a solution for B = 0.50. In terms of amplitude response, this would translate into having a plot similar to that in Fig. 2.2.6 but with an added closed loop of solutions above those shown for values B $\cong$ 0.50 and no solutions in between. A similar reasoning applies to Fig. 4.2.2c. Recently, Staubli [70] found some analytical results similar to the aforementioned. Based on other sets of experimental data [3], however,

it still seems that there must be something wrong with the present data set and that in fact, Figs. 4.2.2b and 4.2.2c should not exhibit any solution for B = 0.50.

5) It is observed that the maximum amplitudes of vibration obtained by the present approach are substantially smaller than those obtained experimentally by Feng [9], as can be seen from Table 4.2.2.

Table 4.2.2

Comparison Between Maximum Amplitudes of Vibration Obtained Experimentally and from Purely Empirical Approach

		B_{max}	
η	ζ	Feng[1]	Model[2]
.00514	.00103	.524	$\cong$ .25
.00514	.00145	.396	$\cong$ .13
.00514	.00181	.204	$<$ .13
.00514	.00257	.146	$<$ .13
.00514	.00324	.082	$<$ .13

[1] Feng's results [9] as digitized by Hall [29].
[2] Purely empirical approach.

6) It is noted that the maximum amplitude of vibration occurs for $V_r \cong 5.00$; that is, where $C_{dh}(V_r,B)$ is a minimum. This also corresponds to the point where $C_{mh}(V_r,B) \cong 0$. It will be shown later that this feature will allow mixing the present experimental data with other sets of experimental observations.

In spite of all the possible problems related to the

presently available experimental data, it is believed that these data still carry the basic information necessary to predict, at least qualitatively, the behavior of the induced vibration of cylinders. A method for accomplishing this is presented.

4.3 AN ANALYTICAL-EMPIRICAL APPROACH

It is clear from the foregoing that some appropriate interpolation of the data will be required in order to produce reasonable model response curves. Sarpkaya, in presenting the experimental data, also included a smoothed version, reproduced in Figs. 2.2.2 and 2.2.3. However, no mention was made as to how this version was obtained from the raw data. As is obvious at this point, the surfaces $C_{mh}(\Omega,B)$ and $C_{dh}(\Omega,B)$ must be well defined and continuous in both Ω and B in order to ensure a continuous solution for the system of Eqs. (3.2.16) and (3.2.17). If there were enough data points in both B and V_r (or Ω), and if these data had a relatively smooth behavior, a numerical interpolation could be employed and the purely empirical approach described in the previous section applied. But this is not the case for the available data and may still not be, even when a more complete experimental set of data becomes available. One must, therefore, resort to some analytical interpolation scheme.

Ideally, the interpolation expressions should be chosen to reflect the very nature of the vortex induced vibration phenomenon. A least square fit in two dimensions could then be applied to the experimental data so as to select the constants appearing in the interpolation

expressions. But if the nature of the fluid-structure interaction was known, there would be no need for an approximate model.

4.3.1 Fitting of Experimental Data

Considering the observations made with respect to the available experimental data, the situation is far from ideal. Instead of attempting to interpolate the actual data points through two dimensional surfaces, which could prove fruitless, an alternate interpolation scheme is adopted based on the smoothed data of Figs. 2.2.2 and 2.2.3.

In this procedure, an expression for the curves in the V_r direction is chosen, in order to retain the characteristics deemed most important, but no attempt is made to make a best fit of the actual data points.

In particular, analysis of $C_{dl}(V_r,B)$ curves presented in Fig. 2.2.3, for the range where Eq. (3.2.18) is satisfied, shows that

1) all curves have a first zero crossing practically at about $V_r = 4.80$;
2) all curves reach a minimum at about the same point, $V_r = 5.00$;
3) there is a second zero crossing for $V_r > 5.00$, that is dependent on B.

Accordingly, an expression for $C_{dl}(V_r,B)$ is chosen as follows:

$$C_{dl}(V_r,B) = \begin{cases} -\dfrac{x}{[d(x-a)^2 + bx]} & , x \leq a \qquad (4.3.1a) \\ -\dfrac{x\left[1 - \left(\dfrac{x-a}{c-a}\right)^2\right]}{[d(x-a)^2 + bx]} & , x > a \qquad (4.3.1b) \end{cases}$$

where

$$x = V_r - 4.80$$

and the other parameters are defined as

a = 0.2 , considered constant. x = a is where the minimum occurs in the local coordinate system.

b = b(B) , function of the amplitude and an approximate value for the inverse of the minimum.

c = c(B) , function of the amplitude, x = c where the second zero crossing occurs in the local coordinate system.

d = 0.1 , controls the broadness of curves.

The relationship between these parameters and the C_{dl} curve is shown in Fig. 4.3.1.

A similar examination of the behaviour of the $C_{ml}(V_r,B)$ curves, presented in Fig. 2.2.3, shows that

1) all curves have a zero crossing practically at $V_r = 5.15$;
2) the slope of the curves at the zero crossing point is dependent on B;
3) the curves tend to have a practically constant behavior for values of V_r slightly greater than 5.5.

The expression for $C_{ml}(V_r,B)$ is chosen as

$$C_{ml}(V_r,B) = \begin{cases} -\dfrac{e\,(V_r - V_{ro})}{\left[1 + \left(\dfrac{V_r - V_{ro}}{f/e}\right)^2\right]^{1/2}} & , V_r > V_{ro} \qquad (4.3.2a) \\ -e\,(V_r - V_{r_o}) & , V_r \leq V_{ro} \qquad (4.3.2b) \end{cases}$$

where the parameters are defined as

V_{ro} , zero crossing of the curves

e = e(B) , slope of the C_{mh} curves at $V_r = V_{ro}$

f = f(B) , assumed as an asymptotic value that C_{mh} would tend to, for relatively large values of V_r.

The relationship between these parameters and the C_{ml} curve is shown in Fig. 4.3.2.

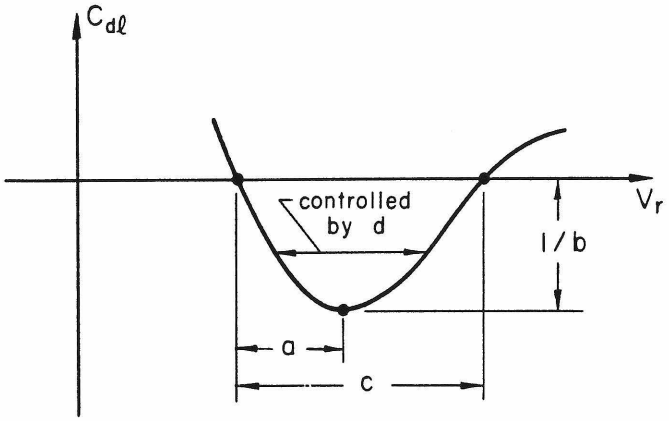

Fig. 4.3.1 Parameters for definition of $C_{dl}(V_r,B)$ surfaces

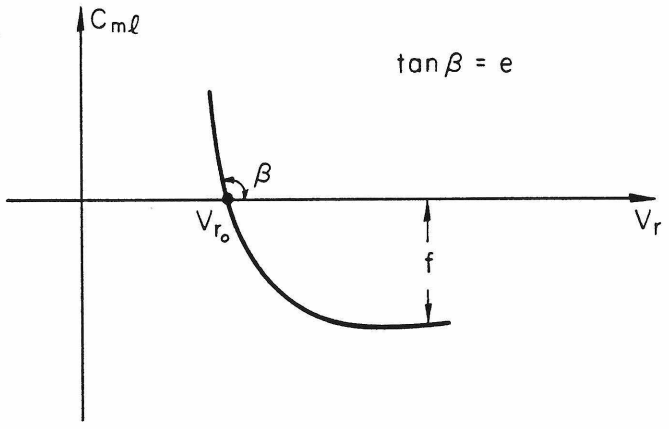

Fig. 4.3.2. Parameters for definition of C_{ml} (V_r,B) surfaces

The $C_{dl}(V_r,B)$ and $C_{ml}(V_r,B)$ curves, being smoother than the $C_{dh}(V_r,B)$ and $C_{mh}(V_r,B)$ curves, have been chosen for interpolation. However, one set of coefficients can easily be recovered from the other by using the following equations:

$$C_{mh}(V_r,B) = \frac{2\pi^3 B}{V_r^2} \; C_{ml}(V_r,B) \tag{4.3.3}$$

$$C_{dh}(V_r,B) = \frac{32\pi B^2}{3V_r^2} \; C_{dl}(V_r,B) \tag{4.3.4}$$

It should be stated that the above expressions have been arrived at after a relatively extensive examination of other possible expressions. Among all the possibilities considered, it is felt that Eqs. (4.3.1) and (4.3.2) are the ones that best match the smoothed data of Fig. 2.2.3.

As has been indicated, several of the parameters appearing in Eq. (4.3.1) and (4.3.2) were defined as functions of B so the complete two-dimensional surfaces for $C_{ml}(V_r,B)$ and $C_{dl}(V_r,B)$ surfaces can be generated. These functions were chosen, bearing in mind the simplest possible expressions and considering only the present set of experimental data to the extent possible.

Specification of the parameter b.

As can be seen from Table 4.2.2, the present experimental data yield maximum amplitudes of vibration far below the values experimentally found by Feng [9]. Since the prediction of amplitude is one of the most important aspects of the capability of any model, it is felt that some improvement should be made in this area. Experimental data[1] exactly simi-

[1] As of this writing Staubli [70] has not published his complete work.

lar to the present set have not, as of yet, been published . However, as mentioned before, the maximum amplitude of vibration occurs at $V_r \cong 5.00$, corresponding to minimum values of C_{dh} (V_r,B) and close to zero values of C_{mh} (V_r,B). Data corresponding to forces acting at peak response on flexibly mounted cylinders are used to supplement Sarpkaya's data, based upon the assumption that both phenomena are similar. Mixing of the results from forced cylinder experiments with those obtained from flexibly mounted cylinder experiments is, admittedly, not a very desirable procedure. Nevertheless, in doing so, the prediction capability of the model is so greatly enhanced that this by far offsets any of the procedure's undesirable effects.

Evaluating Eq. (4.3.1) for $V_r = 5.0$ and using Eq. (4.3.4), yields

$$b(B) = -\frac{32\pi B^2}{75} \quad \frac{1}{C_{dh}(5.0,B)} \tag{4.3.5}$$

Values for $C_{dh}(5.0,B)$ from Blevins [9] are mixed with corresponding values from Sarpkaya and a smooth curve, given by the expression that follows, drawn through the experimental points.

$$C_{dh}(V_r = 5.0,B) = -1.375B^2 + 1.483B + 0.200 \tag{4.3.6}$$

This curve is shown, along with the experimental points, in Fig. 4.3.3. Note that the empirical relationship gives results which are larger than those obtained by Sarpkaya, for $B = 0.13$ and $B = 0.25$, and gives a smaller coefficient for $B = 0.50$.

For all the other parameters, function of B, appearing in Eqs. (4.3.1) and (4.3.2) no similar measurements have been found. Consequently,

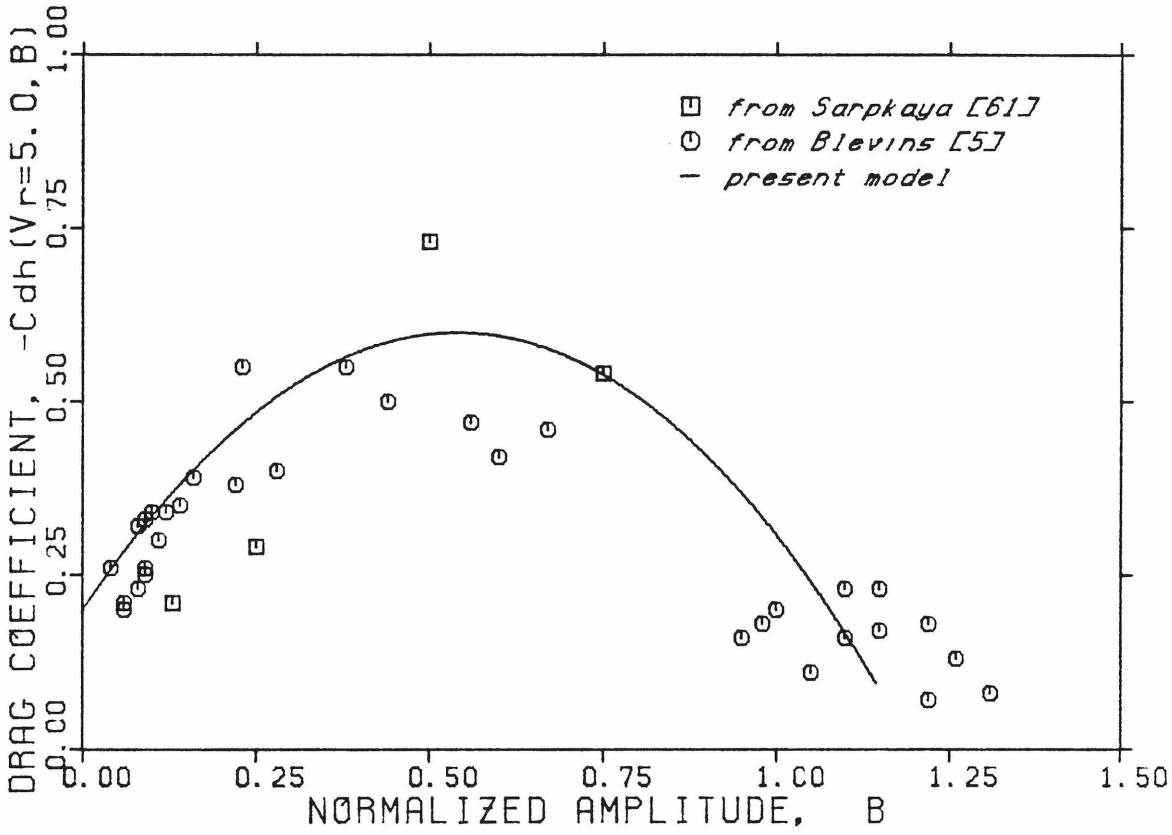

Figure 4.3.3

Force Coefficients at Peak Amplitude Response

all remaining interpolation functions are based only on the experimental results obtained by Sarpkaya. This necessarily implies some degree of arbitrariness since there are, at most, five experimental data points to be interpolated. Nevertheless, there is the indirect constraint of what the amplitude and frequency response should look like for given value of η and ζ. Within this framework, some alternatives have been tried and the expressions chosen for the present model are hereupon presented.

Specification of the parameter c

The parameter c represents the second zero crossing of $C_{dl}(V_r,B)$

curves in the local coordinate system. An interpolation expression of the form

$$c(B) = \frac{1}{3.2B} \tag{4.3.7}$$

has been selected. The constant was determined through a least square fit of the data. Table 4.3.1 compares experimental and predicted values for the parameter c.

Table 4.3.1

Experimental and Predicted Values for Parameter c

	c(B)	
B	experimental	predicted
0.13	2.70 [1]	2.40
0.25	1.60	1.25
0.50	0.65	0.63
0.75	0.40	0.42

[1] Estimated

Specification of the parameter e

The parameter e controls the slope at the zero crossing V_{ro} of $C_{ml}(V_r,B)$ curves. Let

$$e(B) = \frac{1}{2.043B^3 - 2.560B^2 + 1.105B} \tag{4.3.8}$$

The constants in the expression above were determined through a least square fit of the experimental data. Experimental and predicted values are compared in Table 4.3.2.

Table 4.3.2

Experimental and Predicted Values for Parameter e

	e(B)	
B	experimental	predicted
0.13	15.0 [1]	9.54
0.25	7.50	6.75
0.50	6.00	5.96
0.75	3.70	3.99
1.03	1.30	1.53

[1] Estimated

Specification of the parameter f

The parameter f controls the "asymptotic" value of $C_{ml}(V_r,B)$. The following expression has been selected and the constants determined through a least square fit.

$$f(B) = 2.076B^2 - 3.173B + 1.767 \qquad (4.3.9)$$

Experimental and predicted values are presented next

Table 4.3.3

Experimental and Predicted Values for Parameter f

	f(B)	
B	experimental	predicted
0.13	1.40	1.39
0.25	1.00	1.10
0.50	0.75	0.70
0.75	0.60	0.56
1.03	0.70	0.70

Specification of the parameter V_{ro}

In section 4.2.1, it is mentioned that close examination of the actual experimental data shows that there is a shift between the C_{mh} and C_{dh} coefficients obtained for a same V_r. But solely based upon the analysis of these coefficients, one cannot tell which coefficient is actually shifted with respect to which.

In comparing results, obtained in Chapter II, for the Wake Oscillator with those obtained by Sarpkaya, it is clear in Fig. 2.3.1, that if the C_{dh} coefficients, as obtained by the latter, are assumed correct, then the C_{mh} coefficients should be shifted to the left. A left or right shift in the analytical interpolation expression for C_{mh} is accomplished by varying the value of the parameter V_{ro}. Thus, if $V_{ro} = 5.15$ is chosen, the interpolated C_{mh} curves will cross the V_{ro} axis at the same point as the C_{mh} curves published in [61].

Based again on the results of Chapter II, the aformentioned shift can be compensated by choosing $V_{ro} = 5.00$, which will be assumed herein. It will be noted whenever the parameter V_{ro} takes on a different value.

Once all parameters are defined, $C_{ml}(V_r,B)$ and $C_{dl}(V_r,B)$, and corresponding $C_{mh}(V_r,B)$ and $C_{dh}(V_r,B)$ can be plotted, as in Fig. 4.3.4 and 4.3.5 for comparison with Fig. 2.2.3 and 2.2.2. Although, the interpolation procedure had a smoothing effect upon the experimental data, it may be easily verified that the overall fitting is reasonable. It is still observed that the fitting approach used herein, being modular, allows for independent changes in each of the parameters.

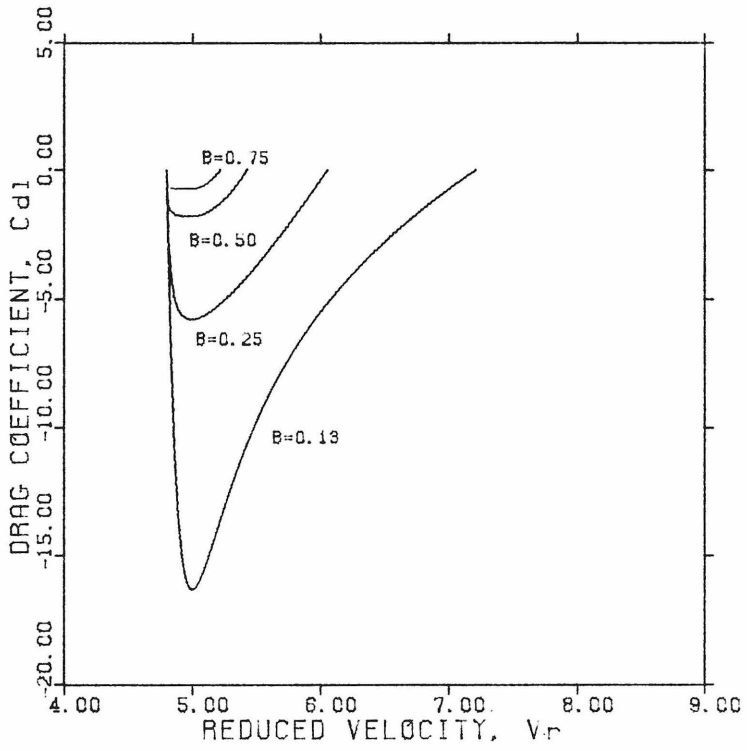

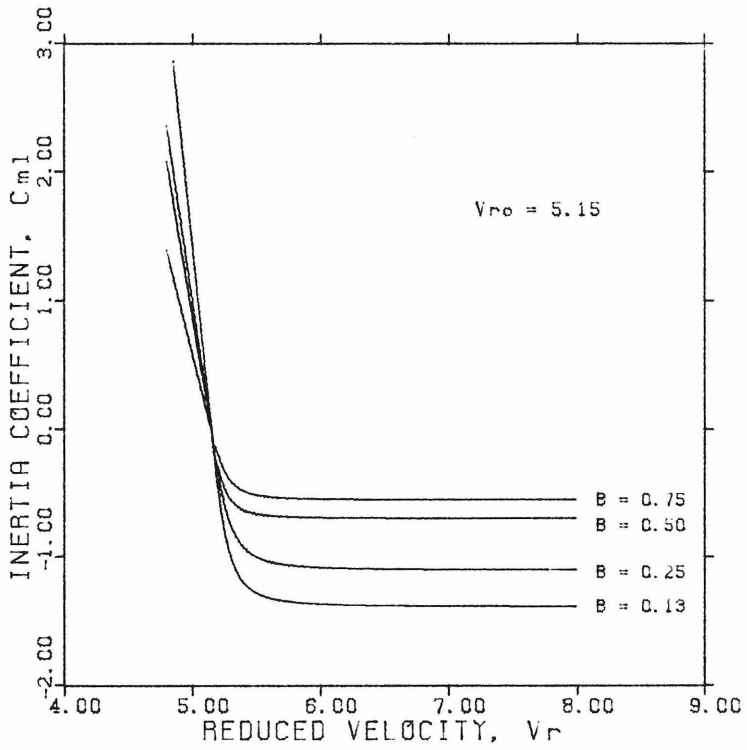

Fig. 4.3.4

Interpolation Surfaces for C_{ml} (V_r,B) and C_{dl} (V_r,B)

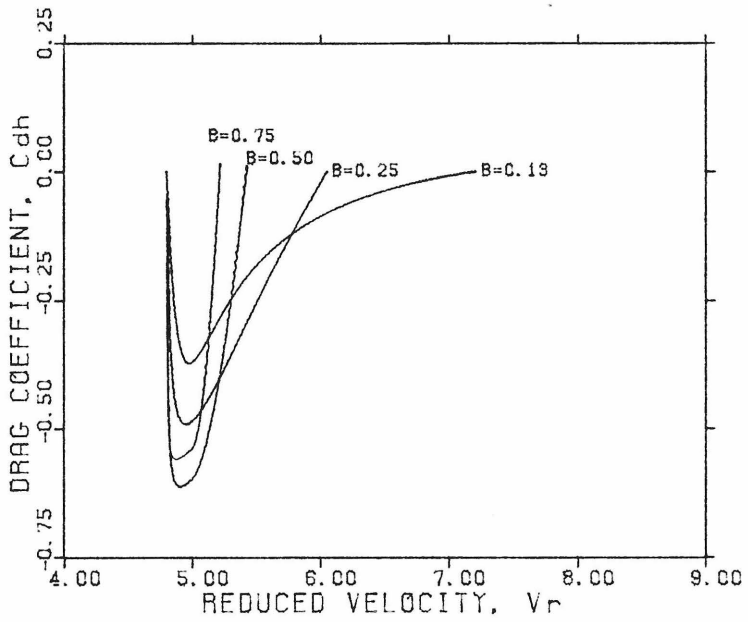

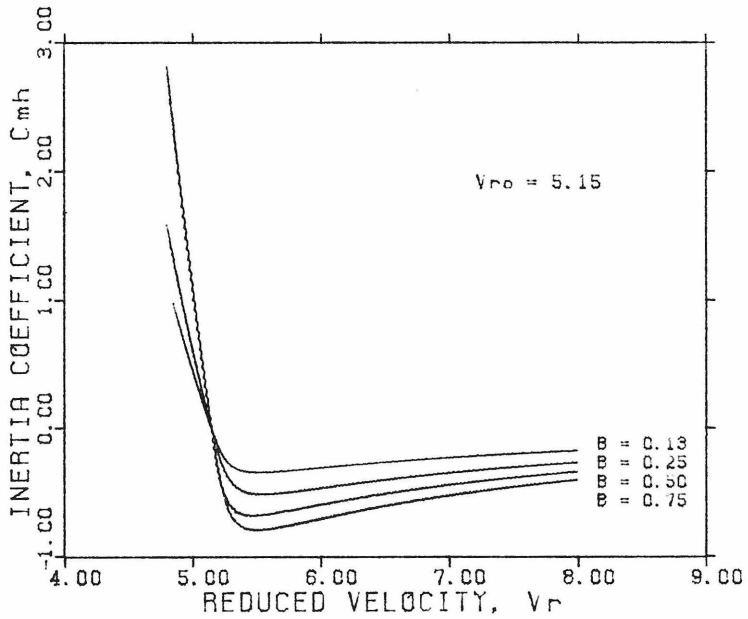

Fig. 4.3.5

Interpolation Surfaces for C_{mh} (V_r,B) and C_{dh} (V_r,B)

4.3.2 Amplitude and Frequency Responses

Having characterized $C_{mh}(V_r,B)$ and $C_{dh}(V_r,B)$ at all points where Eq. (3.2.18) is satisfied, the locked-in response and the non-locked-in response given by Eq. (3.2.16) and (3.2.17) and Eqs. (3.2.25), (3.2.26) and (3.2.27), respectively, can be solved for each set of parameters η, ζ, and ω_n. To enable direct comparison with the experimental results from Feng [9], the model predictions for amplitude and frequency are plotted versus the normalized velocity V_n, defined as

$$V_n = \frac{\omega_s}{\omega_n} = \frac{2\pi S\ V}{\omega_n D} \qquad (4.3.10)$$

Furthermore, the frequency is normalized by ω_n so the response curves for the lock-in case (i.e., $\omega \cong \omega_n$), may lie along the horizontal $\omega/\omega_n = 1$ and for the non-lock-in case (i.e., $\omega \cong \omega_s$), on the diagonal $\omega/\omega_n \cong \omega_s/\omega_n$.

In Figs. 4.3.6 to 4.3.10, the mass parameter η is kept constant while the damping ratio ζ is varied so as to cover all cases studied by Feng. The results from one case to another are very similar and one can note that the model exhibits many of the characteristics associated with the vortex induced vibration phenomenon. The lock-in response presents large amplitudes of vibration at $\omega \cong \omega_n$, where the vortex shedding frequency is known to lock onto the structural frequency of vibration. Relatively smaller amplitudes of vibration are yielded by the non-lock-in model, at a frequency of vibration equal to the Strouhal frequency. The lock-in model clearly exhibits a region of double responses. In this particular region, the stability analysis developed in section 3.3 shows

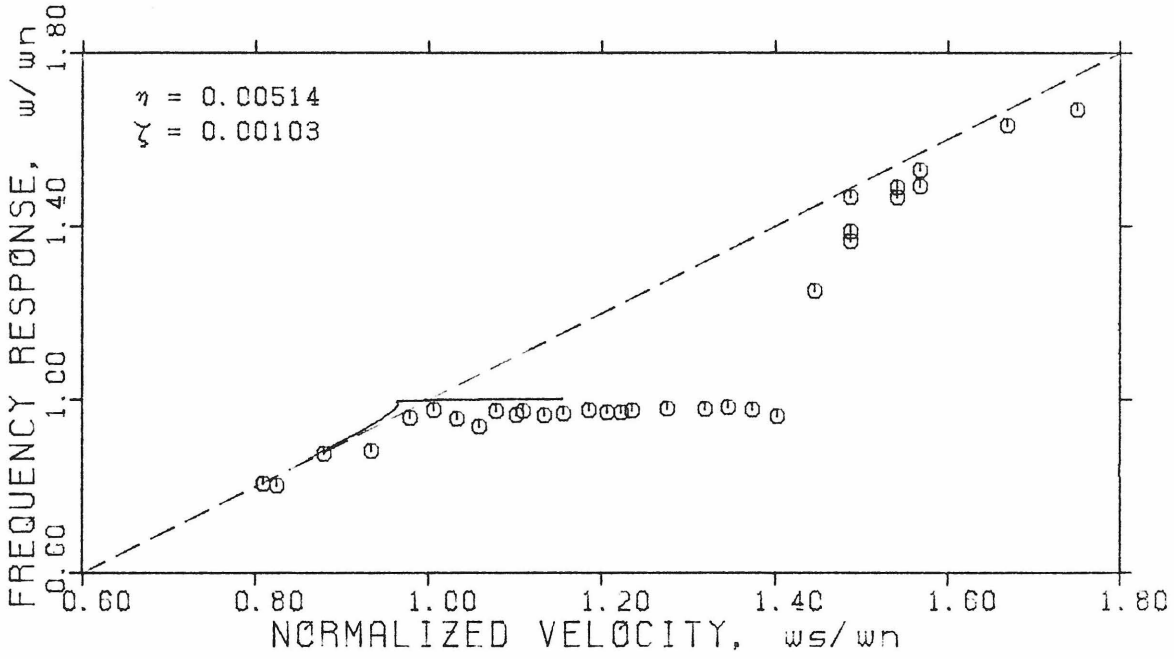

Fig. 4.3.6a

Model Versus Experimental Frequency Response

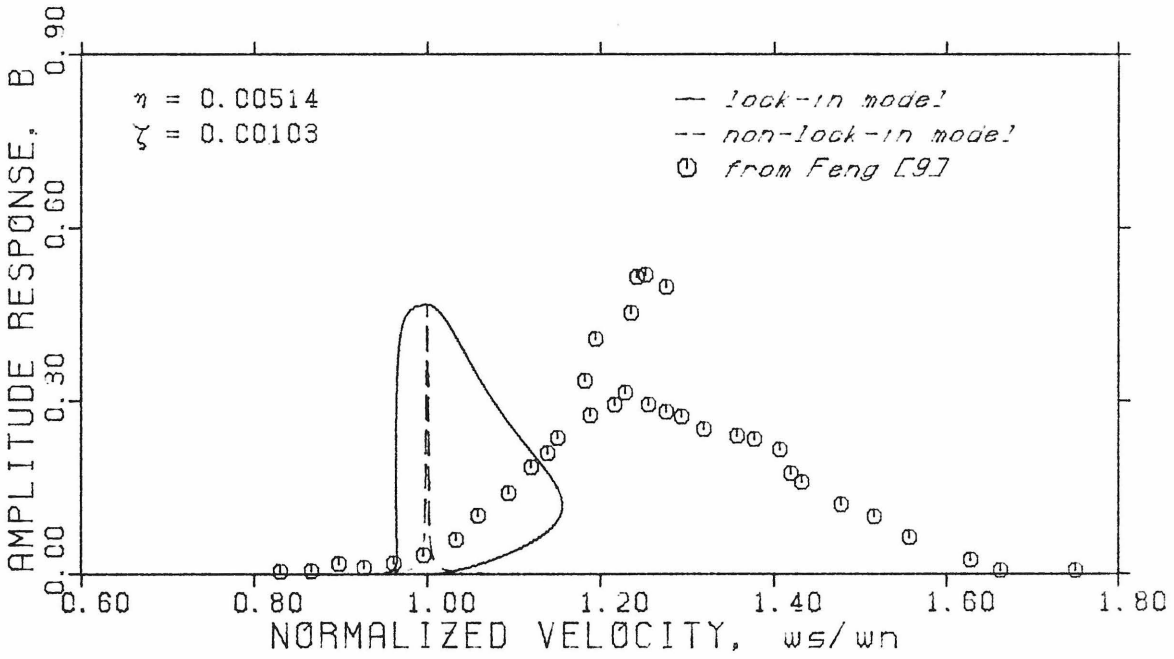

Fig. 4.3.6b

Model Versus Experimental Amplitude Response

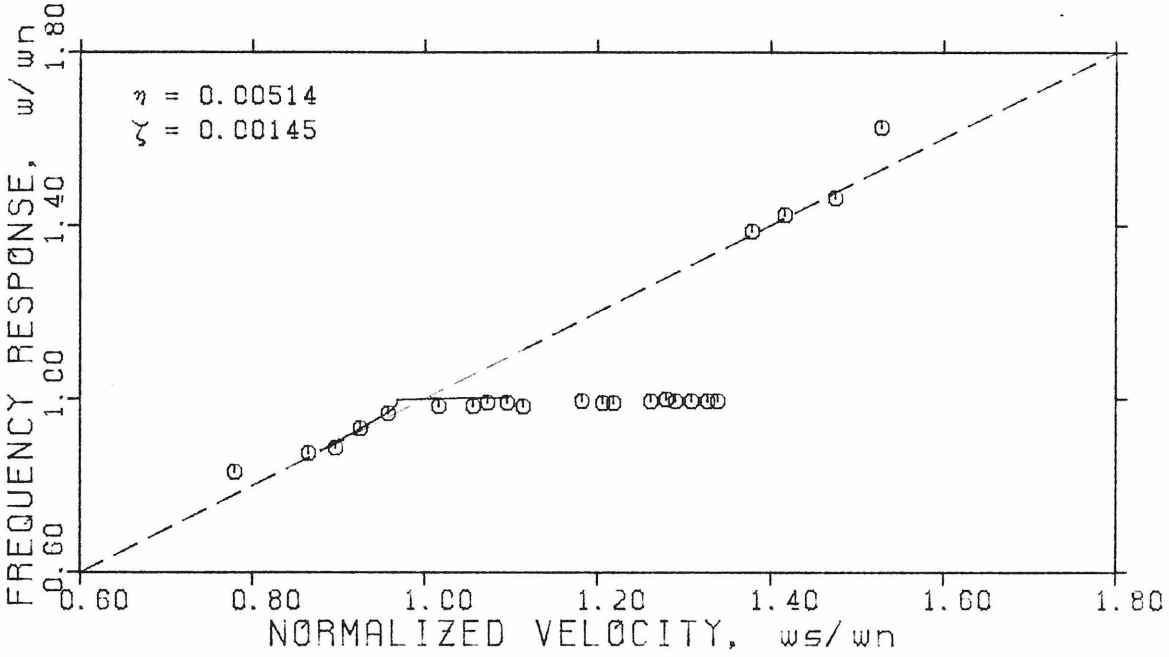

Fig. 4.3.7a

Model Versus Experimental Frequency Response

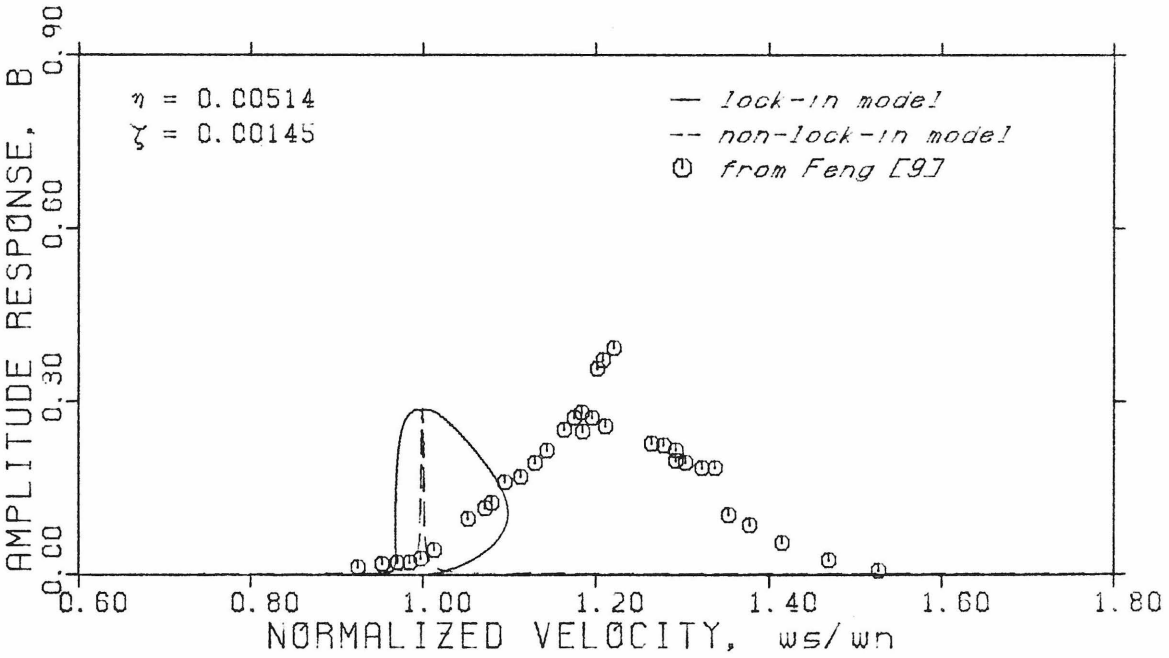

Fig. 4.3.7b

Model Versus Experimental Amplitude Response

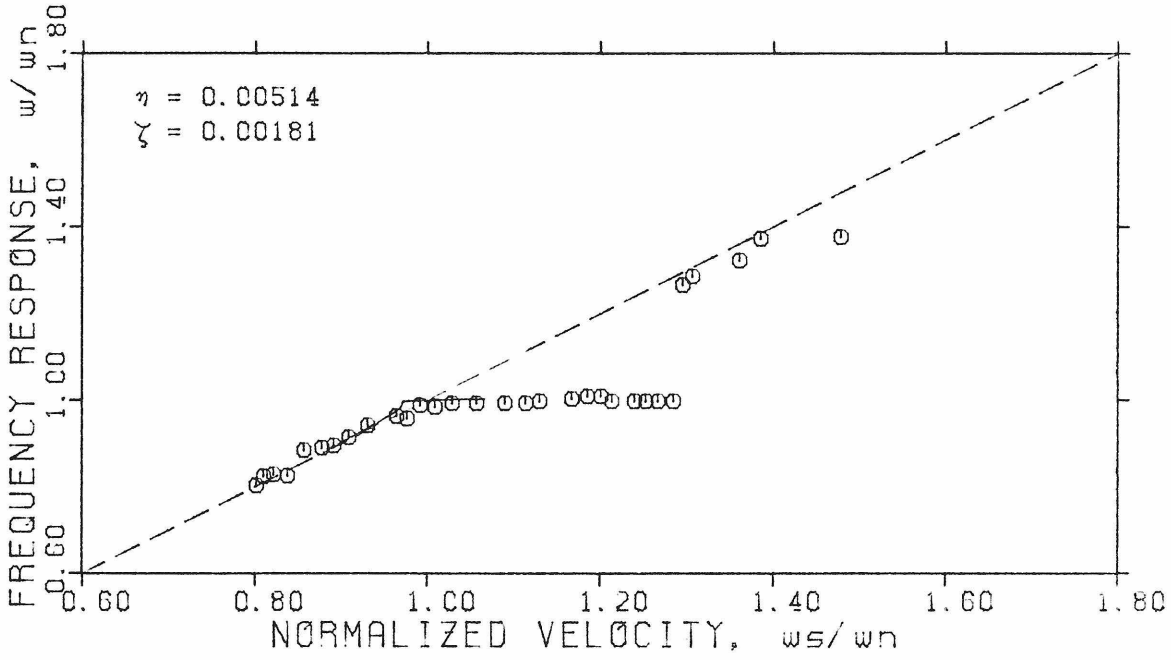

Fig. 4.3.8a

Model Versus Experimental Frequency Response

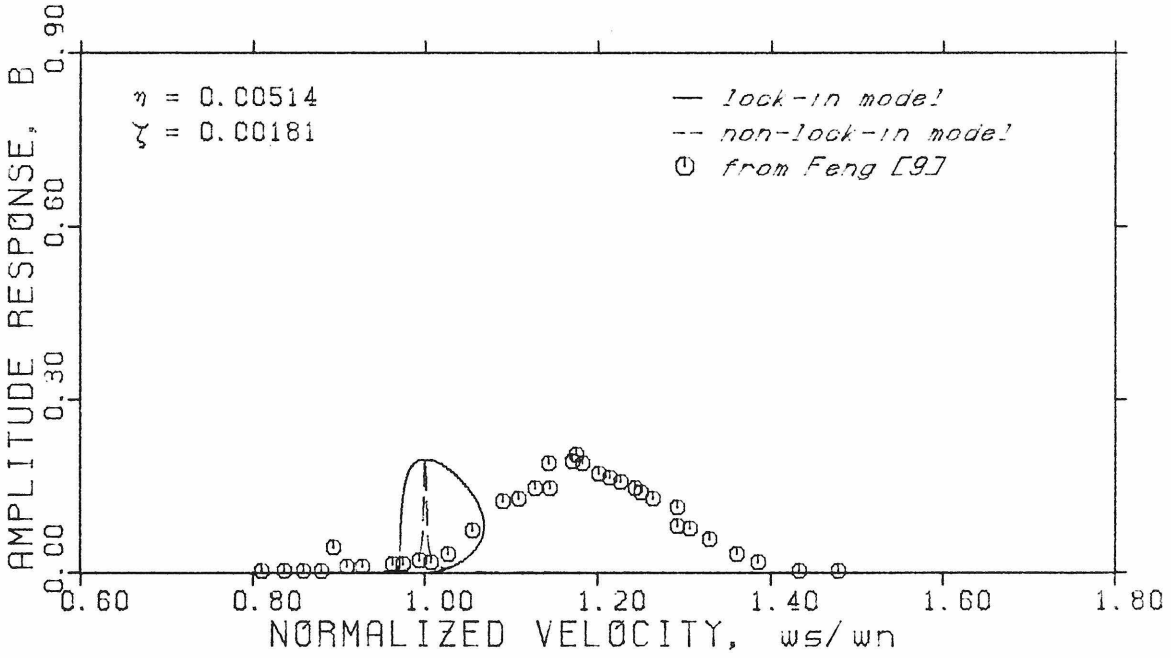

Fig. 4.3.8b

Model Versus Experimental Amplitude Response

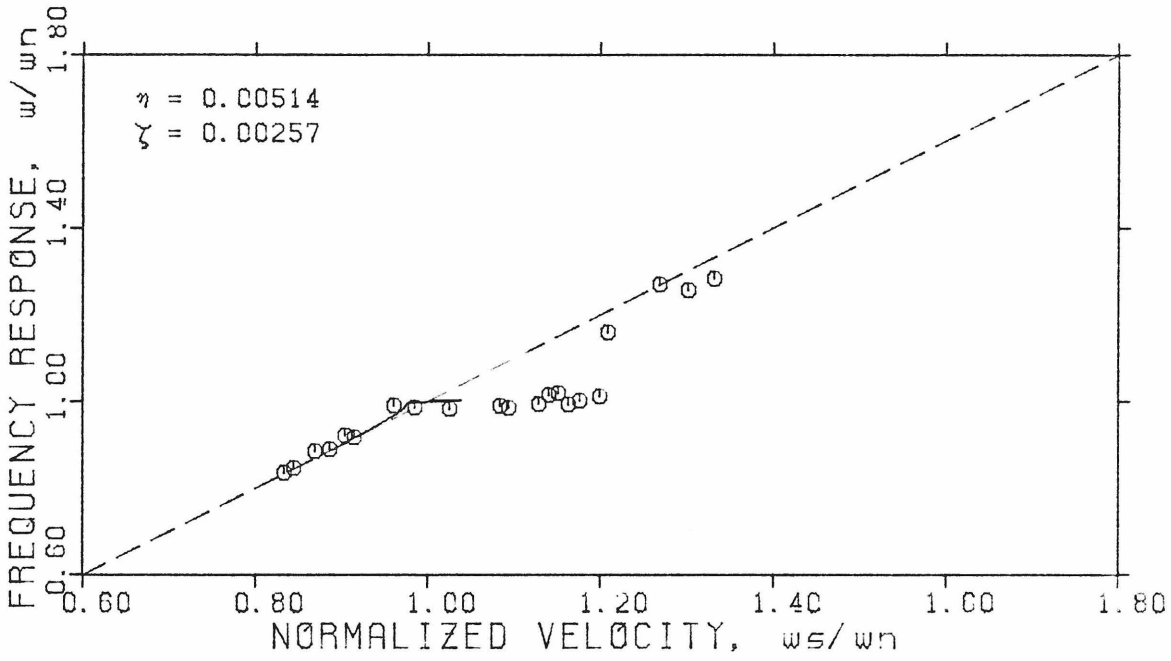

Fig. 4.3.9a

Model Versus Experimental Frequency Response

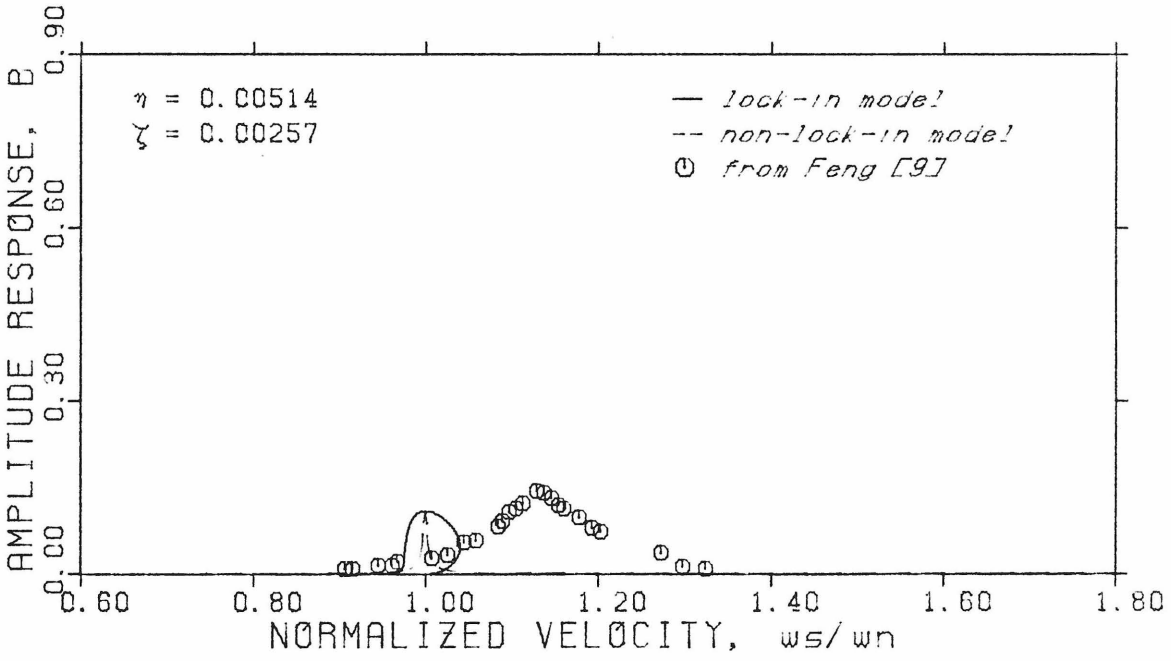

Fig. 4.3.9b

Model Versus Experimental Amplitude Response

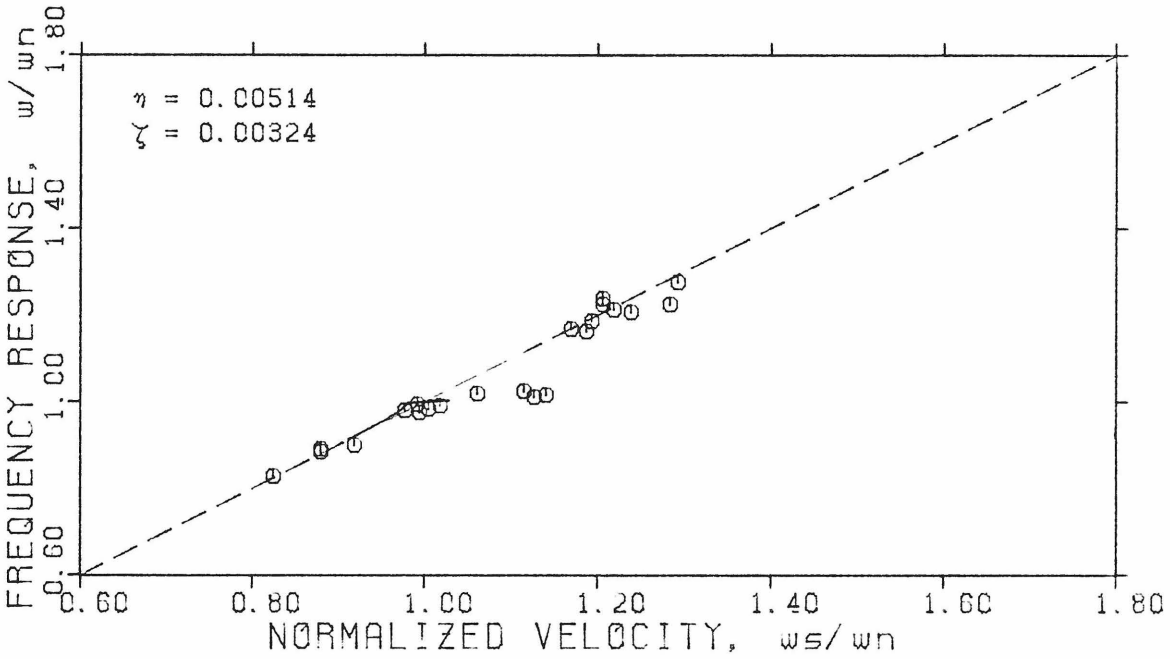

Fig. 4.3.10a

Model Versus Experimental Frequency Response

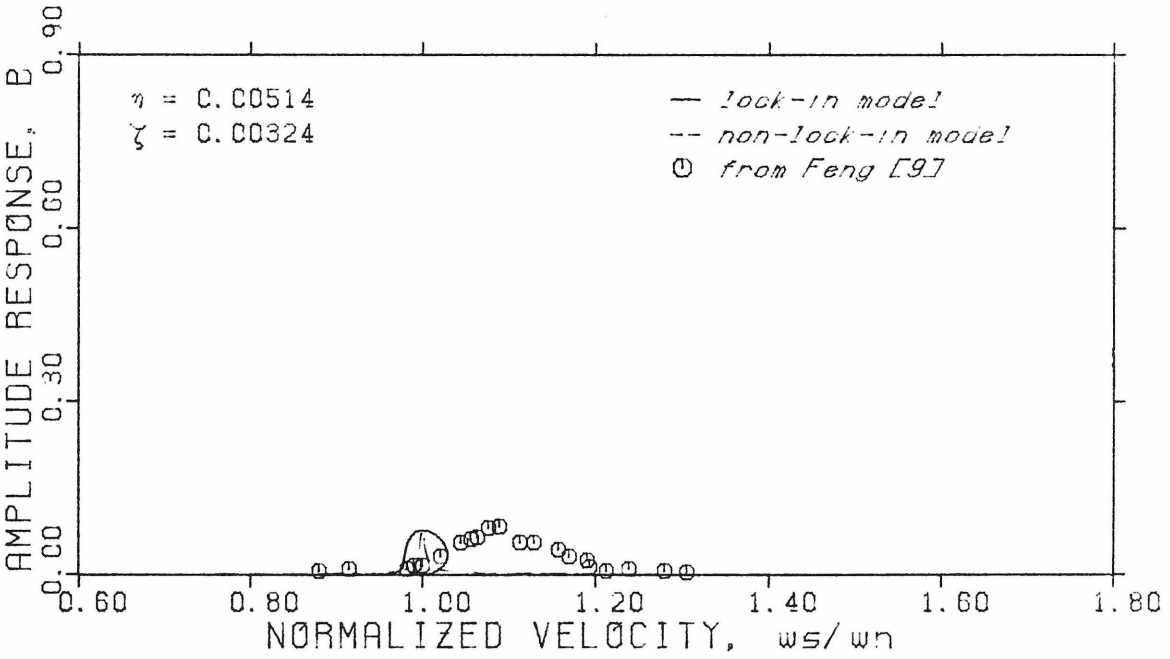

Fig. 4.3.10b

Model Versus Experimental Amplitude Response

that the response corresponding to the smaller amplitudes is always unstable. However, the same stability analysis applied to the non-locked-in response shows that solutions are stable everywhere. A jump in the solution is expected when transition from the locked-in to the non-locked-in solution occurs at increasing flow velocities.

The model predicted and experimentally observed maximum amplitudes of vibration are summarized in Table 4.3.4. It shows that maximum amplitudes are fairly accurately predicted by the present model.

Table 4.3.4

Comparison Between Experimental and Model Predictions for Maximum Amplitudes of Vibration

		B_{max}	
η	ζ	Feng [1]	Model [2]
.00514	.00103	.524	.468
.00514	.00145	.396	.288
.00514	.00181	.204	.198
.00514	.00257	.146	.110
.00514	.00324	.082	.077

[1] Feng's results [9] as digitized by Hall [29].
[2] Analytical-empirical approach

In spite of the good agreement between predicted and experimentally measured maximum amplitudes of vibration, the overall amplitude response curve for the model is consistently shifted to the left with respect to the experimental data. Furthermore, the lock-in band is roughly centered about $\omega_s/\omega_n \cong 1$. At this time, there is no totally convincing explanation as to why this difference occurs. Yet, some possible hypotheses

are, hereby, discussed:

1) It is possible that the forced cylinder experimental data have the "centered" lock-in bandwidth characteristic built in, thus, not allowing for a skewed lock-in band such as exhibited by the flexibly mounted experiments [9]. Koopman's [36] experimental results for a forced cylinder in air also show lock bandwidths centered about $\omega/\omega_s \cong 1$. This tend to lend support to this hypothesis.

2) In an attempt to compensate for the relative shift between experimental C_{mh} and C_{dh} points, the present model considers C_{dh} coefficients correct and shifts C_{mh} coefficients accordingly to the left. Then, the C_{mh} and C_{dh} coefficients, around $V_r = 5.00$, look rather like those predicted by the Wake Oscillator Model and presented in Fig. 2.3.1. Force coefficients with these characteristics, however, are bound to yield responses centered about $\omega = \omega_n = \omega_s$, similar to those shown in Fig. 2.3.2. A correction in C_{dh} coefficients (instead of in C_{mh} coefficients) has not been attempted but it is anticipated that such a correction would shift the model predictions to the right of these model predictions presented herein.

Although one could go on discussing other hypotheses that may help establish why the shift occurred, it is also important to look into why the model consistently underestimates the size of the lock-in bandwidth as shown in Figs. 4.3.6 to 4.3.10. If Feng's and Sarpkaya's experimental data are completely accurate, then this difference of almost 50% between

the size of the experimental and the predicted lock-in bandwidth seem to suggest that the results obtained in air may not be compared with those obtained in water after all. In principle, there seems to be no reason to believe that the force coefficients C_{mh} and C_{dh} would attain the same values for the same experiment performed in different fluid mediums (e.g. air, water).

In order to assess the differences of model response in air and in water, parameters η and ζ are varied according to Table 4.3.5 to simulate several fluid mediums ranging from a light fluid like air to a heavier one like water and these results are shown in Figs. 4.3.11 to 4.3.13.

Table 4.3.5

Values for η and ζ Parameters Used to Simulate Varying Fluid Media

Case #	Fluid Medium	η	ζ
1	Light	.0070	.0001
2		.0700	.0010
3	Heavy	.7000	.0100

In case 1, the mass parameter value adopted is within the range Feng used in his experiments and behavior of the model is essentially similar to that previously described. The lock-in bandwidth and amplitude are, as expected, larger since the damping ratio assumed is an order of magnitude smaller than the values used by Feng, but the overall shape of the amplitude response does not look at all like the previous model response curves pictured in Fig. 4.3.6 to 4.3.10.

The results obtained in case 2 are similar to those in case 1. The lock-in bandwidth is slightly larger and one can observe in the frequency

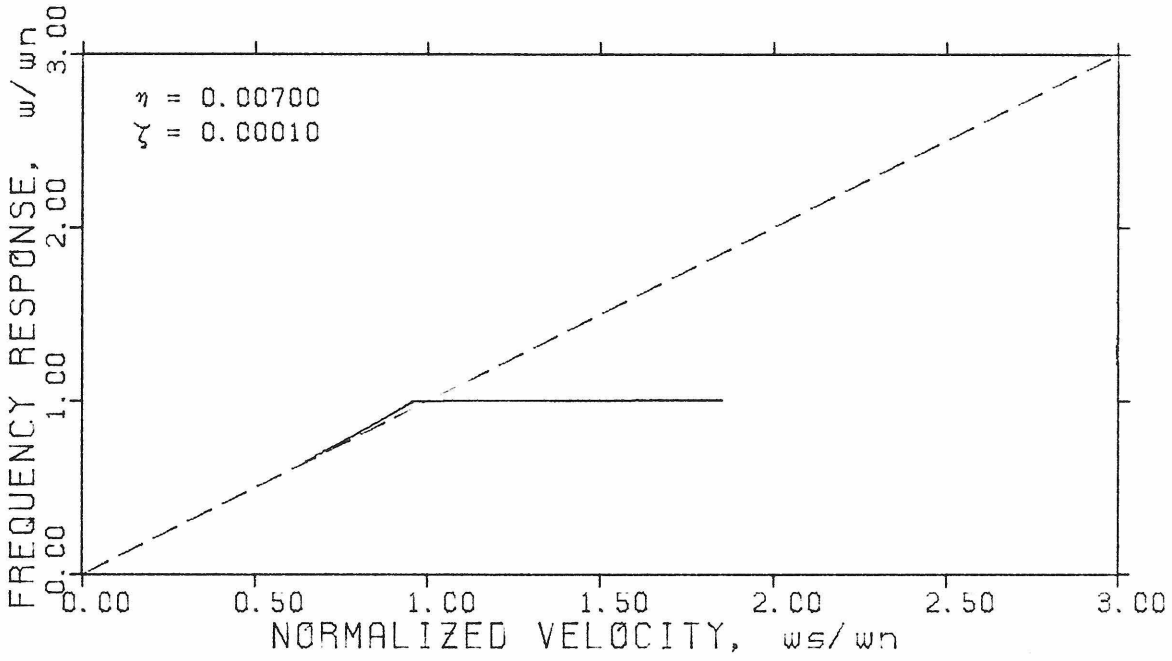

Fig. 4.3.11a

Model Prediction of Frequency Response

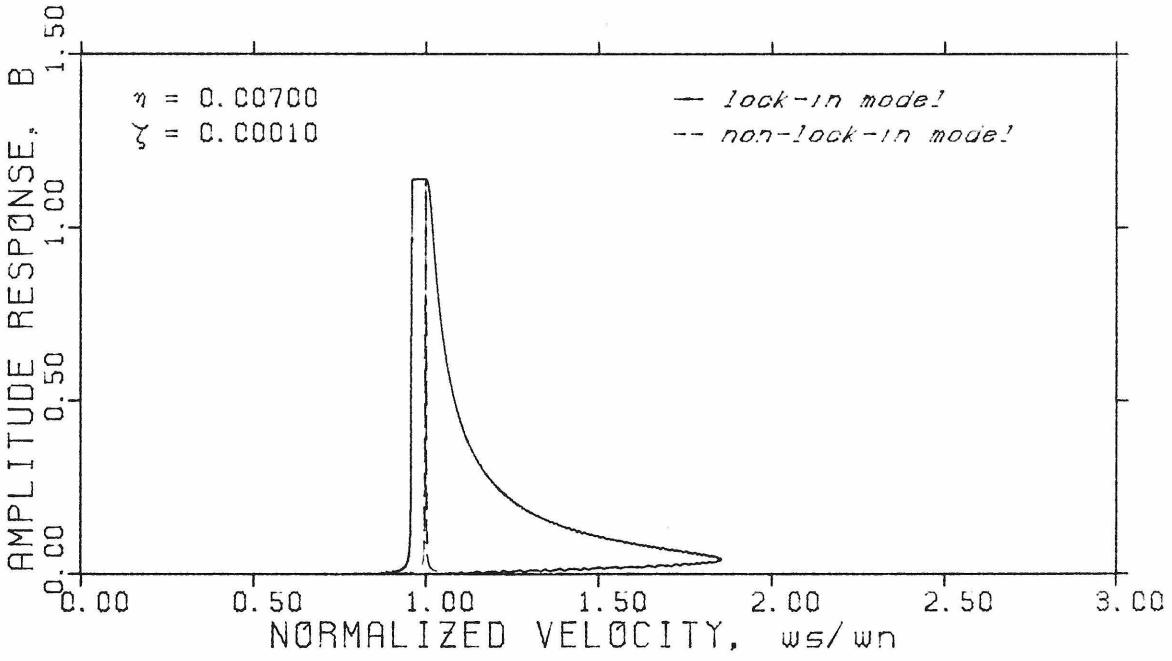

Fig. 4.3.11b

Model Prediction of Amplitude Response

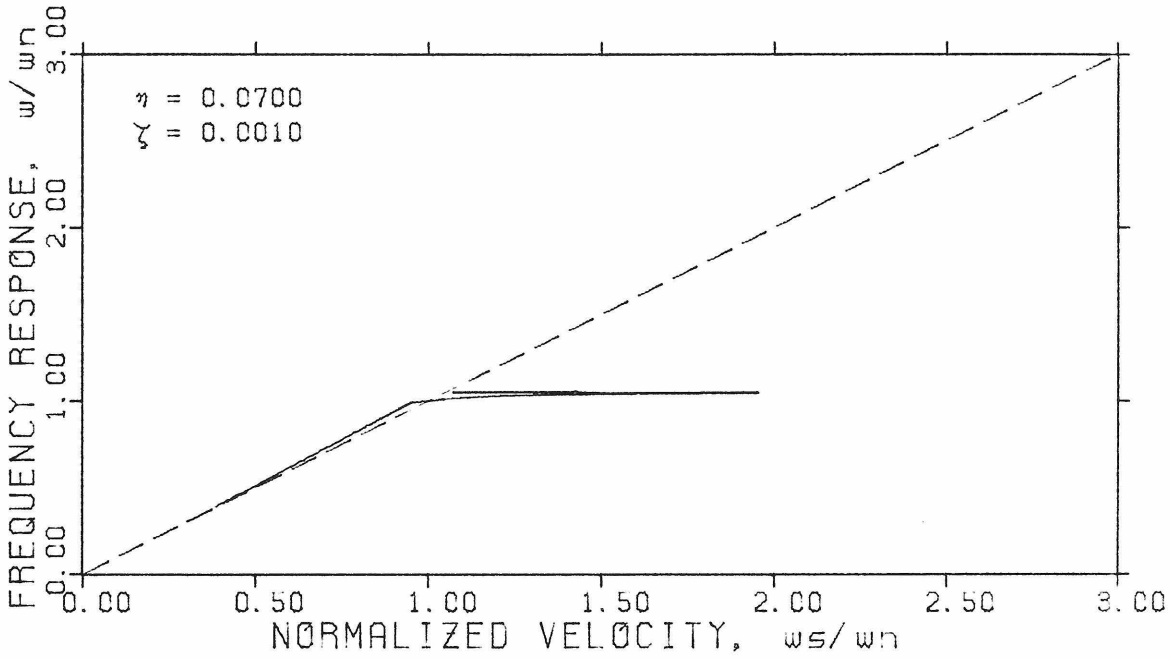

Fig. 4.3.12a

Model Prediction of Frequency Response

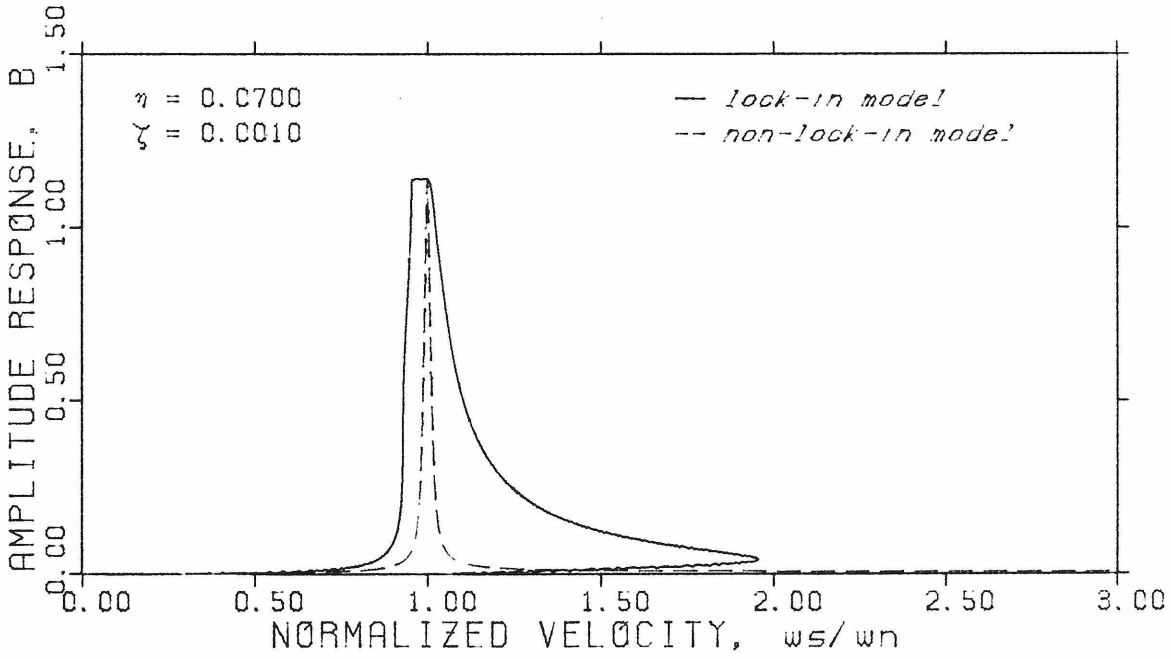

Fig. 4.3.12b

Model Prediction of Amplitude Response

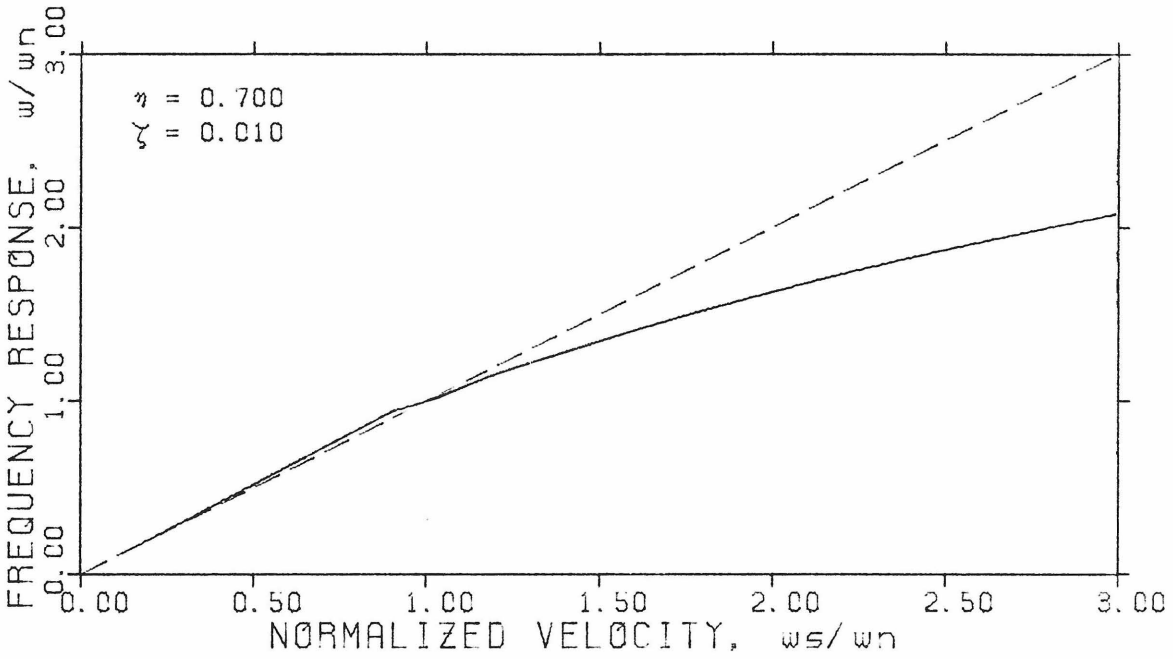

Fig. 4.3.13a

Model Prediction of Frequency Response

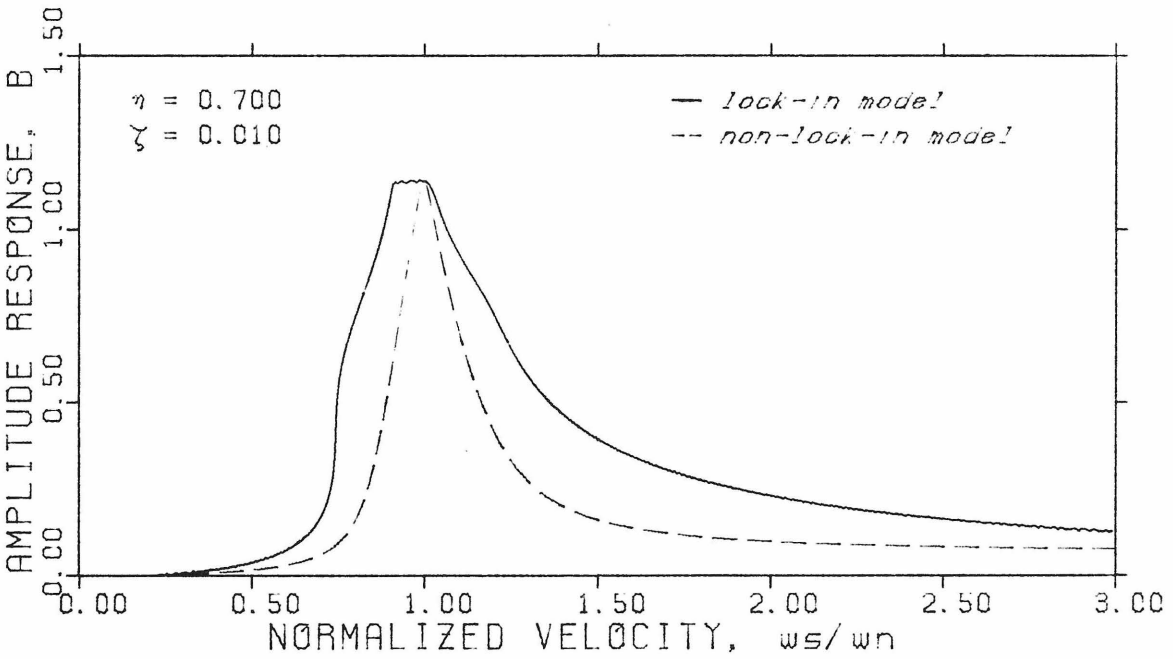

Fig. 4.3.13b

Model Prediction of Amplitude Response

plot, the incipient unfolding of the branch of unstable solutions from that of stable solutions.

Model behavior in case 3, however, is considerably different from that of cases 1 and 2. The amplitude response shows a much wider region of relatively larger amplitudes of vibration. The frequency response has a very small lock-in region (where $\omega \cong \omega_n$) next to a substantially large region of frequency entrainment within which the system responds at a frequency that is neither $\omega \cong \omega_n$ (lock-in frequency) nor $\omega \cong \omega_s$ (non-lock-in frequency). One can also note that the branch of unstable solutions has completely unfolded from that of stable solutions. These characteristics of case 3, although not present in Feng's [9] observations, are qualitatively very similar to those of the response curves of an experiment performed in water reported by Griffin [27] and reproduced in Fig. 4.3.14. The fact that the model response curves of structures in water show a better qualitative agreement with experimental data than their counterparts in air raises some doubts concerning the current practice of comparing results obtained by experiments done in water with those done in air. But only more experimental observations will dispel this doubt. However, it is believed that the present model will perform best in predicting response for structures in water.

4.3.3 An Approximate Model for the Maximum Lock-in Amplitude Response

Whether the maximum steady state amplitude of a flexibly mounted cylinder is determined by the ratio of the parameters η and ζ or by each parameter separately is a debatable point [61]. Based upon Eqs. (3.2.16) and (3.2.17), one may easily conclude that the overall response is a

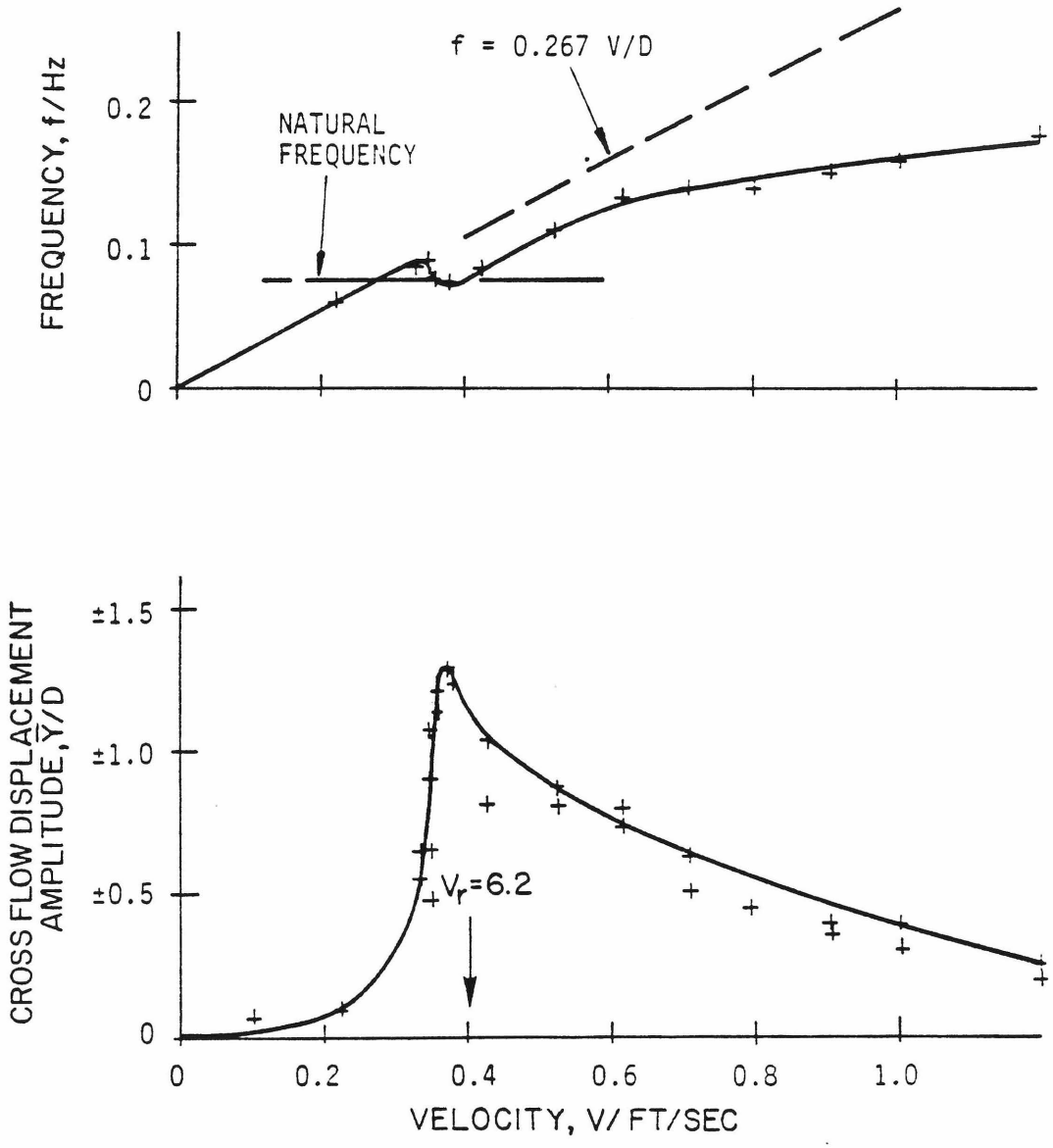

Fig. 4.3.14

Experimental Amplitude and Frequency Responses [27]

function of each parameter separately. Yet, it seems impossible to derive or to conclude any dependency between the maximum amplitude and the parameters η and ζ.

A closer look at Fig. 4.3.6 to Fig. 4.3.13 reveals that maximum amplitude occurs at $\omega_s/\omega_n \cong 1$ and $\omega/\omega_n \cong 1$, for the range of η and ζ used herein. Under these conditions, Eq. (3.2.16) can be considered approximately satisfied and one is left with Eq. (3.2.17) to solve for the amplitude, as follows,

$$2\zeta B_{max} = -\frac{\eta}{2(2\pi S)^2} \quad C_{dh}(\Omega=1,B) \qquad (4.3.11)$$

Therefore, at least in an approximate sense, one may conclude that the maximum amplitude of vibration is indeed a function of the ratio ζ/η. It should be emphasized that in the previous equation, the structural fraction of critical damping ζ must be measured in vacuum.

Since, Eq. (4.3.11) will clearly only predict approximately the maximum amplitude of vibration, a parametric study in η and ζ is undertaken in the next section, with the purpose of determining how good an approximation is this. One may verify in Figs. 4.3.11 to 4.3.13 that the parameters η and ζ were intentionally varied so to maintain a constant ratio ζ/η. In all three cases, the complete analysis yields approximately the same maximum amplitude.

So that the solution of Eq. (4.3.11) can be directly compared with other published results [25], the variable reduced damping $\hat{\zeta}$ is defined as follows

$$\hat{\zeta} = 2(2\pi S)^2 \frac{\zeta}{\eta} \qquad (4.3.12)$$

Then, Eq. (4.3.11) is rewritten as

$$2\hat{\zeta}B_{max} + C_{dh}(\Omega=1,B) = 0 \qquad (4.3.13)$$

The predicted maximum amplitude response obtained as a function of reduced damping is plotted in Fig. 4.3.15 along with experimental results compiled by Griffin[1] [25]. Agreement among the results seem quite reasonable. This is expected because, after all, this model was developed based upon the fitting of experimental values of $C_{dh}(\Omega=1,B)$. Anyway it is still remarkable that such a simple expression (Eq. (4.3.13)) can yield such good results.

By virtue of the approximations introduced, Eq. (4.3.13) will always yield the correct value for the amplitude at $\omega_s/\omega_n = 1$, even though, it may or may not coincide with that of the maximum amplitude. This will be seen in the next subsection.

4.3.4 A Parametric Study in η and ζ

To evaluate prediction capabilities of the Lock-in Model and to appraise the approximate solutions for the stability boundaries (Eq. 3.3.34)) and for the maximum amplitudes (Eq. (4.3.13)) a parametric study is, hereby, undertaken. The results obtained are presented in Figs. 4.3.16 to 4.3.20.

In Fig. 4.3.16, while the mass ratio η is kept constant, equal to 0.00514, the fraction of critical damping ζ is varied within the range

---

[1] According to private communication, only structural damping measured in still air has been used in compiling these results.

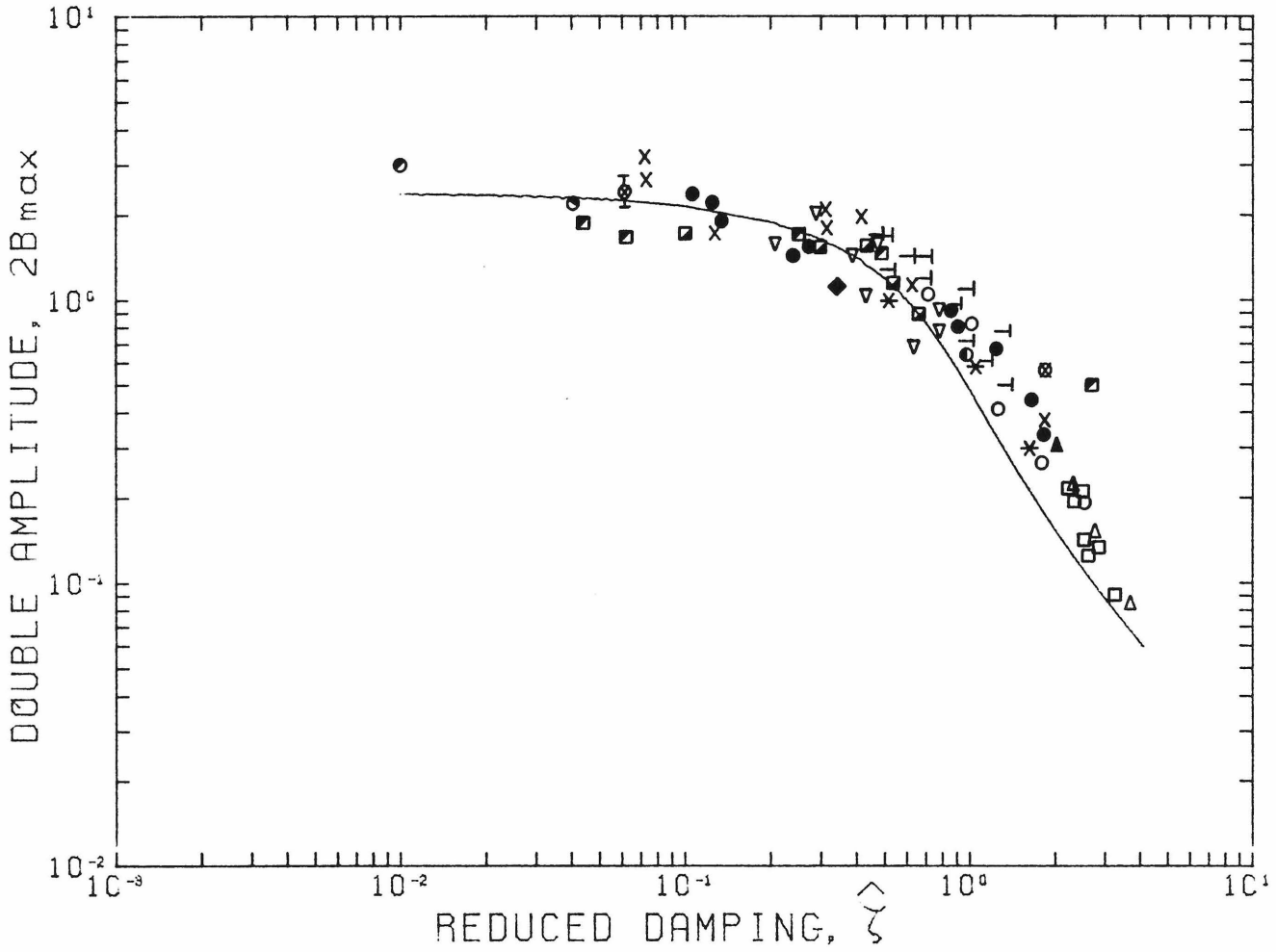

Fig. 4.3.15

Comparison Between Maximum Amplitude Response as Predicted by Eq. (4.3.13) and Experimental Results [25]

considered by Feng [9] in his experiments. Approximate results for both the maximum amplitudes and the stability boundaries, are virtually coincident with those obtained by exact analysis.

In Figs. 4.3.17 to 4.3.20, the mass ratio η takes on the values 0.05, 0.10, 0.20, and 0.50, respectively. In each of the four figures, the corresponding η is kept constant while the fraction of critical damping ζ is varied so the ratio ζ/η takes on the values given in the first column of Table 4.3.6. In this manner, Eq. (4.3.13) for predicting the approximate maximum amplitudes is thoroughly tested for a wide range of values of η. How these results compare with those obtained from the exact analysis is shown in Table 4.3.6.

Table 4.3.6

Comparison of Approximate and Exact Maximum Amplitudes

ζ/η	B_{max} [1] (approximate)	B_{max} [2] (exact)			
		$\eta = 0.05$	$\eta = 0.10$	$\eta = 0.20$	$\eta = 0.50$
1.00	.041	.041	.041	.041	.048
.50	.109	.109	.110	.112	.138
.30	.260	.260	.262	.268	.304
.20	.469	.469	.470	.474	.494
.10	.800	.800	.800	.800	.802
.06	.955	.955	.955	.955	.955

[1] obtained from Eq. (4.3.13).
[2] obtained through the complete analysis.

In general, maximum amplitudes are predicted very well by Eq. (4.3.13), but the results deteriorate as η and ζ increase. The worst results occur where structural damping is high, over 10%. This, however,

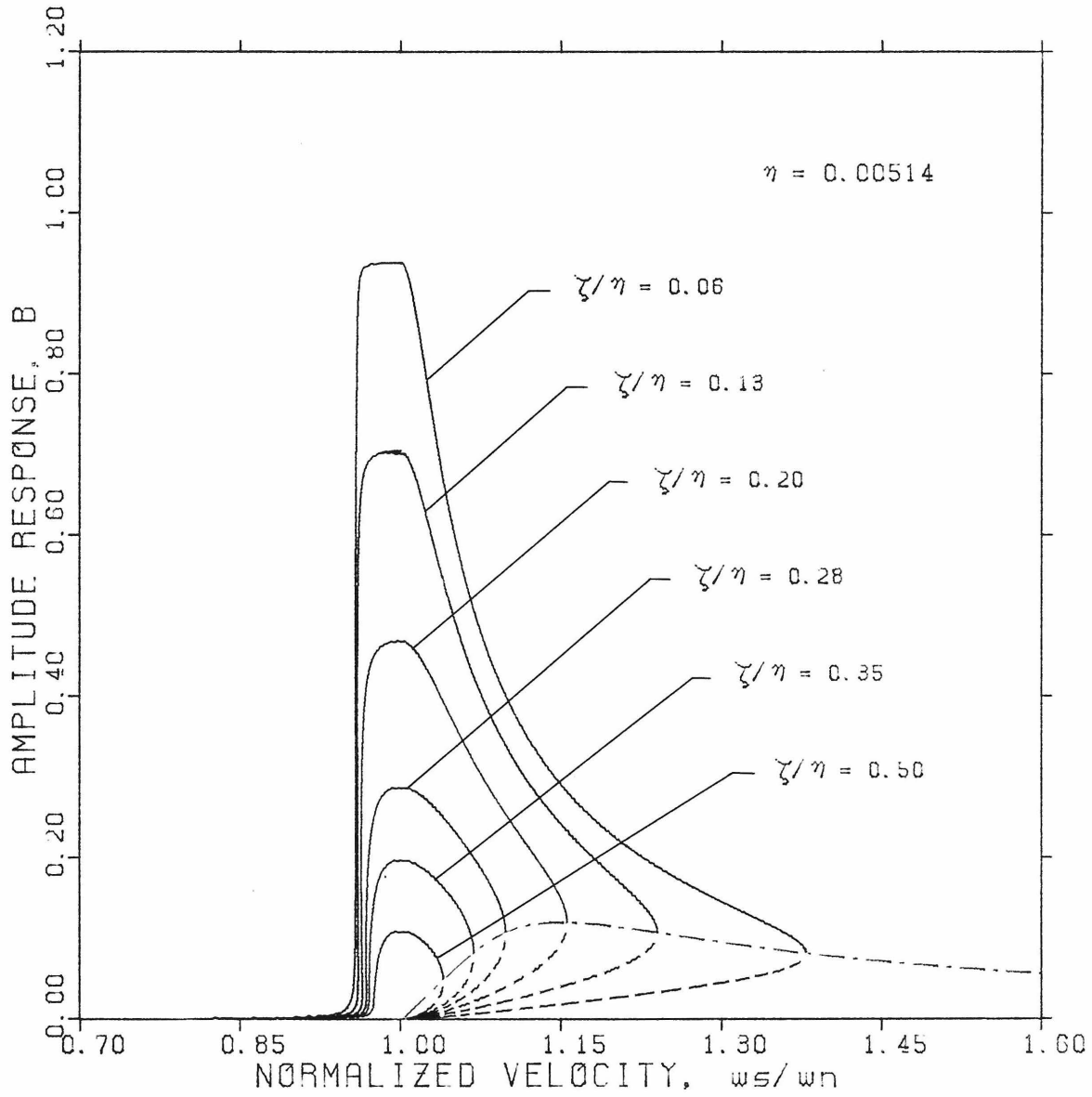

Fig 4.3.16

Parametric Study of Lock-in Model

——— Stable Solutions

– – – – Unstable Solutions

——– – – Approximate Stability Boundary

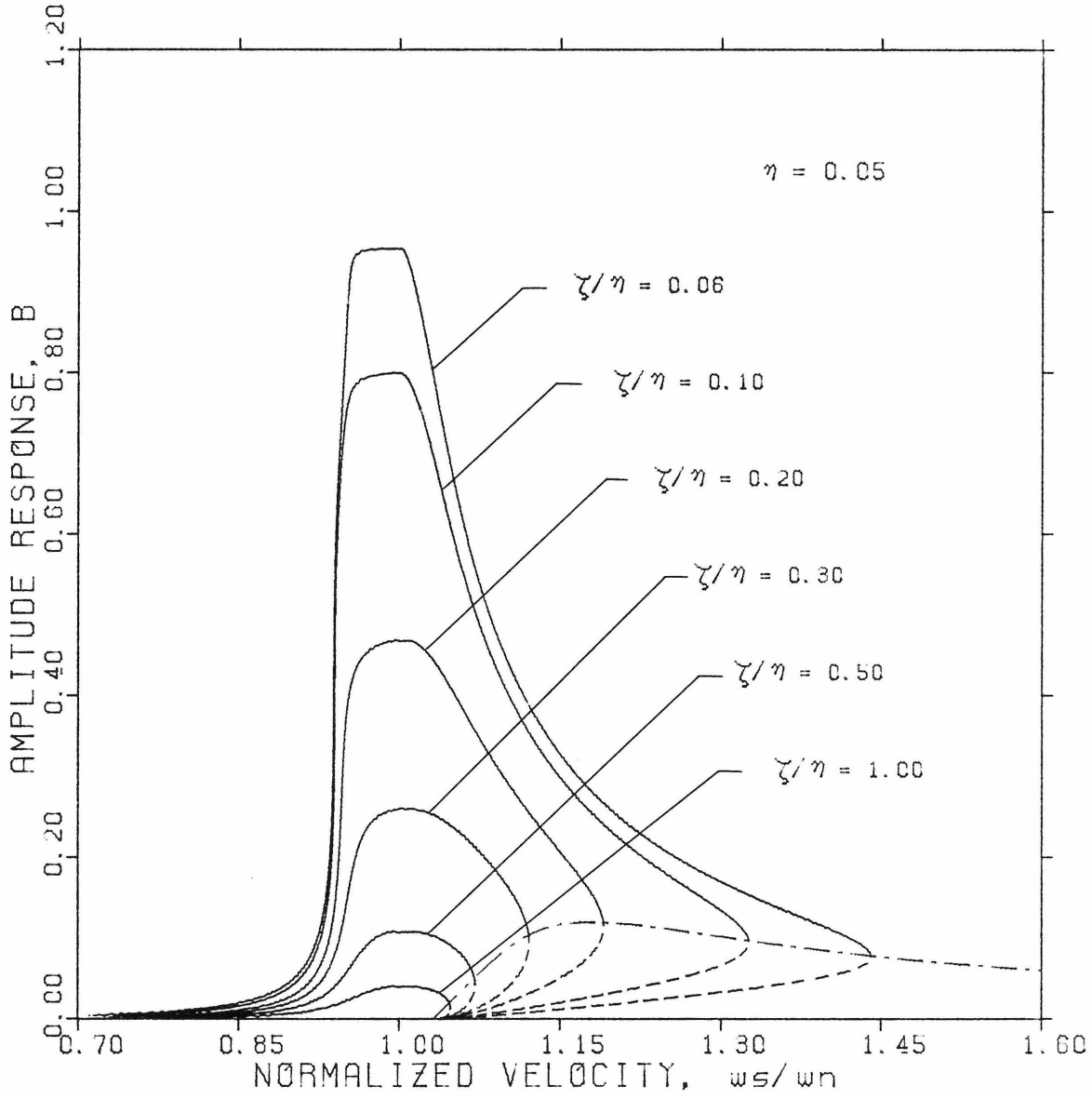

Fig. 4.3.17

Parametric Study of Lock-in Model

——— Stable Solutions

– – – – Unstable Solutions

——– – —— Approximate Stability Boundary

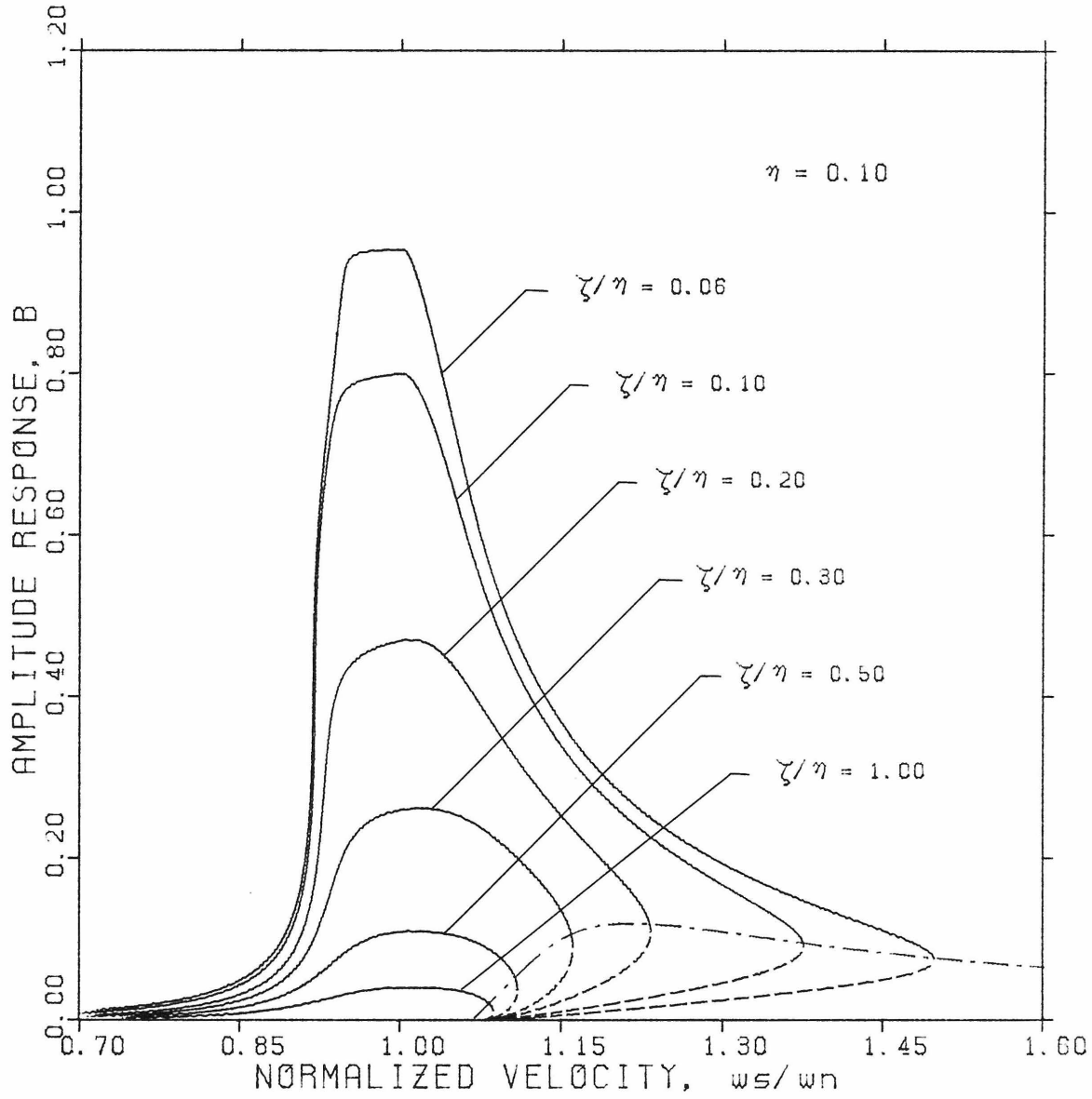

Fig. 4.3.18

Parametric Study of Lock-in Model

——— Stable Solutions

– – – – Unstable Solutions

——– – – Approximate Stability Boundary

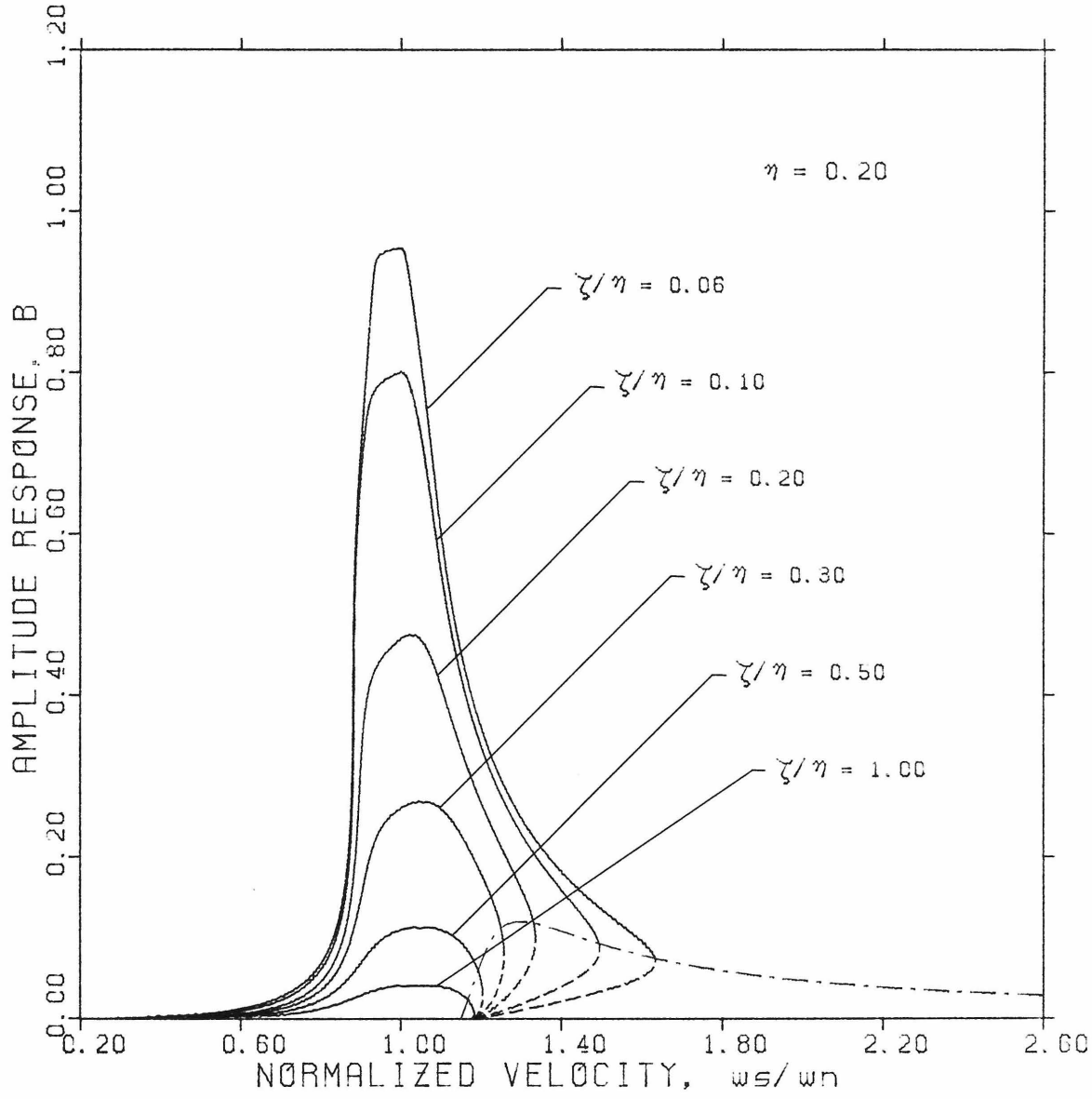

Fig. 4.3.19

Parametric Study of Lock-in Model

——— Stable Solutions

– – – – Unstable Solutions

——– – – Approximate Stability Boundary

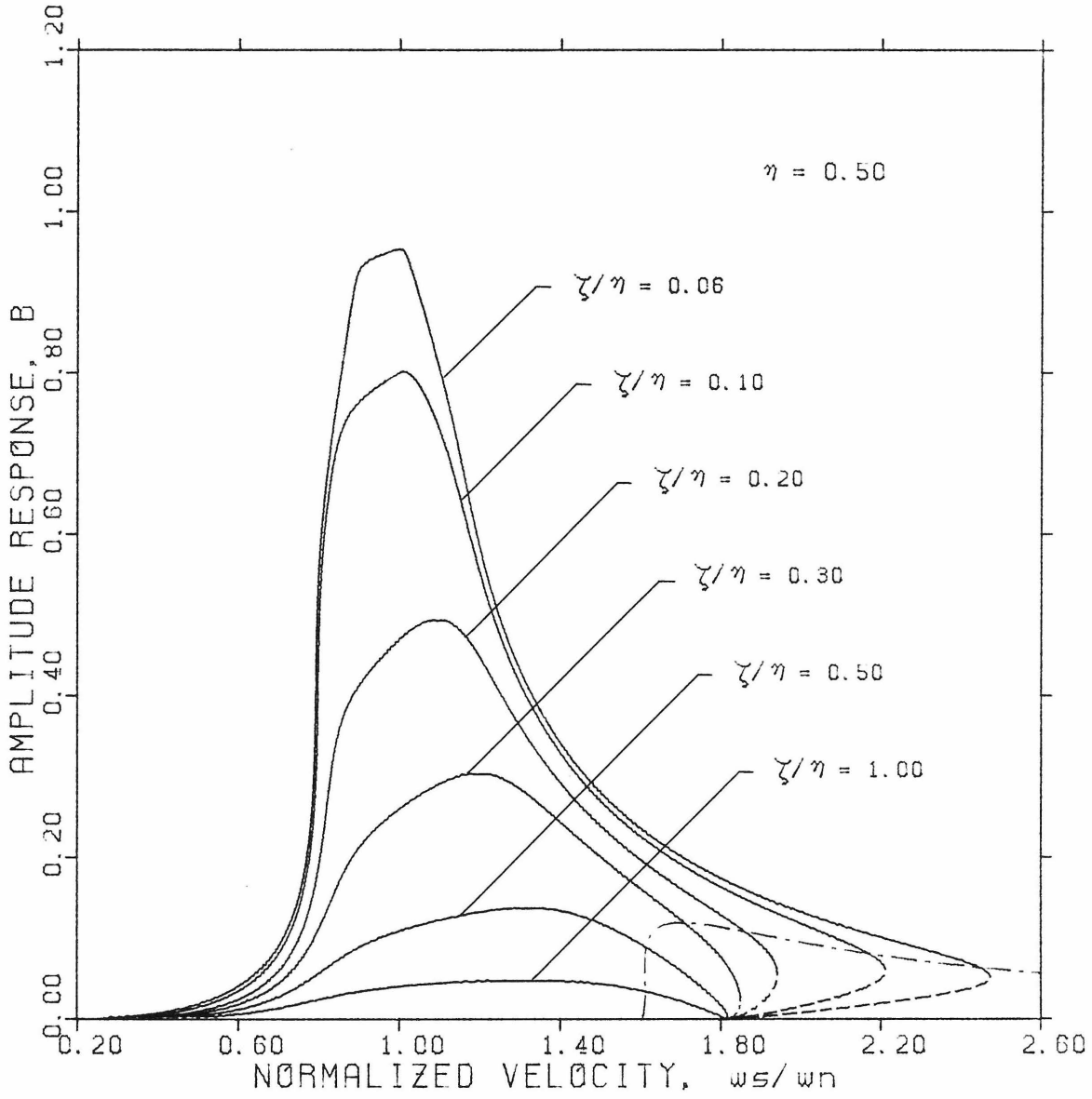

Fig. 4.3.20

Parametric Study of Lock-in Model

——— Stable Solutions

– – – – Unstable Solutions

——– – – Approximate Stability Boundary

does not pose a severe problem since structures, in practice, do not present such large damping. Therefore, it appears reasonable to conclude that maximum amplitudes predicted by Eq. (3.4.15) may be used for all practical purposes.

As for the stability boundaries, the region delimited by Eq. (3.3.34) is, in general, coincident with the actual unstable region. Again, results deteriorate as η and ζ increase, yet all unstable solutions are contained within the approximate stability boundary given by Eq. (3.3.34).

4.3.5 Amplitude Response Bandwidth

From the aforementioned it is now clear that large amplitudes of vibration and frequency entrainment may occur over a wide range of normalized velocities.

In order to have an expeditious way of predicting the characteristics of the amplitude response curves, the following bandwidths are defined:

1) According to the classical half power method, the bandwidth $\Delta\omega_1$ is determined from the frequencies at which the response is reduced to $B_{max}/\sqrt{2}$, as

$$\Delta\omega_1 = \left(\frac{\omega_s}{\omega_n}\right)_b - \left(\frac{\omega_s}{\omega_n}\right)_a$$

where at both points $(\omega_s/\omega_n)_a$ and $(\omega_s/\omega_n)_b$, the amplitude response is $B_{max}/\sqrt{2}$.

2) Alternately, the bandwidth may be defined as the region where the frequency of vibration differs substantially from the Strouhal frequency (i.e., $\omega \neq \omega_s$). The frequency entrainment bandwidth $\Delta\omega_2$ is then given by

$$\Delta\omega_2 = \left(\frac{\omega_s}{\omega_n}\right)_c - \left(\frac{\omega_s}{\omega_n}\right)_a$$

where $(\omega_s/\omega_n)_a$ is the smaller of the normalized frequencies at which amplitude response is $B_{max}/\sqrt{2}$ and $(\omega_s/\omega_n)_c$ corresponds to the normalized frequency at which the amplitude response lies on the stability boundary.

A pictorial representation of each definition is shown in Fig. 4.3.21.

In Fig. 4.3.22, plots for both bandwidths $\Delta\omega_1$ and $\Delta\omega_2$ as functions of η and ζ are presented. In general, one can infer that, for small damping and large mass ratio (e.g. light cylinder in water), the amplitude response curve will be narrow at $B_{max}/\sqrt{2}$ ($\Delta\omega_1 \cong 0.15$) while associated with a relatively larger frequency entrainment region ($\Delta\omega_2 >> 0.60$). As damping increases, one bandwidth tends to the other, then much smaller regions of frequency entrainment can be expected. Note that amplitude and frequency responses for structures in water, that is, for values of $\eta > 0.10$, are expected to be more accurately predicted.

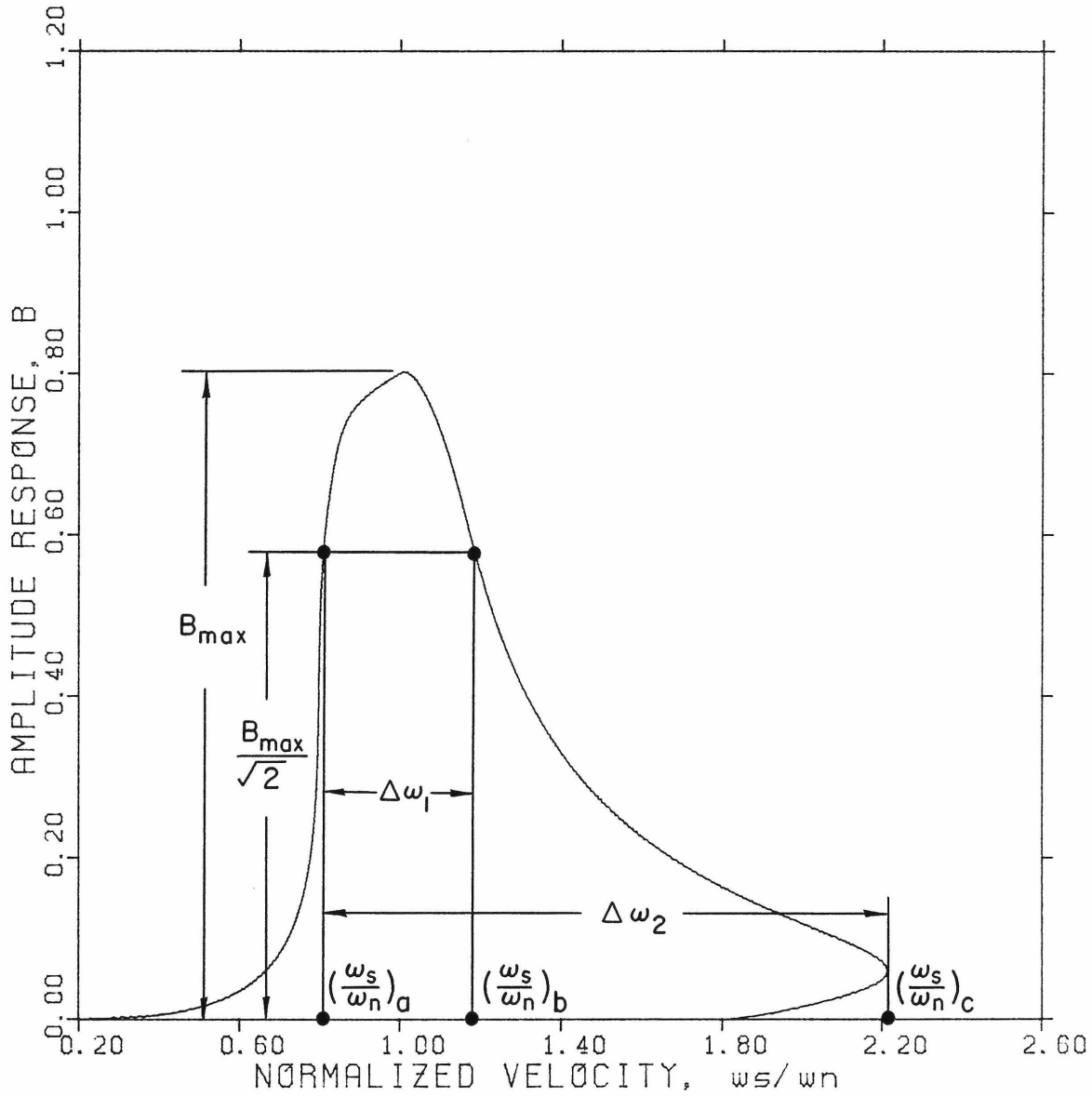

Fig. 4.3.21

Bandwidth Definitions

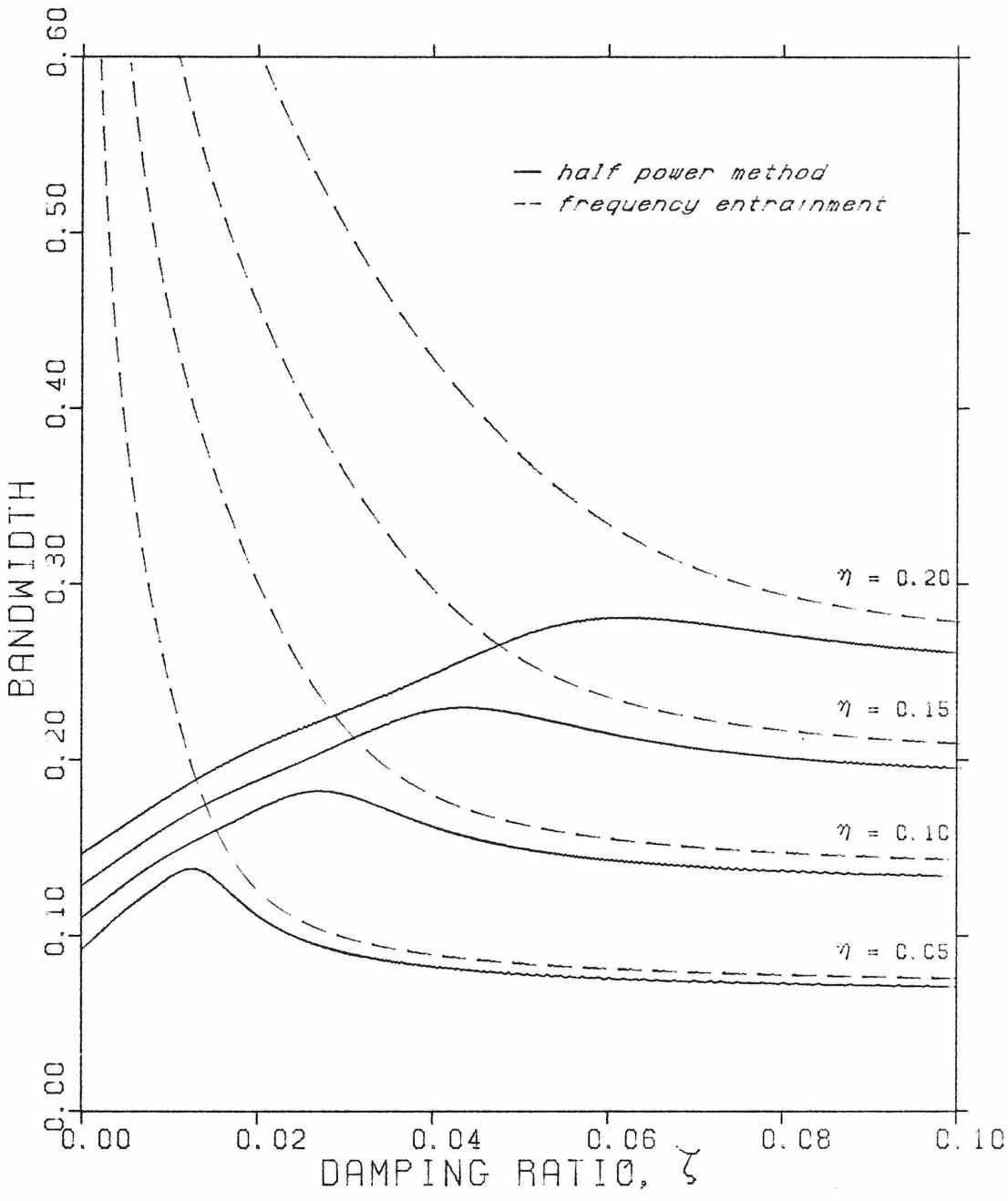

Fig. 4.3.22

Functional Relations of Bandwidths and Damping Ratio

CHAPTER V

SUMMARY AND CONCLUSIONS

Using an analytical-empirical approach in this thesis, the problem of vortex-induced vibration of circular cylinders has been undertaken. A new model has been derived, based solely upon measurements of forces acting on a cylinder forced to vibrate in a uniform aqueous flow. This model predicts response of flexibly-mounted cylinders as a function of the structural system and flow parameters. The predicted model response has been compared to that obtained from flexibly mounted cylinder experiments in a wind tunnel. In Chapter I, the basic phenomena of vortex shedding and lock-in have been reviewed for both structural configurations of interest to this research effort, namely, forced and flexibly mounted cylinders in uniform flow.

Experimental results [61] that constitute the basis for development of the present model have been reviewed and discussed in Chapter II. Also reviewed and discussed in this chapter are the experimental data [9] used to evaluate the response curves predicted by the present model. A short review of previous analytical models for flow induced vibrations with emphasis on the Wake Oscillator Model has also been included. The latter model has been used to predict the forces acting on a cylinder forced to vibrate, in a harmonic motion, transverse to a uniform flow. Subsequently, these predicted forces have been used in the discussion of model results.

In Chapter III, the new model for flow induced steady-state response has been developed. Response under lock-in and non-lock-in conditions

has been treated separately. Model response has been determined to be a function of the following parameters: mass ratio (η), structural damping ratio (ζ), structural natural frequency (ω_n), Strouhal frequency (ω_s) and the Strouhal number (S), each of which can be independently varied. Analysis of model equations has shown that induced oscillations are possible only within certain ranges of reduced velocity, hence better defining the range where necessary experimental efforts should concentrate.

In anticipation to multiple responses, a stability analysis of the steady-state response has been carried out through a perturbation approach that closely resembles the Method of Slowly Varying Parameters. In addition, an expression for an approximate stability boundary, under lock-in conditions has been derived and shown to be dependent only on the mass ratio parameter.

In Chapter IV, the present model has been fully analyzed. First, by a purely empirical approach in which only the actual experimental data points have been used. This analysis has shown that force measurements from forced cylinders experiments can be used to predict amplitude and frequency responses of flexibly mounted cylinders. It has also shown the relative role played by the mass ratio and the structural damping ratio. Furthermore, it has evidenced inconsistencies in the available experimental data allowing some corrective measures to be incorporated into the analytical-empirical approach.

In this analytical-empirical approach, analytical expressions have been used to interpolate the experimental data in order to obtain continuous model prediction curves. Model amplitude and frequency responses have been compared with those observed in flexibly mounted cylinder

experiments in a wind tunnel and have been shown to exhibit several experimentally observed characteristics. Maximum amplitude of vibration is attained within the entrainment band, where the vortex shedding frequency ω_v is entrained by the natural frequency ω_n of the cylinder. Furthermore, amplitude and frequency jumps are observed at the upper end of the entrainment band.

Comparison between model and experimental responses also has shown that even though maximum amplitudes of vibration are fairly accurately predicted, the amplitude response curves are consistently shifted to the left with respect to the experimental ones, while entrainment bandwidths are underestimated. Such discrepancies have lead to doubts concerning the validity of comparing results obtained in experiments performed in water with those performed in air. These doubts were further substantiated by the striking similarities observed between model response curves and those obtained from an experiment performed in water. Hence, the model will best predict for structures in water.

An expression to predict maximum amplitudes of vibration as a function of the reduced damping ζ has been derived based on model response predictions. Then a parametric study undertaken has shown this expression to yield results with virtually no errors for a relatively large range of damping values ($0\%<\zeta<10\%$). The maximum amplitudes predicted by the expression compares well with experimental results compiled elsewhere.

Directed toward a better understanding of the manner in which amplitude response curves vary as a function of η and ζ, frequency entrainment bandwidth and the half power bandwidth have been plotted as functions of these parameters.

Suggestions for further research

As an immediate extension of this work, it is suggested that the methodology involved in the application of this present model be extended to flexible structures (i.e. cables and beams). More subtle, however, is the possible application of this model to uniform structures in spanwise sheared velocity flow or spanwise non-uniform structures in uniform velocity flow. It is strongly suggested that this be also pursued.

Certainly, when more experimental data become available, several doubts raised within the context of this work, particularly, concern expressed over the validity of comparing results obtained from experiments done in water with those done in air, will be dispelled. Therefore experimental work directed towards this objective is also suggested.

From the structural engineering point of view, it is important to be able to predict the nature of flow induced vibration whether or not the basic fluid mechanics is completely understood. It is hoped that the present model as well as the proposed future research will make a positive contribution towards this goal.

REFERENCES

[1] Berger, E., "Analysis of Vortex-Induced Vibrations, by an Improved Oscillator Model", Technische Universitat Berlin, Preprint, 1979.

[2] Bishop, R.E.D., and Hassan, A.Y., "The Lift and Drag Forces on a Circular Cylinder in a Flowing Fluid", Royal Society of London, Proc. Ser. A., vol. 277, pp. 32-75, 1964.

[3] Blevins, R.D., "Flow Induced Vibration of Bluff Structures", Ph.D. Thesis, California Institute of Technology, 1974.

[4] Blevins, R.D., and Burton, T.E., "Fluid Forces Induced by Vortex Shedding", Fluids Engineering Conference, paper No. 75-FE-10, Minneapolis, Minn., May 1975.

[5] Blevins, R.D., Flow Induced Vibrations, Van Nostrand Reinhold Company, New York, 1977.

[6] Blevins, R.D., "Flow-Induced Vibrations in Nuclear Reactors: A Review", Progress in Nuclear Energy, vol. 4, pp. 25-49, Pergamon Press, 1979.

[7] Bogoliubov, N.N., and Mitropolsky, Y.A., Asymptotic Methods in the Theory of Non-Linear Oscillations", Hindustan Publishing Company, Delhi, India, 1961.

[8] Dowdy, J.A., and Black, J.L., "Current Induced Motion of an Elastically Supported Circular Cylinder", Chevron Oil Field Research Company, La Habra, CA 1972.

[9] Feng, C.C., "The Measurement of Vortex-Induced Effects in Flow Past Stationary and Oscillating Circular and D-Section Cylinders", M.A.Sc. Thesis, University of British Columbia, 1968.

[10] Every, M.J., King, R., and Griffin, O.M., "Hydrodynamic Loads on Flexible Marine Structures Due to Vortex Shedding", ASME Winter Meeting, paper No. 81-WA/FE-24, Washington, D.C., November 1981.

[11] Ferguson, N., "The Measurement of Wake and Surface Effects in the Subcritical Flow Past a Circular Cylinder at Rest and in Vortex-Excited Oscillations", M.A.Sc. Thesis, University of British Columbia, 1965.

[12] Fortik, D.F., "Forced Oscillations of a Cylinder in Uniform Flow", M.S. Thesis, Naval Postgraduate School, Monterey, CA 1976.

[13] Gardner, T.N. and Cole, M.W., "Deep Water Drilling in High Current Environment", Offshore Technology Conference, Houston, Texas, May 1982.

[14] Griffin, O.M. and Votaw, C.W., "The Vortex Street in the Wake of a Vibrating Cylinder", J. Fluid Mech., vol. 51, part 1, pp. 31-48, 1972.

[15] Griffin, O.M., "Flow Near Self-Excited and Forced Vibrating Circular Cylinders", J. Eng. for Ind., vol. 94, pp. 539-547, May 1972.

[16] Griffin, O.M., Skop, R.A., and Koopman, G.H., "The Vortex-Excited Resonant Vibrations of Circular Cylinders", J. Sound and Vibration, vol. 31, part 2, pp. 235-249, 1973.

[17] Griffin, O.M. and Ramberg, S.E., "The Vortex-Street Wakes of Vibrating Cylinders", J. Fluid Mech., vol. 66, part 3, pp. 553-576, 1974.

[18] Griffin, O.M., Skop, R.A., and Ramberg, S.E., "The Resonant, Vortex-Excited Vibrations of Structures and Cable Systems", Offshore Technology Conference, paper No. OTC 2319, Dallas, TX, 1975.

[19] Griffin, O.M., "Vortex-Induced Lift and Drag on Stationary and Vibrating Bluff Bodies", J. Hydronautics, vol. 9, No. 4, pp. 160-164, October 1975.

[20] Griffin, O.M. and Koopman, G.H., "The Vortex-Excited Lift and Resistance Forces on Resonantly Vibrating Cylinders", Advance Copy, 1976.

[21] Griffin, O.M., Ramberg, S.E., and Skop, R.A., "Flow-Induced Vibrations of Mooring Arrays", FY1977 Final Report, Ocean Technology Division, Naval Research Laboratory, Washington, D.C., November 15, 1977.

[22] Griffin, O.M., "Vortex-Excited Unsteady Forces on Resonantly Vibrating, Bluff Structures", Naval Research Laboratory, Memorandum Report 3820, August 1978.

[23] Griffin, O.M., Ramberg, S.E., and Skop, R.A., "Flow-Induced Vibrations of Mooring Arrays", FY1979 Final Report, Ocean Technology Division, Naval Research Laboratory, Washington, D.C., September 30, 1979.

[24] Griffin, O.M., et. al., "Vortex-Excited Vibrations of Marine Cables", J. Waterway, Port, Coastal and Ocean Div., ASCE, vol. 106, No. WW2, pp. 183-204, May 1980.

[25] Griffin, O.M., "OTEC Cold Water Pipe Design for Problems Caused by Vortex-Excited Oscillations", Naval Research Laboratory, Memorandum Report 4157, March 14, 1980.

[26] Griffin, O.M., "Vortex-Shedding from Stationary and Vibrating Bluff Bodies in a Shear Flow", Naval Research Laboratory, Memorandum Report 4287, August 11, 1980.

[27] Griffin, O.M., "Steady Hydrodynamic Loads Due to Vortex Shedding from the OTEC Cold Water Pipe", Naval Research Laboratory, Memorandum Report 4698, January 13, 1982.

[28] Hartlen, R.T., and Currie, I.G., "Lift-Oscillator Model of Vortex-Induced Vibration", J. Eng. Mech. Div., ASCE, vol. 96, No. EM5, pp. 577-591, 1970.

[29] Hall, S.A., "Vortex-Induced Vibrations of Structures", Ph.D. Thesis, California Institute of Technology, 1981.

[30] Iwan, W.D., and Blevins, R.D., "A Model for Vortex Induced Oscillation of Structures", J. Applied Mech., vol. 41, No. 3, pp. 581-586, September 1974.

[31] Iwan, W.D., "The Vortex Induced Oscillation of Elastic Structural Elements", J. Eng. for Ind., vol. 97, pp. 1378-1382, November 1975.

[32] Iwan, W.D., "Calculation of the Natural Frequencies, Mode Shapes and Strumming Amplitude of Nonuniform Cable Structures" submitted to the Civil Engineering Laboratory, Port Hueneme, CA, May 1979.

[33] Jones G.W., Jr., "Unsteady Lift Forces Generated by Vortex Shedding About a Large, Stationary, and Oscillating Cylinder at High Reynolds Numbers", ASME, Symposium on Unsteady Flow at the Fluids Engineering Conference, paper No. 68-FE-36, Philadelphia, PA, May 1968.

[34] Kennedy, M.B., "A Linear Random Vibrations Model for Cable Strumming", Ph.D. Thesis, Massachusetts Institute of Technology, 1979.

[35] King, R., "The 'Added Mass' of Cylinders", British Hydrodynamics Research Association paper TN1100, 1971.

[36] Koopmann, G.H., "The Vortex Wakes of Vibrating Cylinders at Low Reynolds Numbers", J. Fluid Mech., vol. 28, part 3, pp. 501-512, 1967.

[37] Kretschmer, T.R., Edgerton, G.A., and Albertsen, N.D., "Seafloor Construction Experiment, Seacon II - An Instrumented Tri-Moor for Evaluating Undersea Cable Structure Technology", Naval Facilities Engineering Command, Technical Report R848, December 1976.

[38] Krylov, N.N., and Bogoliubov, N.N., Introduction to Non-Linear Mechanics, Princeton University Press, N.J., 1947, Kraus Reprint Company, NY, 1970.

[39] Kwok, K.C.S., and Melbourne, W.H., "Wind-Induced Lock-in Excitation of Tall Structures", J. Structural Div., ASCE, vol. 107, No. ST1, January 1981.

[40] Mackovsky, M.S., "Vortex-Induced Vibration Studies", Navy Department, David Taylor Model Basin, Report 1190, July 1958.

[41] Marris, A.W., "A Review on Vortex Streets, Periodic Wakes, and Induced Vibration Phenomena", J. Basic Eng., vol. 86, pp. 185-196, June 1964.

[42] Mazel, C.H., "Vortex-Excited Vibrations of Marine Cables", M.S. Thesis, Massachusetts Institute of Technology, 1976.

[43] Minorsky, N., Nonlinear Oscillations, D. Van Nostrand Company, Princeton, NJ, 1962.

[44] Morrinson, J.R., O'Brian, M.P., Johnson, J.W., and Schaaf, S.A. "The Force Exerted by Surface Waves on Piles", Petroleum Transactions, AIME, vol. 189, pp. 149-154, 1950.

[45] Novak, M., and Tanaka, H., "Pressure Correlations on Vibrating Cylinder", London, Heathrow, 1975.

[46] Overik, T., Moe, G. and Hjorth-Hansen, E., "Flow-Induced Motions of Multiple Risers", ASME Winter Meeting, paper 81-WA/FE-26, Washington, D.C., 1981.

[47] Parkinson, G.V., Feng, C.C. and Ferguson, N., "Mechanisms of Vortex-Excited Oscillation of Bluff Cylinders", Proceedings of the Symposium on Wind Effects on Buildings and Structures, Loughborough University of Technology, vol. 2, paper 27, April 1968.

[48] Parkinson, G.V., "Mathematical Models of Flow-Induced Vibrations of Bluff Bodies", IUTAM-IAHR Symposium, Karlsrühe 1972, Technical Session B, pp. 81-127, Springer-Verlag, 1974.

[49] Pattison, J.H., "Measurement Technique to Obtain Strumming Characteristics of Model Mooring Cables in Uniform Currents", DWTNSRDC, Report SPD 766-01, Bethesda, MD, April 1977.

[50] Peltzer, R.D., and Rooney, D.M., "Wake Characteristics of High Aspect Ratio Cylinders in Subcritical Spanwise Sheared Flows", ASME Winter Meeting, paper 81-WA/FE-10, Washington, D.C., 1981.

[51] Ramberg, S.E., Griffin, O.M., "Vortex Formation in the Wake of a Vibrating Flexible Cable", J. Fluids Eng., vol. 96, pp. 317-322, December 1974.

[52] Ramberg, S.E., Griffin, O.M., and Skop, R.A., "Some Resonant Vibration Properties of Marine Cables with Application to the Prediction of Vortex-Induced Structural Vibrations", ASME Winter Meeting, Ocean Eng. Div., vol. 1, pp. 29-42, Houston, TX, 1975.

[53] Ramberg, S.E., and Griffin, O.M., "Velocity Correlation and Vortex Spacing in the Wake of a Vibrating Cable", ASME, Fluids Eng. Confer., paper No. 75-FE-7, Minneapolis, MN, May 1975.

[54] Ramberg, S.E., and Griffin, O.M., "The Effects of Vortex Coherence, Spacing, and Circulation on the Flow-Induced Forces on Vibrating Cables and Bluff Structures", Naval Research Laboratory, Report 7945, January 1976.

[55] Ramberg, S.E., "The Influence of Yaw Angle Upon the Vortex Wakes of Stationary and Vibrating Cylinders", Naval Research Laboratory, Memorandum Report 3822, August 1978.

[56] Raposo, P.A., "Transverse Oscillations of a Cylinder in Uniform Flow", M.S. Thesis, Naval Postgraduate School, Monterey, CA, June 1976.

[57] Rayleigh, J.W.S., Scientific Papers, vol. I-II, § 61, pp. 413-414, Dover Publications, NY, 1964.

[58] Roshko, A., "On the Drag and Shedding Frequency of Two-Dimensional Bluff Bodies", TN 3169, National Advisory Committee for Aeronautics, July 1954.

[59] Russel, J.J., "A Finite Element Analysis of Vortex-Induced Cable Oscillations", Student Research Report 2080-79, Air Command and Staff College, Air University, Maxwell Air Force Base, AL, 1979.

[60] Sarpkaya, T., "An Analytical and Experimental Study of the In-Plane and Transverse Oscillations of a Circular Cylinder in Uniform Flow", Report No. NPS-59SL75051-B, Naval Postgraduate School, Monterey, CA, May 30, 1975.

[61] Sarpkaya, T., "Transverse Oscillations of Circular Cylinder in Uniform Flow, Part I", Report No. NPS-69SL77071-R, Naval Postgraduate School, Monterey, CA, December 25, 1977.

[62] Sarpkaya, T., "Fluid Forces on Oscillating Cylinders", J. Waterway, Port, Coastal and Ocean Div., ASCE, No. WW4, pp. 275-290, August 1978.

[63] Sarpkaya, T., and Shoaff, R.L., "A Discrete Vortex Analysis of Flow About Stationary and Transversely Oscillating Circular Cylinders", Report No. NPS-69SL79011, Naval Postgraduate School, Monterey, CA, January 1979.

[64] Sarpkaya, T., "Vortex-Induced Oscillations: A Selective Review", J. Applied Mech., vol. 46, pp. 241-258, June 1979.

[65] Shiraishi, T., "The Vortex Induced Oscillation of Elastic Structural Elements", M.E. Thesis, California Institute of Technology, 1977.

[66] Skop, R.A., and Griffin, O.M., "A Model for the Vortex-Excited Resonant Response of Bluff Cylinders", J. Sound and Vib., vol. 27, pp. 225-233, 1973.

[67] Skop, R.A., and Griffin, O.M., "On a Theory for the Vortex-Excited Oscillations of Flexible Cylindrical Structures", J. Sound and Vib., vol. 41, part 3, pp. 263-274, 1975.

[68] Skop, R.A., Ramberg, S.E., and Ferer, K.M., "Added Mass and Damping Forces on Circular Cylinders", Naval Research Laboratory, Report 7970, March 19, 1976.

[69] Skop, R.A., Griffin, O.M., and Ramberg, S.E., "Seacon II Strumming Predictions", Naval Research Laboratory, Memorandum Report 3383, October 1976.

[70] Staubli, T., "Calculation of the Vibration of an Elastically Mounted Cylinder Using Experimental Data from Forced Oscillation", ASME Winter Meeting, Fluid/Structure Interactions in Turbomachinery, pp. 19-24, Washington, D.C., 1981.

[71] Staubli, T., Private Communication.

[72] Stoker, J.J., Nonlinear Vibrations in Mechanical and Electrical Systems, Interscience Publishers, Inc. NY, 1950.

[73] Strouhal, V., "Ueber eine Besondere Art der Tonerregung", Ann. Physik (Leipzig), 1878.

[74] Toebes, G.H., "The Unsteady Flow and Wake Near an Oscillating Cylinder", ASME Winter Meeting, paper No. 68-WA/FE-23, NY, 1968.

[75] Vandiver, B.J., and Pham, T.Q., "Performance Evaluation of Various Strumming Suppression Devices", Report No. 77-2, M.I.T., Ocean Engineering, March 1977.

[76] Vickery, B.J., "Fluctuating Lift and Drag on a Long Cylinder of Square Cross-Section in a Smooth and in a Turbulent Stream" J. Fluid Mech., vol. 25, part 3, pp. 481-494, 1966.

[77] von Kármán, T., "On the Mechanism of the Resistance Experienced by a Moving Body in a Liquid", Nachrichten der K. Gessellschaft der Wissenschaften zu Göttinger Mathematisch-Physikalische Klasse, pp. 547-556, translated by the National Translation Center, No. 76-51072.